uicc
global cancer control

IJC
International Journal of Cancer

NF-κ B-dependent upregulation of ICAM-1 by HPV16-E6/E7 facilitates NK cell/target cell interaction

Sonja Textor[1], Rosita Accardi[2], Tereza Havlova[1], Ishraq Hussain[3], Bakary S. Sylla[2], Lutz Gissmann[4,5] and Adelheid Cerwenka[1]

[1] German Cancer Research Center, Research Group Innate Immunity, Heidelberg, Germany
[2] International Agency for Research in Cancer, Infections and Cancer Biology Group, Lyon, France
[3] SK University of Agricultural Sciences & Technology of Kashmir, Division of Veterinary Biochemistry FVSc & AH, Shuhama, Alusteng, Kashmir, Jammu and Kashmir, India
[4] Department of Genome Modifications and Carcinogenesis, German Cancer Research Center, Heidelberg, Germany
[5] Department of Botany and Microbiology, King Saud University, Riyadh, Saudi Arabia

NK cell recognition of tumor cells is mediated by a delicate balance of signals received by MHC class I-binding inhibitory NK cell receptors and activating NK cell receptors, which mainly bind to virus-, stress- or tumor-induced ligands. In addition, adhesion molecules such as the intercellular adhesion molecule-1 (ICAM-1) and its receptors, the lymphocyte function-associated antigen-1 (LFA-1) and Mac-1, are crucial for immune synapse formation and NK cell-mediated killing. In this study, we show that expression of the adhesion molecule ICAM-1 was rapidly induced by E6 and -E7 oncoproteins of HPV16, -18, -5 and -8, but not of HPV38 and -6 in primary human keratinocytes after retroviral transduction. ICAM-1 was upregulated in E6E7-expressing keratinocytes both at mRNA and protein levels. The observed ICAM-1 upregulation in HPV16-E6E7-expressing keratinocytes was partially dependent on activation of the NF-κB pathway. Importantly, the upregulated ICAM-1 expression in HPV16-E6E7-expressing keratinocytes led to enhanced conjugate formation with NK cells. We previously showed that HPV16-positive cervical carcinomas frequently express low levels of inhibitory NK cell ligands and high levels of activating NK cell ligands. Moreover, levels of the adhesion molecule ICAM-1 are enhanced by HPV16-E6/E7. Therefore, strategies that aim at harnessing NK cells might be beneficial for the treatment of cervical carcinoma.

Human papillomaviruses (HPV) are a family of small double-stranded DNA viruses including more than 100 different members that cause diseases in humans ranging from benign warts to malignant cancers. The two main HPV genera are the Alpha and Beta papillomaviruses.[1] Alpha papillomaviruses include the so-called "high-risk" mucosal HPV types, *e.g.*, HPV16 and HPV18 that are the causal agents of the development of malignant cancer of the cervix.[2] Beta papillomaviruses, including HPV5, HPV8 and HPV38, are typically associated with unapparent cutaneous infections in humans. Nevertheless, in particular, in immunocompromised individuals, these viruses are associated with nonmelanoma skin cancer (NMSC).[3] The two early viral proteins E6 and E7 of "high-risk" Alpha papillomaviruses, such as HPV16, are well-characterized oncogenes leading to a severe deregulation of the cell cycle by degradation of p53[4] or inhibition of pRb,[5,6] respectively. Little is known about the signaling pathways affected by E6 and E7 from Beta papillomaviruses.[3]

Activation of NK cells is mediated by a delicate balance of signals received by inhibitory and activating receptors.[7] Inhibitory receptors mostly recognize self-MHC class I molecules and activating receptors interact with virus-, stress- or transformation-induced ligands.[8,9] Thus, low MHC class I expression combined with high levels of activating NK cell receptor ligands make cells susceptible to NK cell-mediated killing. In addition to the "right" combination of activating and inhibitory NK cell receptor ligands on target cells, adhesion molecules on targets and NK cells are crucial for immune synapse formation and NK cell-mediated killing.[10] Firm NK cell/target cell adhesion is mainly mediated by the two integrins, LFA-1 and Mac-1, on NK cells and ICAM-1 on target cells.[11] The adhesion molecule ICAM-1 mediates not only cell–cell but also cell–matrix interactions.[12] ICAM-1 is expressed on hematopoietic and nonhematopoietic cells[13] and is rapidly upregulated in response to inflammatory stimuli, including virus infections or pro-inflammatory cytokines.[12] Depending on the

Key words: Human Papillomavirus, cervical cancer, NK cells, ICAM-1, NF-κB

Abbreviations: CxCa: cervical carcinoma; HPV: Human Papillomavirus; ICAM-1: intercellular adhesion molecule-1; IFN-γ, interferon-γ; I-κBα: NF-κB inhibitor alpha; LFA-1: lymphocyte function-associated antigen-1; NF-κB: nuclear factor kappa-light-chain-enhancer of activated B cells; NK cell: natural killer cell; NMSC: nonmelanoma skin cancer

DOI: 10.1002/ijc.25442
History: Received 5 Nov 2009; Accepted 12 Apr 2010; Online 6 May 2010

Correspondence to: Adelheid Cerwenka, German Cancer Research Center/D080, Im Neuenheimer Feld 280, 69120 Heidelberg, Germany, Tel: 0049-6221-424480, Fax: 0049-6221-423755, E-mail: a.cerwenka@dkfz.de

stimulus, ICAM-1 expression is regulated by several signal transduction pathways, including protein kinase C (PKC), mitogen-activated protein (MAP) kinases, Janus kinases (JAKs), signal transducers and activators of transcription (STAT) or NF-κB signaling pathway.[14]

In HPV-associated diseases, high ICAM-1 expression was observed *in situ* by immunohistochemistry.[15,16] Furthermore, increased expression of ICAM-1 in *high-grade* cervical intraepithelial neoplasia (CIN)[15] and cervical carcinoma (CxCa) specimen[16] was reported. Studies using immortalized or transformed *in vitro*-cultured HPV16-positive cell lines confirmed these results. ICAM-1 was reported to be upregulated in HPV16-immortalized human oral keratinocytes compared to normal human oral keratinocytes.[17] In contrast, Coleman *et al.* described ICAM-1 expression only in fully transformed tumorigenic cells such as in the $HPV16^+$ CxCa cell lines SiHa and CaSki, but not in HPV16-immortalized nontumorigenic human keratinocytes.[15] In these studies, the mechanisms of ICAM-1 upregulation were not addressed.

Here, we describe for the first time that E6 and E7 of HPV16 rapidly induced ICAM-1 surface expression in their natural host cells, primary human keratinocytes. This ICAM-1 upregulation was partially mediated by the NF-κB pathway. Furthermore, our results reveal that significantly more conjugates were formed between NK cells and HPV16-E6E7-expressing cells as compared to control cells. Thus, expression of HPV16-E6/E7 in primary human keratinocytes might alert the immune system by upregulation of ICAM-1 that facilitates immune cell adhesion.

Material and Methods

Cell culture

Phoenix ampho cells were cultured in DMEM containing 4.5 g/ml glucose and 2 mM *l*-glutamine (Sigma-Aldrich, Munich, Germany) supplemented with 10% FBS (PAA, Pasching, Austria). Primary human epidermal keratinocytes from adult or neonatal foreskin were obtained from Invitrogen and cultured in EpiLife® medium supplemented with 1% human keratinocyte growth supplement, HKGS, containing 0.2 % bovine pituitary extract, 5 μg/ml bovine insulin, 0.18 μg/ml hydrocortisone, 5 μg/ml bovine transferrin and 0.2 ng/ml human epidermal growth factor (Invitrogen, Karlsruhe, Germany). The cervical cancer-derived cell line, CaSki, was maintained in DMEM containing 1 g/ml glucose and 2 mM L-glutamine supplemented with 10% FBS. The human NK cell line, NKL,[18] was cultured in RPMI containing 1 g/ml glucose and 2 mM L-glutamine supplemented with 10% FBS and 100 U/ml human IL-2 (Chiron Corporation, Emeryville, CA). All cells were cultured in the presence of 100 U/ml penicillin G and 100 μg/ml streptomycin (Gibco/BRL, Karlsruhe, Germany).

Retroviral transduction

The plasmids pLXSN, pLXSN-16E6, pLXSN-16E7, pLXSN-16E6E7, pLXSN-38E6E7, pLXSN-5E6E7, pLXSN-8E6E7, pLXSN-18E6E7, pLXSN-6E6E7 and pBabepuro-16E7 were kindly provided by M. Tommasino (IARC, Lyon, France) and the plasmids pBabe-puro and pBabe-puro-ΔN-I-κBα by B. Sylla (IARC, Lyon, France). The pBabe-puro-ΔN-I-κBα was generated by inserting the coding sequence of I-κBα lacking the first 32 amino acids into the pBabe-puro retroviral vector. An IRES-EGFP sequence was cloned 3′ of the multiple cloning site in pLXSN, pLXSN-16E6, pLXSN-16E7 and pLXSN-16E6E7 plasmids as a marker genes. Retroviral supernatants generated by transfection of the pLXSN and pBabe-puro constructs into Phoenix ampho cells were used to transduce primary human epidermal keratinocytes as previously described.[19] Forty-eight hours after transduction, keratinoctyes were analyzed by flow cytometry for expression of the gene of interest gating on EGFP-positive cells and/or selection with 100 μg/ml G418 (Gibco/BRL, Karlsruhe, Germany) or 0.2 μg/ml puromycin (Sigma-Aldrich, Munich, Germany) was started.

RNA extraction, reverse transcription and PCR

Total RNA was extracted with the RNeasy Mini Kit (Qiagen, Hilden, Germany) according to the manufacturer's instructions. Residual contaminating DNA was removed with the TURBO DNA-*free*™ Kit (Ambion, Huntingdon, UK). One microgram RNA was reversely transcribed using the SuperScript™ First-Strand Synthesis system for RT-PCR (Invitrogen, Karlsruhe, Germany) and Oligo $(dT)_{12-18}$ primer. To exclude false positive results due to contaminating genomic DNA, samples without reverse transcriptase were included.

Nonquantitative PCR experiments for HPV-E6/E7 transcripts were performed on a Mastercycler (Eppendorf, Hamburg, Germany) with the following program: 95°C for 4 min; 30 cycles at 95°C for 1 min/55°C for 1 min/72°C for 1 min; 72°C for 10 min. *Taq* DNA polymerase (Invitrogen, Karlsruhe, Germany) with its respective buffer, 100 ng forward and reverse primers (Table 1) and a cDNA equivalent to 10 ng RNA was used.

All real-time PCR experiments were carried out on an ABI 7300 SDS system (Applied Biosystems, Darmstadt, Germany). Reactions were performed in duplicates using the RT^2 Real-Time™ SYBR Green/ROX PCR Master Mix (Biomol, Hamburg, Germany) containing 300 nm forward and reverse primer (Table 2) and a cDNA equivalent to 10 ng RNA. The PCR program was the following: 50°C for 2 min; 95°C for 10 min; 40 cycles at 95°C for 15 sec/60°C for 60 sec. Threshold cycle (Ct) values were determined using Sequence Detection Software version 1.2 (Applied Biosystems, Darmstadt, Germany). Transcripts were considered present at a $Ct \leq 35$. Relative ICAM-1 mRNA expression was calculated as: $2^{-\Delta Ct}$, where $\Delta Ct = Ct_{ICAM\text{-}1} - Ct_{GAPDH}$.

Western blotting

Whole cell lysates were prepared using 1× Cell Lysis Buffer from Cell Signaling Technology (Danvers, MA) according to the manufacturer's instructions. For the separation of nuclear

Table 1. Oligonucleotide primers for RT-PCR

Gene		Sequence 5′ → 3′
HPV16-E6	F	AAAAAGAATTCATGTTTCAGGACCCACAG
	R	AAAAAGTCGACTTACAGCTGGGTTTCTCTA
HPV16-E7	F	ACATTGCATGAATATATGTTAGATTTGCAA
	R	TCTGAGAACAGATGGGGCATC
HPV18-E7	F	GACCTTCTATGTCACGAGCAATTA
	R	TGCACACCACGGACACACAAAG
HPV5-E7	F	CGTTAACATGATTGGTAAAGAGGTCACC
	R	CCTCGAGCTACCTTTAGAATTAGGATC
HPV8-E7	F	CGAATTCATGATTGGTAAAGAGGTCAC
	R	CGGATCCCCCTTCTTTAGATGTACTAC
HPV38-E7	F	AGAGGAGGAGCCAGCATA
	R	TGCGAATGTCTTCTCGACA
HPV6-E7	F	ATGCATGGCAGGCACGTGACCCTGAAG
	R	TTGGGGGCGCAGATGGGGCACACGATGTTC
GAPDH	F	AAAAAGGTGGTGAAGCAGGCGT
	R	AAAGAGGAGTGGGTGTCGCTGTT

Abbreviations: F, forward; R, reverse.

Table 2. Oligonucleotide primers for quantitative real-time PCR

Gene		Sequence 5′ → 3′
CD54	F	GCTGACGTGTGCAGTAATACTGG
	R	TTCTGAGACCTCTGGCTTCGT
GAPDH	F	CCCATGTTCGTCATGGGTGT
	R	TGGTCATGAGTCCTTCCACGATA

Abbreviations: F, forward; R, reverse.

and cytosolic proteins, the NucBuster™ Protein Extraction Kit from Novagen (Madison, WI) was used. Equal amounts of protein lysates (50 μg per lane) were separated by 12% SDS-polyacrylamide gel electrophoresis and transferred to Immobilon-P® PVDF membranes (Millipore, Bedford, MA). Subsequently, membranes were blocked in PBS/0.05% Tween 20/5% milk for 1 hr at RT. Rabbit Abs specific for phospho-I-κBα (Ser32), I-κBα, phospho-p65 (Ser536), p65 and p105/p50 (Cell Signaling Technology, Danvers, MA) were added at an 1:1,000 dilution in PBS/0.05% Tween 20/5% BSA for an overnight incubation at 4°C. Equal loading was controlled by reprobing the membranes with a rabbit Ab for the nuclear Poly (ADP-ribose) polymerase (PARP) (Cell Signaling Technology, Danvers, MA) at a final dilution of 1:1,000 and/or a mAb specific for actin (clone C4, MP Biomedicals, Solon, OH) at a final dilution of 1:10,000. Horseradish-peroxidase (HRP)-coupled anti-rabbit antibody at a final dilution of 1:2,000 (Cell Signaling Technology) or HRP-conjugated anti-mouse Ab at a final dilution of 1:5,000 (Dianova, Hamburg, Germany) were applied for 1 hr at RT. Signals were visualized by enhanced chemiluminescence (ECL Plus Western Blotting Detection Reagents, GE Healthcare, Chalfont St. Giles, UK). Western Blot signals were quantified using ImageJ (*rsbweb.nih.gov/ij/*).

p65/p-p65-specific ELISA

Nuclear and cytosolic extracts were prepared using the NucBuster™ Protein Extraction Kit from Novagen (Madison, WI). Equal amounts of protein (30 μg per well) in nuclear and cytosolic extracts were loaded on a 96-well plate. Phospho-p65 or p65-specific signals were quantified with the PathScan® Phospho-NF-κB p65 (Ser536) Sandwich ELISA Kit or with the PathScan® Total NF-κB p65 Sandwich ELISA Kit, respectively (both Cell Signaling Technology, Danvers, MA) following the manufacturer's instructions.

Flow cytometry

Transduced keratinocytes and CaSki cells of less than 70% confluence were harvested by trypsinization and washed twice with FACS-buffer consisting of PBS containing 0.02% NaN_3 (Applichem, Darmstadt, Germany) and 3% FBS (PAA). 1×10^5 cells were resuspended in 50 μl FACS buffer containing PE-labeled anti-CD54 mAb (clone HA58; BD Pharmingen, San Jose, CA) at a 1:50 dilution in 96-well plates. After washing, 7-AAD (Sigma-Aldrich, Munich, Germany; 2 μg/ml) was added and incubated for 20 min on ice. Flow cytometric analysis was performed using a FACS Calibur® and CellQuest Pro® software (BD Biosiences, San Jose, CA).

Cytotoxicity assay

A 5 hr standard ^{51}Cr release cytotoxicity assay was carried out as previously described.[19] Blockage of LFA-1 was accomplished by adding anti-LFA-1 (clone L130; BD Pharmingen, San Jose, CA) or isotype control $mIgG_1$ (clone 11711; R&D Systems, Wiesbaden, Germany) mAbs at 20 μg/ml final concentration to the effector cells 10 min before coculture with target cells.

Flow cytometry-based conjugation assay

The flow cytometry-based conjugation assay was performed as previously described.[20] Briefly, effector cells (NKL) and target cells were harvested and washed once with HBSS containing $CaCl_2$ and $MgCl_2$ (Gibco/BRL, Karlsruhe, Germany) 2×10^6 target cells/ml were resuspended in 40 nM Calcein AM (Molecular Probes/Invitrogen, Karlsruhe, Germany) in HBSS and 1×10^6 effector cells/ml were resuspended in 0.2 μm-filtered 253 μM DHE (Molecular Probes/Invitrogen, Karlsruhe, Germany) in HBSS. Cells were incubated with the dyes for 30 min at 37°C with slow agitation every 10 min. Staining was stopped by washing twice with HBSS. Conjugate formation was achieved by mixing 2×10^5 Calcein AM-labeled target cells with 1×10^5 DHE-labeled effector cells. The cell mixture was slowly vortexed and spun down for 3 min at 300 rpm at 4°C followed by incubation for the indicated time periods at 37°C and 5% CO_2. Conjugate

formation was stopped by addition of ice-cold 1% paraformaldehyde. Conjugate formation was analyzed using a FACSCalibur™ and CellQuest™ software (BD Biosciences, San Jose, CA). Blockage of LFA-1 was performed as described for the cytotoxicity assay.

Statistical analysis

For the calculation of statistical significances of differences between experimental groups two-tailed Student's *t* tests for unpaired data were used. *p* values of less than 0.05 were considered as significant.

Results

HPV16-E6E7 expression induces rapid upregulation of the adhesion molecule ICAM-1 in primary human keratinocytes

To investigate the impact of the two viral oncoproteins E6 and E7 on the expression of ICAM-1, we transduced primary human keratinocytes, the natural host cells of HPV, with a retroviral vector system containing E6/E7 of HPV type 16 and IRES-EGFP as a marker gene. Transduction efficiencies were $\geq$ 80%. After transduction, E6 and E7 expression were confirmed by RT-PCR (Fig. 1*a*). Full-length E7 and E6 transcripts were detectable as well as the two splice variants of E6, E6*I and E6*II (Fig. 1*a*). Importantly, HPV16-E6E7-expressing EGFP-positive keratinocytes expressed higher levels of surface ICAM-1 as compared to vector control (VC)-transduced keratinocytes 48 h after transduction (Fig. 1*B*, left and middle panel). ICAM-1 expression was significantly upregulated on protein level as determined by flow cytometry (Fig. 1*b*, middle panel) and at mRNA level as detected by Real-time quantitative PCR (Fig. 1*b*, right panel). Expression of other molecules, including the NKG2D ligand ULBP1, was unchanged (data not shown) indicating selective upregulation of ICAM-1 by HPV16-E6E7. Neither HPV16-E6 nor HPV16-E7 by itself was able to significantly upregulate ICAM-1 mRNA or protein in primary human keratinocytes (Fig. 1*c*). Taken together, our data indicate that E6 and E7 of HPV16 are potent inducers of ICAM-1 expression in primary human keratinocytes and that the two oncoproteins act synergistically.

ICAM-1 expression on target cells enhances adhesion and killing susceptibility to the NK cell line NKL

In a next step, we analyzed the influence of the enhanced ICAM-1 expression in transduced keratinocytes on the ability to form conjugates with the NK cell line, NKL that expresses high levels of LFA-1.[21] Figure 2*a* shows that significantly more conjugates were formed between NKL cells and HPV16-E6E7-expressing keratinocytes as compared to VC-expressing keratinocytes. This enhanced conjugate formation between NKL cells and HPV16-E6E7-expressing keratinocytes was significantly reduced by addition of a blocking mAb directed against LFA-1 (Fig. 2*b*). In addition, conjugate formation of NKL cells with the HPV16-positive cervical carcinoma cell line, CaSki, which endogenously expresses high levels of ICAM-1 (Fig. 2*c*), was significantly reduced by LFA-1 blockage (Fig. 2*d*). Furthermore, killing of CaSki cells by NKL cells was markedly reduced upon addition of a blocking anti-LFA-1 mAb (Fig. 2*e*). Thus, enhanced ICAM-1 expression by HPV16-E6E7 leads to a better recognition of HPV16-E6E7-expressing cells by LFA-1-expressing NK cells.

The upregulation of ICAM-1 in HPV16-E6E7-expressing keratinocytes correlates with activated components of the NF-κB pathway

A variety of transcription factors, including NF-κB, AP-1, GAS and C/EBP, are implicated in the transcriptional regulation of ICAM-1.[14] It was reported that induction of multiple NF-κB- and AP-1-responsive genes in HPV16-E6E7 expressing keratinocytes correlated with enhanced expression of components of the NF-κB signaling pathway.[22] Thus, we investigated the involvement of NF-κB signaling in the induction of ICAM-1 expression by HPV16-E6E7. NF-κB activation is typically mediated through phosphorylation of its inhibitor Iκ-B by the Iκ-B kinase complex IKKα/IKKβ/IKKγ followed by the ubiquitination of I-κB and its degradation.[23] During this process, NF-κB dimers, in most cells composed of p65 and/or p50, are also phosphorylated by the IKK complex and released from I-κB binding due to I-κB degradation. Phosphorylated NF-κB dimers shuttle into the nucleus and exert their function through binding to NF-κB binding sites upstream of NF-κB-responsive genes. As depicted in Figure 3*a*, we detected decreased levels of I-κBα and increased phosphorylation of p65 at Ser536 in keratinocytes expressing HPV16-E6E7 as compared to VC-expressing keratinocytes. Phosphorylation of additional phosphorylation sites at Ser276 and Ser468 of p65 was not observed (data not shown). Overall levels of p65 and p50 remained unchanged in whole cell lysates. After separation of the nuclear from the cytosolic cell fraction, more phosphorylated p65 and more total p65 and p50 were detected in nuclei of HPV16-E6E7-expressing keratinocytes than in nuclei of VC-expressing keratinocytes as assessed by Western blotting (Fig. 3*b*) and specific ELISAs (Fig. 3*c*). In the cytosolic cell fraction levels of phosphorylated and total p65 and p50 were similar in VC- and HPV16-E6E7-expressing cells (Figs. 3*d* and 3*e*). Hence, low levels of Iκ-Bα, phosphorylation of p65 at Ser536 and enhanced levels of p65/p50 in the cell nuclei indicate a constitutively activated NF-κB pathway in HPV16-E6E7-expressing cells.

NF-κB signaling is required for the upregulation of ICAM-1 surface expression in HPV16-E6E7-expressing keratinocytes

Next, we investigated whether NF-κB signaling is involved in the increased ICAM-1 expression in HPV16-E6E7-expressing cells. For this purpose, we employed a NF-κB superrepressor (ΔN-I-κBα), a deletion mutant of I-κBα lacking the phosphorylation sites Ser32 and Ser36. Hence, VC- or HPV16-E6E7-expressing keratinocytes were transduced with a

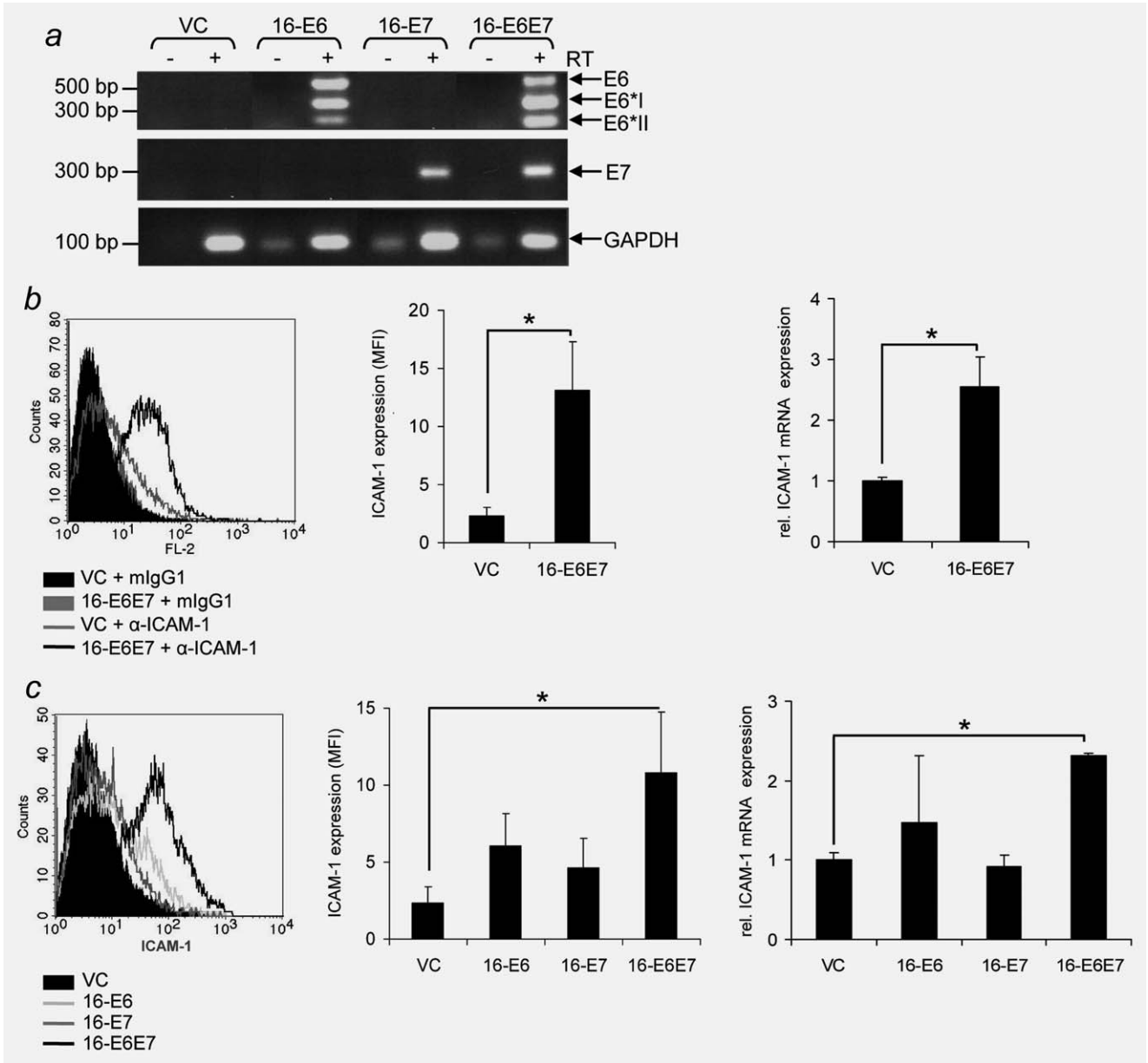

Figure 1. ICAM-1 is upregulated in HPV16-E6E7 expressing cells. Primary human epidermal keratinocytes were transduced with an IRES-EGFP-containing retroviral vector carrying HPV16-E6E7 (16-E6E7), HPV16-E6 (16-E6), HPV16-E7 (16-E7) or with the respective empty vector control (VC). (*a*) E6, E6*I, E6*II (upper panel), E7 (middle panel) and GAPDH (lower panel) transcripts in transduced keratinocytes were determined by RT-PCR. (*b, c*) ICAM-1 surface or relative ICAM-1 mRNA expression was monitored on transduced keratinocytes by flow cytometric analysis or Real-time quantitative PCR analysis, respectively, 48 hr after transduction. For the flow cytometric analysis, ICAM-1 expression was monitored on 7-AAD$^-$ EGFP$^+$ cells. Left panel: One representative histogram overlay showing ICAM-1 surface expression in transduced keratinocytes. Middle panel: ICAM-1 surface expression: The mean of three independently performed experiments with three different keratinocytes donors ± SD is shown. Right panel: Relative ICAM-1 mRNA expression: ICAM-1 mRNA expression levels are depicted relative to GAPDH mRNA expression levels (set as 100). The mean of two independently performed experiments with two representative keratinocyte donors ± SD is shown. *$p < 0.05$ determined by Student's *t* test. RT, reverse transcriptase.

retroviral vector (pBabe) carrying ΔN-I-κBα (Fig. 4*a*). In HPV16-E6E7-expressing keratinocytes transduced with the superrepressor degradation of I-κBα was greatly impaired (data not shown). Three days after start of antibiotic selection, ICAM-1 expression was significantly reduced in HPV16-E6E7-expressing cells that were transduced with the NF-κB superrepressor. The expression of other cell surface molecules, like ULBP1, was unchanged (Fig. 4*b*). Moreover, the viability of target cells was not influenced by the NF-κB superrepressor at this time point (data not shown). In

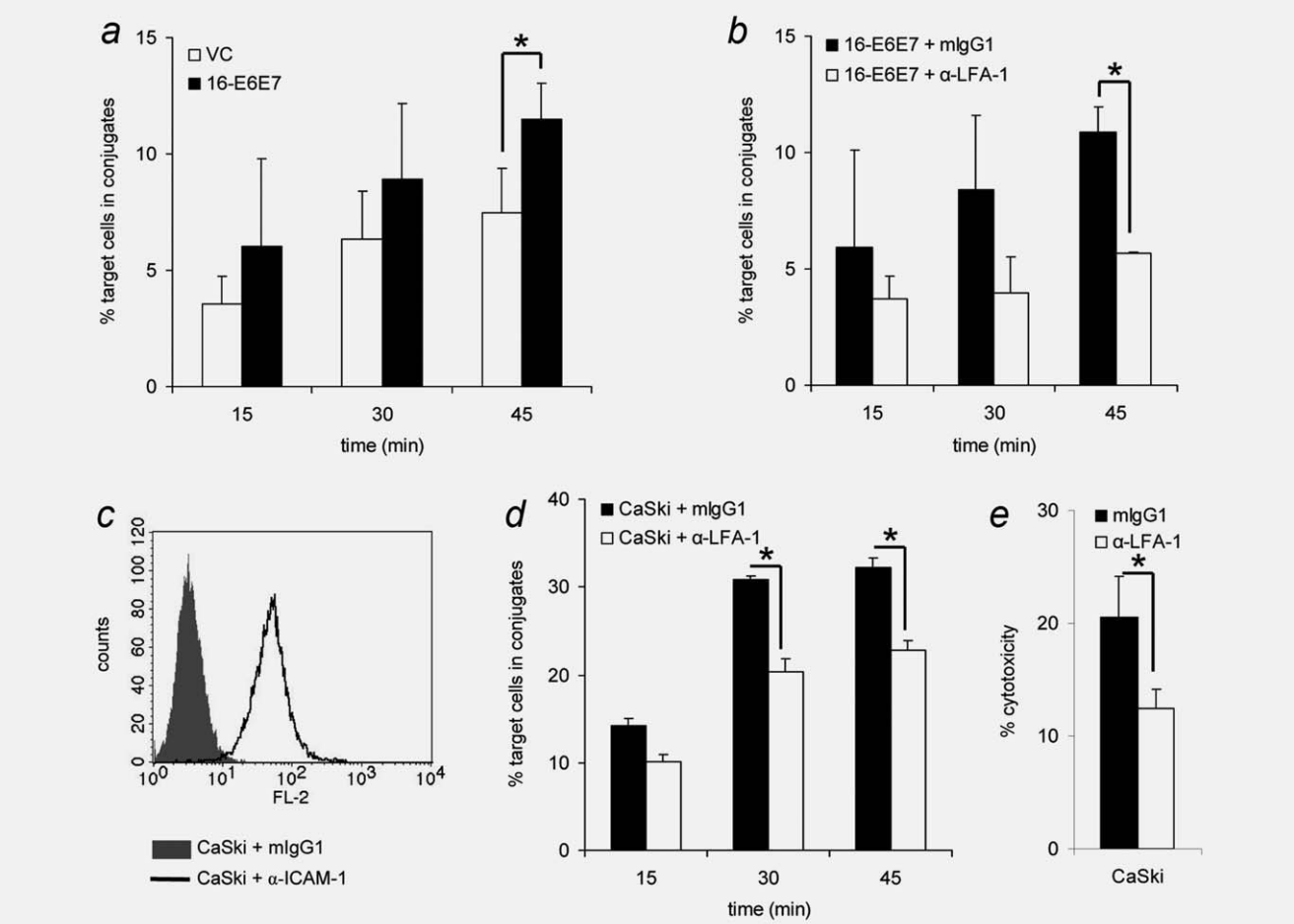

Figure 2. ICAM-1 expression in HPV16-E6E7$^+$ cells mediates NK cell-dependent adhesion and killing. (*a*) Flow cytometry-based conjugate formation assay using NKL cells as effector cells and vector control (VC) or HPV16-E6E7 (16-E6E7)-expressing keratinocytes as target cells at the indicated time points. (*b*) Blockage of LFA-1 in a flow cytometry-based conjugate formation assay using NKL cells as effector cells and HPV16-E6E7-expressing keratinocytes as target cells. (*a, b*) The mean of four independently performed experiments with two different keratinocyte donors ± SD is depicted. (*c*) One representative histogram overlay depicting ICAM-1 surface expression on the HPV16$^+$ CxCa cell line, CaSki. (*d*) Blockage of LFA-1 in a flow cytometry-based conjugate formation assay using NKL cells as effector cells and CaSki cells as target cells. The mean of two independently performed experiments ± SD is depicted. (*e*) Blockage of LFA-1 in a standard ^{51}Cr-release cytotoxicity assay using NKL cells as effector cells and CaSki cells as target cells (E:T ratio 50:1). One representative experiment out of two independently performed experiments is shown. The mean of triplicates ± SD is indicated. *$p < 0.05$ determined by Student's *t* test.

summary, these data indicate that the NF-κB pathway in HPV16-E6E7-expressing keratinocytes is, at least, partially responsible for the observed upregulation of ICAM-1 by HPV16-E6E7.

Mucosal and cutaneous HPV types differentially regulate ICAM-1 expression

As ICAM-1 expression was upregulated in HPV16-E6E7-expressing cells, the influence of additional related HPV types on ICAM-1 expression was investigated. Primary human keratinocytes from two different donors were transduced with retroviral vectors expressing HPV18-E6E7 (another mucosal high-risk Alpha PV type), HPV5-E6E7, HPV8-E6E7 and HPV38-E6E7 (cutaneous Beta PV types) and HPV6-E6E7 (a mucosal low-risk Alpha PV type). Expression of the respective HPV-E7 mRNA was confirmed by RT-PCR (Fig. 5*a*). Figure 5*b* shows that 5 days after transduction HPV16-E6E7 induced the strongest upregulation of ICAM-1 compared to E6 and E7 of other HPV types. E6 and E7 from HPV18 induced an intermediate upregulation of ICAM-1. In contrast to HPV38-E6E7, which did not upregulate ICAM-1 expression, E6 and E7 from the two other cutaneous Beta PV types, HPV5 and 8, significantly enhanced ICAM-1 expression. E6 and E7 of the low-risk mucosal Alpha PV type, HPV6, did not significantly change levels of ICAM-1. Analysis of components of the NF-κB pathway in whole cell lysates of these HPV types revealed that only in HPV16-E6E7 expressing cells I-κBα expression was diminished and p65

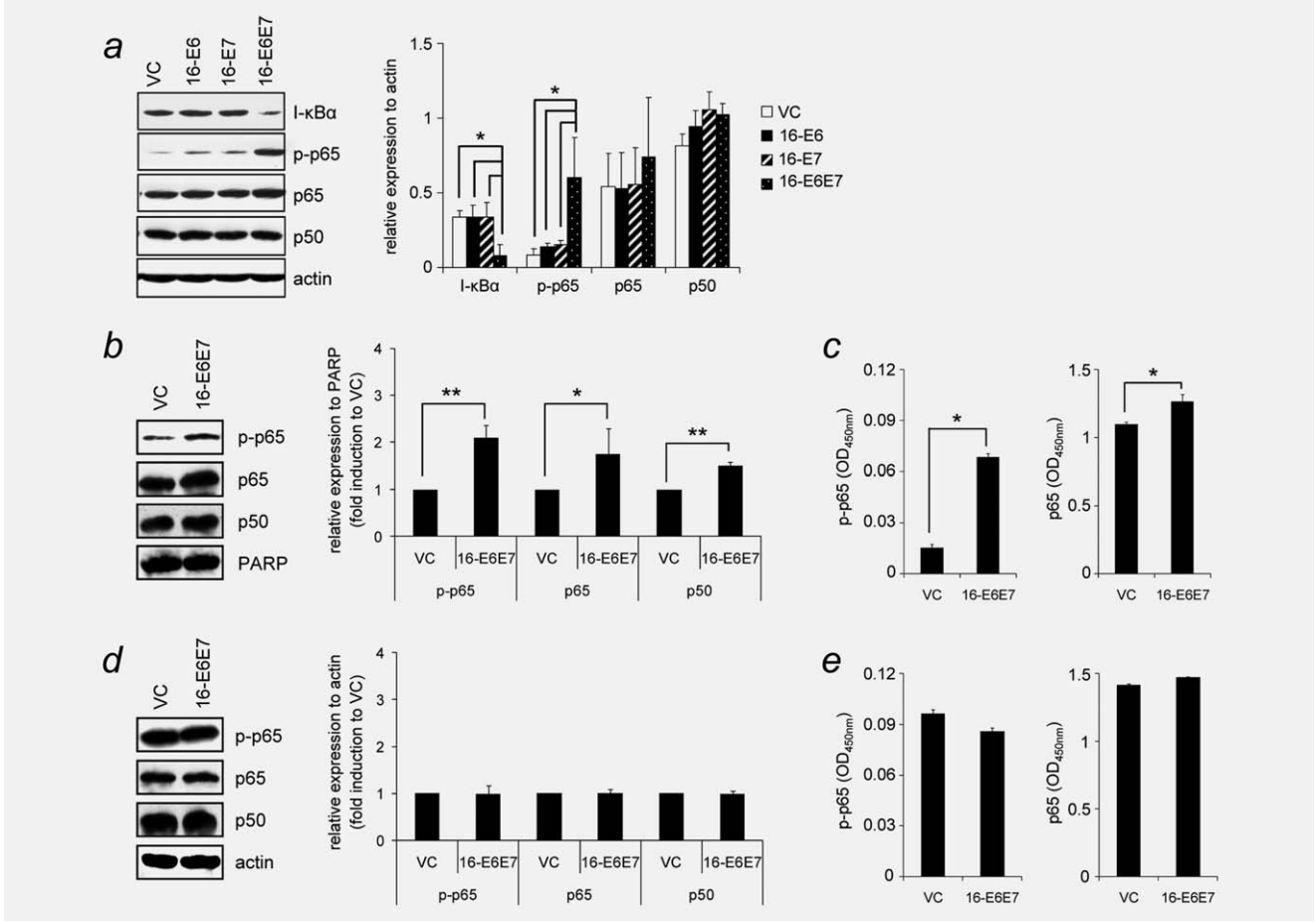

Figure 3. Components of the NF-κB pathway are activated in HPV16-E6E7 expressing cells. (*a*) Whole cell lysates: Western blot analysis of p50, p65, phospho-p65 (Ser536), I-κBα and actin expression in transduced keratinocytes 7 days after transduction. (*b, c*) Nuclear extracts: (*b*) Western Blot analysis of p50, p65, phospho-p65 (Ser536) and Poly (ADP-ribose) polymerase (PARP) expression in transduced keratinocytes 7 days after transduction. (*c*) Sandwich ELISA showing levels of phospho-p65 (Ser536) and total p65 in nuclear extracts in transduced keratinocytes 7d after transduction. (*d, e*) Cytosolic extracts: (*d*) Western Blot analysis of p50, p65, phospho-p65 (Ser536) and actin expression in transduced keratinocytes 7 days after transduction. (*e*) Sandwich ELISA showing levels of phospho-p65 (Ser536) and total p65 in cytosolic extracts in transduced keratinocytes 7 days after transduction. Western Blot signals were quantified relative to actin (*a, d*) or the nuclear protein PARP (*b*) and fold induction by HPV16-E6E7 compared to VC (set as 1) was calculated (*b, d*). (*a, b, d*) The mean of three independently performed experiments with three different keratinocyte donors ± SD is indicated. (*c, e*) One representative experiment is shown. Standard deviations of duplicates are indicated.*$p < 0.05$ determined by Student's *t* test. **$p < 0.01$ determined by Student's *t* test. VC, vector control

phosphorylated at Ser536 at this time point post-transduction (Fig. 5*c*). In HPV18-E6E7-expressing cells higher levels of phosphorylated p65 were detectable, whereas I-κBα expression was not altered. In HPV5- and HPV8-E6E7-expressing cells, the upregulated ICAM-1 expression did not correlate with activated components of the NF-κB pathway suggesting that in these HPV types additional signaling pathways are involved.

Discussion

It is well established that ICAM-1 expression in cells is often induced during viral infections by viral proteins, pro-inflammatory cytokines and interferons.[12,24] Thereby, ICAM-1 promotes interactions between infected cells and immune cells by allowing immune synapse formation.[25] Here, we show that in primary human keratinocytes expression of HPV16-E6 and -E7 leads to a pronounced and rapid induction of ICAM-1 at mRNA- and protein levels already 48 hr after transduction (Fig. 1*b*). A previous study by Huang *et al.* described induction of ICAM-1 expression in HPV16-E6E7-immortalized human oral epithelial cells compared to normal oral epithelial cells without elucidating the mechanisms underlying the observed ICAM-1 upregulation in HPV16-E6E7-expressing cells.[17] In addition, a study by Coleman *et al.* reported a significant induction of ICAM-1 in high-grade cervical intraepithelial neoplasia (CIN), in which the

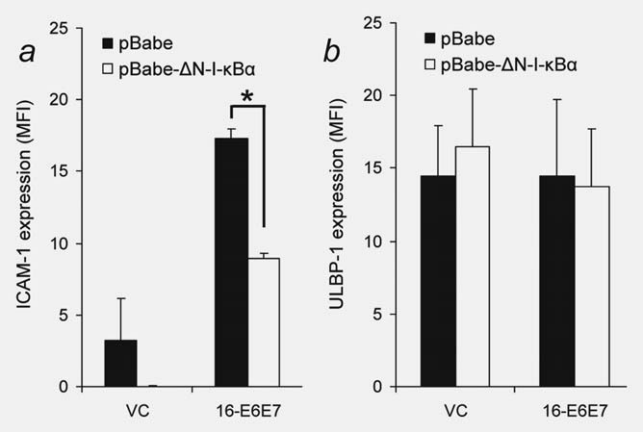

Figure 4. Upregulation of ICAM-1 in HPV16-E6E7 expressing cells is partially NF-κB-dependent. (*a, b*) Keratinocytes expressing either HPV16-E6E7 (16-E6E7) or the respective vector control (VC) were transduced on day 3 after transduction with an empty retroviral vector (pBabe) or with a retroviral vector carrying a NF-κB superrepressor (pBabe-ΔN-I-κB). Seven days after transduction ICAM-1 (*a*) and ULBP1 (*b*) surface expression was monitored by flow cytometry on 7-AAD$^-$ EGFP$^+$ cells. The mean of two independently performed experiments with two different keratinocyte donors ± SD is shown. *$p < 0.05$ determined by Student's *t* test.

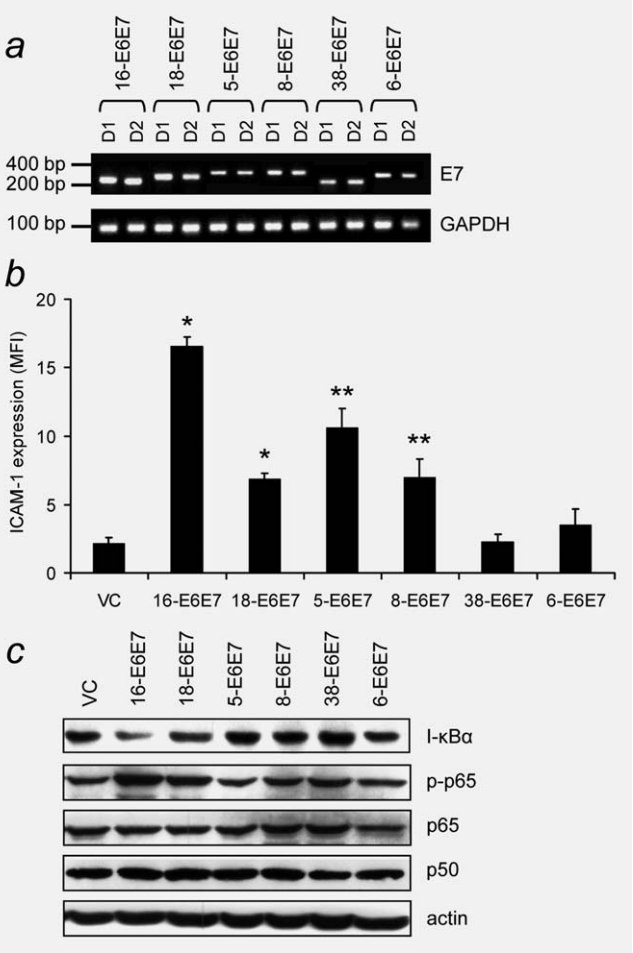

Figure 5. HPV16-E6E7 induces the highest upregulation of ICAM-1 compared to E6 and E7 from other HPV types. Keratinocytes of two different donors (D1 and D2) were transduced with a retroviral vector carrying HPV16-E6E7 (16-E6E7), HPV18-E6E7 (18-E6E7), HPV5-E6E7 (5E6E7), HPV8-E6E7 (8-E6E7), HPV38-E6E7 (38-E6E7), HPV6-E6E7 (6-E6E7) or with the respective empty vector control (VC). (*a*) E7 transcript expression in transduced keratinocytes was determined by RT-PCR. (*b*) Expression of ICAM-1 was monitored on transduced keratinocytes by flow cytometry 5 days after transduction after antibiotic selection. The mean of two independently performed experiments with two different keratinocyte donors ± SD is shown. (*c*) Western Blot analysis of p50, p65, phospho-p65 (Ser536), I-κBα and actin expression in transduced keratinocytes 7 days after transduction. *$p < 0.01$ determined by Student's *t* test comparing 16-E6E7 and 18-E6E7 with VC; **$p < 0.05$ determined by Student's *t* test comparing 5-E6E7 and 8-E6E7 with VC.

two HPV oncoproteins E6 and E7 are highly expressed.[15] In this study, ICAM-1 expression was only detected in fully transformed tumorigenic cells, such as in HPV16$^+$ CxCa cell lines, but not in HPV16-immortalized non-tumorigenic human keratinocytes. These data led to the assumption that the observed upregulation is not directly linked to E6 and E7 expression, but rather represents a late effect of transformation.[15] However, our results demonstrate that ICAM-1 upregulation was already detectable 48 hr after transduction with HPV16-E6E7-expressing vectors suggesting that E6 and E7 expression in primary human keratinocytes directly led to increased ICAM-1 expression. Moreover, transfer of cell culture supernatant from HPV16-E6E7-expressing primary human keratinocytes to VC-expressing primary keratinocytes did not induce ICAM-1 expression (data not shown) indicating that ICAM-1 induction in HPV16-E6E7-expressing cells was not mediated indirectly by soluble factors.

Our data suggest a critical involvement of the NF-κB signaling pathway in the regulation of ICAM-1 in HPV16-E6E7-expressing cells. ICAM-1 upregulation in HPV16-E6E7-expressing cells correlated with decreased I-κBα expression, increased p65 phosphorylation at Ser536 and enhanced levels of p50 and p65 in cell nuclei (Figs. 3*b* and 3*c*). Most importantly, inhibition of the NF-κB pathway with a NF-κB superrepressor significantly reduced surface ICAM-1 expression (Fig. 4). Recently, Nees et al. also described activation of components of the NF-κB pathway in HPV16-E6E7-expressing keratinocytes compared to vector control-expressing cells.[22] Furthermore, constitutive NF-κB activation in high-grade squamous intraepithelial lesions (SIL) and CxCa was detected *in situ*.[26] In agreement with our study, these reports demonstrated that mainly p65/p50 NF-κB heterodimers translocated to cell nuclei. Of note, other studies reported an inhibition of NF-κB activity in HPV16-E6 or -E7-expressing

cells.[27–29] Harvard et al. described reduced activity of NF-κB associated with modulation of expression and subcellular localization of the NF-κB1/2 precursors p100 and p105 in long-term cultured HPV16-E6 or -E7 expressing keratinocytes compared to normal keratinocytes of different origin.[27,28] Furthermore, an inhibition of IKKα activity and TNF-α induced translocation of p65 by HPV16-E7 was reported.[29] It is likely that the conflicting results regarding the modulation of NF-κB activity by HPV16-E6/E7 are due to different cell types and cell culture conditions used in these studies.

Not only HPV16-E6E7, but also E6 and E7 proteins from other HPV types led to an upregulation of ICAM-1 in primary human keratinocytes (Fig. 5). E6/E7 from another high-risk mucosal HPV type, HPV18, and E6/E7 from the two cutaneous HPV types, HPV5 and HPV8, led to a significant increase in ICAM-1 expression (Fig. 5*b*). Noteworthy, E6/E7 from a low-risk mucosal HPV type, HPV6, and E6/E7 from another cutaneous HPV type, HPV38, did not significantly increase ICAM-1 expression (Fig. 5*b*). Although HPV38 belongs to the group of Beta papillomaviruses, like HPV5 and HPV8, it is located distantly from these types in the phylogenetic tree[1] and, in contrast to HPV5 and -8, it is not regarded as a "high-risk" cutaneous HPV type.[30] Thus, ICAM-1 upregulation in E6/E7-expressing cells appears to be associated with the oncogenicity of the respective HPV type. In this context, we observed that ICAM-1 expression in HPVE6E7-expressing keratinocytes increases with the number of cell doublings. Analysis at later time points after transduction ($\geq$ 9 days) revealed that ICAM-1 upregulation in HPV5- and HPV8-E6E7 expressing cells even exceeded ICAM-1 expression in HPV16-E6E7-expressing cells (data not shown). Furthermore, it was reported that senescent cells upregulate ICAM-1 ([31] and our unpublished observation). Keratinocytes transduced with the cutaneous HPV-E6E7-expressing vectors were not or less efficiently immortalized than HPV16-E6E7-expressing keratinocytes and usually became senescent soon after transduction. A recent study detected a most pronounced upregulation of ICAM-1 by HPV5-E6E7-expressing cells and to a lower extent by HPV38-E6E7- and HPV16-E6E7-expressing cells.[32] In this study, the number of cell doublings or time after transduction of keratinocytes was not specified. Thus, it is possible that the experimental conditions and time of analysis after transduction were responsible for the different observations. Our results indicate that ICAM-1 upregulation in HPV5- and HPV8-E6E7-expressing cells did not correlate with decreased I-κBα expression and enhanced phosphorylation of p65 at Ser536 (Fig. 5*c*). These data suggest that additional mechanisms of ICAM-1 upregulation in cells expressing HPV-E6/E7 proteins exist.

The increased ICAM-1 expression in HPV16-E6E7-expressing cells led to enhanced conjugate formation with the NK cell line, NKL (Figs. 2*a*, and 2*b*). In addition, NKL cell-mediated killing of the HPV16$^+$ CxCa cell line CaSki was significantly reduced by addition of a blocking LFA-1 mAb (Fig. 2*e*). In the study of Huang *et al.*, increased ICAM-1 expression in HPV16-E6E7-immortalized human oral epithelial cells also correlated with enhanced adhesion to PBMCs and enhanced lymphokine-activated-killer cell cytotoxicity.[17] Thus, ICAM-1 expression on tumor cells might contribute to lymphocyte retention and activation in cervical carcinoma. In this context, it was shown that ICAM-1 expression in breast cancer correlated with a better prognosis and survival rates of patients.[33] In contrast, ICAM-1 expression in certain other cancer entities was associated with cancer progression. In melanoma and liver cancer patients, high ICAM-1 expression on tumor cells corresponded with an increased risk for metastasis.[34–36] So far, there are no reports describing the impact of ICAM-1 expression on prognosis of cervical cancer or its precursors. Thus, it is unclear whether induction of ICAM-1 expression by high-risk HPV types is beneficial for tumor immunosurveillance or supports tumor progression.

Our previous study revealed that activating NK cell receptor ligands, such as CD155 and MICA, are often up-regulated and inhibitory NK cell receptor ligands, like MHC class I, are frequently down-modulated in CxCa *in situ*.[19] In addition, here we demonstrate that ICAM-1 that is critical for conjugate formation of effector to target cells is induced by HPV16-E6E7 and high ICAM-1 expression was reported on CxCa *in situ*.[16] These data suggest that CxCa should be well recognized by NK cells. However, in cancer patients NK cells are frequently inactive due to multiple suppressive forces exerted by other immune cells or the tumor microenvironment. Strategies that lead to the efficient activation of NK cells might be promising for successful treatment of CxCa.

Acknowledgements

We would like to thank Dr. Massimo Tommasino for providing valuable reagents and advice. We thank Dr. Carsten Watzl for helping to establish the FACS-based conjugate formation assay and Dr. Angelika Bierhaus for helpful discussions concerning NF-κB signaling.

References

1. de Villiers EM, Fauquet C, Broker TR, Bernard HU, zur Hausen H. Classification of papillomaviruses. *Virology* 2004;324:17–27.
2. Walboomers JM, Jacobs MV, Manos MM, Bosch FX, Kummer JA, Shah KV, Snijders PJ, Peto J, Meijer CJ, Munoz N. Human papillomavirus is a necessary cause of invasive cervical cancer worldwide. *J Pathol* 1999;189:12–19.
3. Akgul B, Cooke JC, Storey A. HPV-associated skin disease. *J Pathol* 2006;208:165–75.
4. Scheffner M, Werness BA, Huibregtse JM, Levine AJ, Howley PM. The E6 oncoprotein encoded by human papillomavirus types 16 and 18 promotes the degradation of p53. *Cell* 1990;63:1129–36.
5. Dyson N, Howley PM, Munger K, Harlow E. The human papilloma virus-16 E7 oncoprotein is able to bind to the retinoblastoma gene product. *Science* 1989;243:934–7.

6. Munger K, Baldwin A, Edwards KM, Hayakawa H, Nguyen CL, Owens M, Grace M, Huh K. Mechanisms of human papillomavirus-induced oncogenesis. *J Virol* 2004;78:11451–60.
7. Cerwenka A, Lanier LL. Natural killer cells, viruses and cancer. *Nat Rev Immunol* 2001; 1:41–9.
8. Zompi S, Colucci F. Anatomy of a murder–signal transduction pathways leading to activation of natural killer cells. *Immunol Lett* 2005;97:31–9.
9. Lanier LL. NK cell recognition. *Annu Rev Immunol* 2005;23:225–74.
10. Patarroyo M, Prieto J, Rincon J, Timonen T, Lundberg C, Lindbom L, Asjo B, Gahmberg CG. Leukocyte-cell adhesion: a molecular process fundamental in leukocyte physiology. *Immunol Rev* 1990; 114:67–108.
11. Orange JS. Formation and function of the lytic NK-cell immunological synapse. *Nat Rev Immunol* 2008;8:713–25.
12. van de Stolpe A, van der Saag PT. Intercellular adhesion molecule-1. *J Mol Med* 1996;74:13–33.
13. Springer TA. Adhesion receptors of the immune system. *Nature* 1990;346:425–34.
14. Stratowa C, Audette M. Transcriptional regulation of the human intercellular adhesion molecule-1 gene: a short overview. *Immunobiology* 1995;193: 293–304.
15. Coleman N, Greenfield IM, Hare J, Kruger-Gray H, Chain BM, Stanley MA. Characterization and functional analysis of the expression of intercellular adhesion molecule-1 in human papillomavirus-related disease of cervical keratinocytes. *Am J Pathol* 1993;143:355–67.
16. Davidson B, Goldberg I, Kopolovic J. Inflammatory response in cervical intraepithelial neoplasia and squamous cell carcinoma of the uterine cervix. *Pathol Res Pract* 1997;193:491–5.
17. Huang GT, Zhang X, Park NH. Increased ICAM-1 expression in transformed human oral epithelial cells: molecular mechanism and functional role in peripheral blood mononuclear cell adhesion and lymphokine-activated-killer cell cytotoxicity. *Int J Oncol* 2000;17:479–86.
18. Robertson MJ, Cochran KJ, Cameron C, Le JM, Tantravahi R, Ritz J. Characterization of a cell line. NKL, derived from an aggressive human natural killer cell leukemia. *Exp Hematol* 1996;24:406–15.
19. Textor S, Durst M, Jansen L, Accardi R, Tommasino M, Trunk MJ, Porgador A, Watzl C, Gissmann L, Cerwenka A. Activating NK cell receptor ligands are differentially expressed during progression to cervical cancer. *Int J Cancer* 2008;123: 2343–53.
20. Jackson AM, Alexandroff AB, Lappin MB, Esuvaranathan K, James K, Chisholm GD. Control of leucocyte function-associated antigen-1-dependent cellular conjugation by divalent cations. *Immunology* 1994;81: 120–6.
21. Garcia-Penarrubia P, Lorenzo N, Galvez J, Campos A, Ferez X, Rubio G. Study of the physical meaning of the binding parameters involved in effector-target conjugation using monoclonal antibodies against adhesion molecules and cholera toxin. *Cell Immunol* 2002;215: 141–50.
22. Nees M, Geoghegan JM, Hyman T, Frank S, Miller L, Woodworth CD. Papillomavirus type 16 oncogenes downregulate expression of interferon-responsive genes and upregulate proliferation-associated and NF-kappaB-responsive genes in cervical keratinocytes. *J Virol* 2001;75:4283–96.
23. Ghosh S, Karin M. Missing pieces in the NF-kappaB puzzle. *Cell* 2002;109 Suppl: S81–S96.
24. Roebuck KA, Finnegan A. Regulation of intercellular adhesion molecule-1 (CD54) gene expression. *J Leukoc Biol* 1999;66: 876–88.
25. Bromley SK, Burack WR, Johnson KG, Somersalo K, Sims TN, Sumen C, Davis MM, Shaw AS, Allen PM, Dustin ML. The immunological synapse. *Annu Rev Immunol* 2001;19:375–96.
26. Nair A, Venkatraman M, Maliekal TT, Nair B, Karunagaran D. NF-kappaB is constitutively activated in high-grade squamous intraepithelial lesions and squamous cell carcinomas of the human uterine cervix. *Oncogene* 2003;22: 50–8.
27. Havard L, Delvenne P, Frare P, Boniver J, Giannini SL. Differential production of cytokines and activation of NF-kappaB in HPV-transformed keratinocytes. *Virology* 2002;298:271–85.
28. Havard L, Rahmouni S, Boniver J, Delvenne P. High levels of p105 (NFKB1) and p100 (NFKB2) proteins in HPV16-transformed keratinocytes: role of E6 and E7 oncoproteins. *Virology* 2005;331:357–66.
29. Spitkovsky D, Hehner SP, Hofmann TG, Moller A, Schmitz ML. The human papillomavirus oncoprotein E7 attenuates NF-kappa B activation by targeting the Ikappa B kinase complex. *J Biol Chem* 2002;277:25576–82.
30. Pfister H. Chapter 8: Human papillomavirus and skin cancer. *J Natl Cancer Inst Monogr* 2003:52–6.
31. Kletsas D, Pratsinis H, Mariatos G, Zacharatos P, Gorgoulis VG. The proinflammatory phenotype of senescent cells: the p53-mediated ICAM-1 expression. *Ann N Y Acad Sci* 2004;1019: 330–2.
32. De Andrea M, Mondini M, Azzimonti B, Dell'Oste V, Germano S, Gaudino G, Musso T, Landolfo S, Gariglio M. Alpha- and betapapillomavirus E6/E7 genes differentially modulate pro-inflammatory gene expression. *Virus Res* 2007;124: 220–5.
33. Ogawa Y, Hirakawa K, Nakata B, Fujihara T, Sawada T, Kato Y, Yoshikawa K, Sowa M. Expression of intercellular adhesion molecule-1 in invasive breast cancer reflects low growth potential, negative lymph node involvement, and good prognosis. *Clin Cancer Res* 1998;4: 31–6.
34. Johnson JP, Stade BG, Holzmann B, Schwable W, Riethmuller G. De novo expression of intercellular-adhesion molecule 1 in melanoma correlates with increased risk of metastasis. *Proc Natl Acad Sci USA* 1989;86:641–4.
35. Natali P, Nicotra MR, Cavaliere R, Bigotti A, Romano G, Temponi M, Ferrone S. Differential expression of intercellular adhesion molecule 1 in primary and metastatic melanoma lesions. *Cancer Res* 1990;50:1271–8.
36. Sun JJ, Zhou XD, Liu YK, Tang ZY, Feng JX, Zhou G, Xue Q, Chen J. Invasion and metastasis of liver cancer: expression of intercellular adhesion molecule 1. *J Cancer Res Clin Oncol* 1999;125:28–34.

THE JOURNAL OF BIOLOGICAL CHEMISTRY VOL. 286, NO. 22, pp. 19617–19629, June 3, 2011

PRR7 Is a Transmembrane Adaptor Protein Expressed in Activated T Cells Involved in Regulation of T Cell Receptor Signaling and Apoptosis*

Received for publication, August 13, 2010, and in revised form, March 20, 2011 Published, JBC Papers in Press, April 1, 2011, DOI 10.1074/jbc.M110.175117

Matouš Hrdinka[1], Peter Dráber[1], Ondřej Štěpánek[1], Tereza Ormsby[1], Pavel Otáhal, Pavla Angelisová, Tomáš Brdička, Jan Pačes, Václav Hořejší, and Karel Drbal[2]

From the Institute of Molecular Genetics, Academy of Sciences of the Czech Republic, Videnska 1083, 142 20 Prague 4, Czech Republic

Transmembrane adaptor proteins (TRAPs) are important organizers and regulators of immunoreceptor-mediated signaling. A bioinformatic search revealed several potential novel TRAPs, including a highly conserved protein, proline rich 7 (PRR7), previously described as a component of the PSD-95/*N*-methyl-D-aspartate receptor protein complex in postsynaptic densities (PSD) of rat neurons. Our data demonstrate that PRR7 is weakly expressed in other tissues but is readily up-regulated in activated human peripheral blood lymphocytes. Transient overexpression of PRR7 in Jurkat T cell line led to gradual apoptotic death dependent on the WW domain binding motif surrounding Tyr-166 in the intracellular part of PRR7. To circumvent the pro-apoptotic effect of PRR7, we generated Jurkat clones with inducible expression of PRR7 (J-iPRR7). In these cells acute induction of PRR7 expression had a dual effect. It resulted in up-regulation of the transcription factor c-Jun and the activation marker CD69 as well as enhanced production of IL-2 after phorbol 12-myristate 13-acetate (PMA) and ionomycin treatment. On the other hand, expression of PRR7 inhibited general tyrosine phosphorylation and calcium influx after T cell receptor cross-linking by antibodies. Moreover, we found PRR7 constitutively tyrosine-phosphorylated and associated with Src. Collectively, these data indicate that PRR7 is a potential regulator of signaling and apoptosis in activated T cells.

Activation of leukocytes through multichain immunoreceptors (TCR,[3] BCR, FcRs) involves a complex array of membrane-linked and cytoplasmic proteins, including transmembrane and cytoplasmic adaptor proteins (1). Several of the transmembrane adaptors (TRAPs) are associated with lipid rafts, namely LAT (2, 3), PAG (4, 5), NTAL (6, 7), and LIME (8, 9), whereas others (LAX, SIT, TRIM, GAPT) are present in non-raft membrane (10–13). All of these proteins are composed of a short N-terminal extracellular peptide, a single transmembrane segment, and a cytoplasmic part containing multiple tyrosine and other protein interaction motifs. In the case of the raft-associated proteins, a palmitoylation motif (*CXXC* or *CXC*) lies between the transmembrane segment and the intracellular part (14). TRAPs play positive and negative regulatory roles in immunoreceptor signaling. The most prominent role is played by LAT, which is essential for several aspects of TCR signaling and plays an important role in the immunoreceptor signaling in other leukocyte subsets (15). In addition, experiments on genetic models have assigned important regulatory functions to other members of TRAP family, including NTAL, LAX, TRIM, and SIT (16, 17).

In an effort to discover additional TRAPs of functional importance, we performed an *in silico* search for proteins possessing the features characteristic of known TRAPs. Among 149 candidate genes, one of the best hits was PRR7. Previously, PRR7 was identified in the PSD fraction of rat forebrain tissue by a proteomic approach (18). It was shown to associate with PSD-95 (via a PDZ domain binding motif) and was found in a protein complex containing the *N*-methyl-D-aspartate receptor subunits NR1 and NR2B. These biochemical data suggested that PRR7 could be potentially involved in modulation of neural activities.

In the present study we found that PRR7 is weakly expressed in many other tissues, including immune cells, and is up-regulated during T cell activation. Moreover, we show that PRR7 overexpression in Jurkat cells substantially affected TCR signaling and cell survival.

EXPERIMENTAL PROCEDURES

Bioinformatic Search—The *in silico* search in human genome (USCS build hg16) for proteins possessing the features characteristic of known TRAPs was done with following parameters: a short extracellular N-terminal sequence, a single hydrophobic sequence starting at amino acids (aa) 5–50 (prediction using TMHMM Version 2.0) (19), a palmitoylation motif at aa 20–60 (*CXC* or *CXXC*), tyrosine-based phosphorylation motifs (*YXX*(I/L/V/A)) and/or C-terminal Group I PDZ binding motifs ((S/T)*X*(L/V)).

* This work was supported in part by Academy of Sciences of the Czech Republic Project AV0Z50520514, GACR (Project MEM/09/E011), and by the Center of Molecular and Cellular Immunology (Project 1M0506, Ministry of Education, Youth, and Sports of the Czech Republic).

[1] Supported in part by the Faculty of Science, Charles University in Prague.

[2] To whom correspondence should be addressed: Videnska 1083, CZ-142 20 Prague 4, Czech Republic. Fax: 420-244472282; E-mail: drbal@img.cas.cz.

[3] The abbreviations used are: TCR, T cell receptor; aa, amino acid; Brij-98, polyoxyethylene 20 oleyl ether; J-iPRR7, Jurkat clones with PRR7-inducible expression; LM, lauryl maltoside (*n*-dodecyl-β-D-maltoside); PBL, peripheral blood lymphocytes; PSD, postsynaptic density; RSL1, RheoSwitch Ligand 1, diacylhydrazine [(*N*-(2-ethyl-3-methoxybenzoyl)-*N*′-(3,5-dimethylbenzoyl)-*N*′-*tert*-butylhydrazine]; SFK, Src family kinase; TRAP, transmembrane adaptor protein; PMA, phorbol 12-myristate 13-acetate; PHA, phytohemagglutinin; qPCR, quantitative PCR; Z-VAD-FMK, carbobenzoxy-valyl-alanyl-aspartyl-[*O*-methyl]-fluoromethylketone; PLC, phospholipase C.

RNA and RT-qPCR—RNA was isolated using a Mini RNA purification kit (Zymo Research, Orange, CA) or TRI Reagent RT (MRC, Cincinnati, OH). Contaminating DNA was removed using a DNAfree kit (Ambion, Austin, TX). A human normal tissue FirstChoice RNA Survey Panel and a lymph node FirstChoice Total RNA were purchased from Ambion. Human hippocampal RNA was purchased from BioChain Institute (Hayward, CA). Total RNA (1 μg) was transcribed using SuperScript III RT (Invitrogen) with a combination of random pentadecamer and anchored oligo$(dT)_{20}$ primers. RT-qPCR was performed using a LightCycler 480 SYBR Green I Master chemistry (Roche Applied Science) and an amount of cDNA equivalent to 20 ng of total RNA. Primers specific for human PRR7 were 5′-tgtccagtgaagcgtctgag-3′ (forward) and 5′-aagcacgtgaggaacgtgta-3′ (reverse). Raw RT-qPCR data (Ct values) were preprocessed (normalization to optimal reference genes, GAPDH or β-microglobulin, relative expression calculation) and analyzed using GenEx Software (MultiD, Göteborg, Sweden).

Northern Blotting—Total RNA was isolated from 1×10^7 cells using TRI Reagent RT. RNA was resolved (15 μg/sample) by formaldehyde-agarose gel electrophoresis, transferred to positively charged nylon membrane, and hybridized to radioactively ([α-^{32}P]dCTP)-labeled probe in Super Hyb solution (MRC). The probe was prepared from cloned PRR7 cDNA using DecaLabel DNA labeling kit (Fermentas, Ontario, Canada).

Cells and Media—Cell line MEG-01 was provided by S. Watson (University of Birmingham, Birmingham, UK), MOLT-4 and HPB-ALL were from the IMG cell line collection (Institute of Molecular Genetics, Prague, Czech Republic), and Caco-2, U937, and THP-1 were from DSMZ (Braunschweig, Germany). Jurkat, Ramos, and COS-7 cell lines were from ATCC (Manassas, VA), and HEK293FT cells were obtained from Invitrogen. Caco-2, HEK293FT, and COS-7 cells were cultured in DMEM supplemented with 10% FCS (Biochrom AG, Berlin, Germany) and antibiotics at 37 °C in 5% CO_2. All other cells were cultured in RPMI 1640 supplemented with 10% FCS and antibiotics at 37 °C in 5% CO_2. Human peripheral blood lymphocytes (PBL) were isolated from whole blood of healthy donors by Ficoll-Paque Plus (GE Healthcare) gradient centrifugation. For depletion of adherent cells, PBL were subjected to plastic adherence for 2 h at 37 °C. PBL were cultured as stated above for Jurkat cells.

DNA Constructs—The coding region of human PRR7 was amplified from human T cell line MOLT-4 cDNA and inserted into mammalian expression plasmid pEFIRES-P, provided by Dr. S. Hobbs (Institute of Cancer Research, London, UK) (20). For inducible expression, PRR7 was subcloned into the pZX-LR vector in-frame with the hemagglutinin (HA) tag. The pZX-LR vector was a kind gift of Dr. Claude Labrie (CHUL Research Center, Quebec, Canada) (21). Deletion mutants of PRR7 (Δ2–39, Δ44–274, Δ114–274, Δ151–274, Δ159–274, Δ171–274, Δ207–274, ΔTAV) were generated by PCR and fused to enhanced green fluorescent protein (EGFP) in the pEGFP vector (Clontech, Palo Alto, CA). A tyrosine mutant of PRR7 (all Tyr residues mutated to Phe) was generated by sequential PCR oligonucleotide-directed site-specific mutagenesis and subcloned into the pEGFP vector (Clontech). For co-transfection experiments in COS-7 cells, the following cDNA constructs were used: Src in the pSM vector provided by Dr. A. Weiss (University of California, San Francisco, CA), FLAG-tagged Lck inserted into the pcDNA3 vector provided by Dr. R. Abraham (Mayo Clinic, Rochester, MN), FynT and FynF (constitutively active Fyn) in the pEF-BOS vector provided by Dr. B. Schraven (Otto-von-Guericke-University, Magdeburg, Germany), Yes in the pSG5 vector provided by Dr. C. Benistant (CRBM, CNRS, Universities of Montpellier I and II, France), Myc-tagged Lyn in the pcDNA3.1 vector provided by Dr. S. Watson (University of Birmingham, Birmingham, UK), FLAG-tagged Hck in the pcDNA1 vector provided by Dr. G. Langsley (Institut Pasteur, Paris, France).

Antibodies—Hybridomas producing monoclonal antibodies (mAbs, TRAP-3/01–13) to human PRR7 were prepared by standard hybridoma techniques using mice immunized with the recombinant protein corresponding to aa 147–274. Using the deletion mutants, the epitope recognized by the mAbs was mapped to the stretch of aa 147–170. The mAbs were cross-reactive with murine and rat PRR7 in immunoblots (not shown). The phosphotyrosine antibody (P-TYR-02) used for detection of phospho-LAT in Jurkat whole cell lysates was developed in our laboratory as well. For cell stimulation, the following non-commercial antibodies were used: C305 IgM mAb to Jurkat cell TCR provided by Dr. A. Weiss and 248.23.2 IgM mAb to CD28 (22). Antibodies to the following antigens were obtained from the indicated commercial sources: LAT (LAT-01), PAG (MEM-255), CD3 (MEM-57), CD5 (MEM-32), Lck (LCK-01), ZAP-70 (ZAP-03), CD69 (FN50, Alexa Fluor 647), tubulin (TU-01), and LAMP-1 (CD107a, B-T47) from Exbio (Vestec, Czech Republic); GAPDH from Sigma; Src (N-16), c-Jun (N), ERK2 (C-14), TCRζ (6B10.2) from Santa Cruz Biotechnology (Santa Cruz, CA); IL-2 (MQ1–17H12, APC) from eBioscience (San Diego, CA); phosphotyrosine (4G10) from Upstate Biotechnology (Lake Placid, NY); HA tag (6E2), pZAP-70 Tyr-319, pPLCγ1 Tyr-783, PLCγ1, pp42/44 ERK1/2 (Thr-202/Tyr-204), pp38 MAPK (T180/Y182), p38 MAPK, pJNK (T183/Y185), JNK, pc-Jun (Ser-63/Ser-73), pSFK (Y416), and pLck (Y505) from Cell Signaling Technology (Beverly, MA).

Inhibitors and Inhibitor Assay—The following inhibitors were used: the inhibitor of the Src family kinases, PP2 (Calbiochem), final concentration 10 μM and the pan-caspase inhibitor, Z-VAD-FMK (Alexis Biochemicals), final concentration 10 μM. Z-VAD-FMK inhibitor assay was performed using 2.5×10^5 cells in 96-well tissue culture plates in triplicates. Viability was assessed by flow cytometry (propidium iodide exclusion and side plus forward scatter gating).

Transfections and Inducible Expression—Jurkat cells (10^7) were transfected with 15 μg of the corresponding plasmid DNA in 300 μl of RPMI medium supplemented with 10% FCS by electroporation (250 V, 950 microfarads) using a GenePulser electroporator (Bio-Rad). For the pZRD-inducible system (21), based on the RheoSwitch Mammalian Inducible Expression System (New England Biolabs, Ipswich, MA), transfectants were selected in the culture medium containing Zeocin (200 μg/ml, Invitrogen). Stably transfected GFP-positive cells were

sorted and further subcloned by limiting dilution. The clones (denoted J-iPRR7) that expressed PRR7 only after induction with RSL1 (500 nM for maximal induction, RheoSwitch Ligand 1, New England Biolabs) were used in further experiments. COS-7 cells were transfected using Lipofectamine 2000 (Invitrogen) according to the manufacturer's instructions.

Cell Stimulation—To analyze PRR7 up-regulation, freshly isolated PBL were stimulated using 1) anti-CD3 IgG (MEM-57) immobilized on tissue culture plastic (10 μg/ml) and soluble anti-CD28 IgM (100× diluted hybridoma supernatant), 2) PHA-L (2.5 μg/ml, Sigma), and 3) a combination of PMA (10 ng/ml, Sigma) and ionomycin (500 ng/ml, Sigma).

For short term activation (Ca^{2+} flux, phospho-Tyr blots), Jurkat cells were stimulated with anti-TCR IgM (C305) (23) (10 μg/ml) at 37 °C for 2 min. For activation of Jurkat cells in an IL-2 production assay, the combination of PMA and ionomycin was used as described above.

Preparation of Cell Lysates, Immunoprecipitations, Biochemical Methods—Generally, 5×10^7 cells were lysed in 1 ml of lysis buffer (20 mM Tris pH 7.5, 100 mM NaCl, 5 mM iodoacetamide, 10 mM EDTA, 50 mM NaF, 10 mM $Na_4P_2O_7$, 10% v/v glycerol, and Protease Inhibitor Mixture III, Calbiochem) containing 1% w/v detergent LM (Calbiochem) or Brij-98 (Sigma) for 30 min on ice. To remove nuclei and other insoluble materials, the lysate was spun down at 16,000 × *g* for 10 min at 4 °C. Density gradient ultracentrifugation and gel filtration on Sepharose 4B were performed as previously described (24). For immunoprecipitation experiments, we coupled the anti-PRR7 IgG (TRAP3-03) to CNBr-Sepharose 4B (Amersham Biosciences) or used soluble antibodies and Protein A/G PLUS-agarose IP Reagent (Santa Cruz). Palmitoylation of PRR7 was examined using the acyl-biotinyl exchange chemistry-based method (25). Briefly, plasma membranes from 5×10^7 cells were isolated, and palmitate protein modifications were removed by hydroxylamine and replaced with biotin. Biotinylated proteins were then immunoprecipitated on streptavidin-agarose beads. Other biochemical methods (SDS-PAGE, immunoblotting) were performed essentially as described before (4).

Microscopy—Jurkat cells were allowed to adhere to polylysine-coated coverslips for 30 min, then fixed with 4% w/v formaldehyde for 15 min at room temperature and permeabilized with 0.1% Triton X-100 (Sigma) for 5 min. Blocking was performed in 2.5% BSA and 10% goat serum (Sigma) in PBS for 30 min. Cells were then incubated with 100×-diluted LAMP-1 antibody followed by 750×-diluted Alexa 647-labeled goat anti-mouse IgG secondary antibody (Molecular Probes, Invitrogen). The DNA dye, Hoechst 33258 (1 μg/ml, Invitrogen), was used to visualize nuclei. Images were captured with a Leica SP5 confocal microscope and a 63× objective lens (Leica Microsystems, Mannheim, Germany).

Flow Cytometry—CD69 surface staining and intracellular IL-2 staining were done according to the standard protocols. To measure apoptosis in cells expressing PRR7, we performed annexin V/Dy-647 (Apronex Biotechnologies, Vestec, Czech Republic) staining in combination with the DNA dye, Hoechst 33258, according to the manufacturer's instructions. To measure calcium response to anti-TCR activation, cells were first loaded with 5 μM Fura Red (Molecular Probes, Invitrogen) in loading buffer (1 × Hanks' balanced salt solution, 2% FCS, without Ca^{2+} or Mg^{2+}) for 30 min at 37 °C. After washing, cells were resuspended in loading buffer supplemented with Ca^{2+} and Mg^{2+} and kept on ice. Cells were warmed up for 10 min at 37 °C and then stimulated with an irrelevant control antibody or the anti-TCR C305 mAb (10 μg/ml). Calcium flux was monitored for 240 s. Flow cytometry was carried out on an LSRII instrument (BD Biosciences), and cells were sorted on FACSVantage (BD Biosciences). Analysis of the data was performed using FlowJo software (Tree Star, Ashland, OR) as specified in the figure legends (Figs. 6 and 8).

RESULTS

PRR7 Sequence Analysis—Human PRR7 (18) is a 274-aa protein with a sequence typical for TRAPs. It has a short N-terminal extracellular peptide, a single transmembrane segment, and a cytoplasmic part containing several conserved binding motifs (Fig. 1*A*). These motifs include multiple SH2 domain binding and/or endocytic tyrosine-based motifs (Y*XX*(I/L/V/A)), multiple proline-rich SH3 binding motifs (P*XX*P), group I WW domain binding motifs (PP*X*Y), and a C-terminal class I PDZ domain binding motif (TTAV). In addition, PRR7 contains a potential submembrane palmitoylation motif (CC*X*C, Fig. 1*A*).

PRR7 is a highly conserved protein. The percentage of aa identity is more than 94% among available sequences from placental mammals, and a substantial level of aa identity is observed even if lower vertebrate species (amphibian, fish) are included (Table 1). The highest degree of conservation of PRR7 protein sequence was observed in the extracellular, transmembrane, and submembrane parts, including the palmitoylation motif. In addition, the region containing three tyrosine residues, Tyr-153, Tyr-166, and Tyr-177, and the C terminus with the PDZ domain binding motif also displayed a very high degree of homology (Fig. 1*B*). Interestingly, N-terminal part of PRR7 as well as sequences surrounding tyrosines 153 and 166 form a putative domain identified in Pfam data base (26) as the WBP-1 domain (PF11669). Among other proteins, this domain is present in WW domain-binding protein 1 (WBP-1) where it mediates the interaction with WW domains of Yes-associated protein (YAP) via tandem PP*X*Y motifs in its C terminus (27). Similar motifs encompass tyrosines 153 and 166 in PRR7, suggesting possible involvement of this region in an interaction with a WW domain containing protein (Fig. 1*C*).

PRR7 Expression Profile—To determine the PRR7 expression pattern in human tissues, we performed RT-qPCR on a panel of multiple tissue RNAs. As shown in Fig. 2*A*, PRR7 mRNA is expressed most strongly in brain tissue and moderately in several other tissues: esophagus, trachea, lung, ovary, cervix, prostate, testes, thyroid, including the immune organs thymus and lymph nodes. We also found low levels of PRR7 mRNA in a number of human cell lines (Jurkat, U937, THP-1, MEG-01, CaCo2, HEK293FT); the only cell line exhibiting relatively high expression was T cell line MOLT-4 (Fig. 2*B*). We next analyzed whether the expression level of PRR7 mRNA in PBL changes after activation. Interestingly, we observed rapid up-regulation of PRR7 mRNA in PHA-stimulated PBL. It was detectable at 1 h and peaked at 8 h after stimulation (Fig. 2*C*).

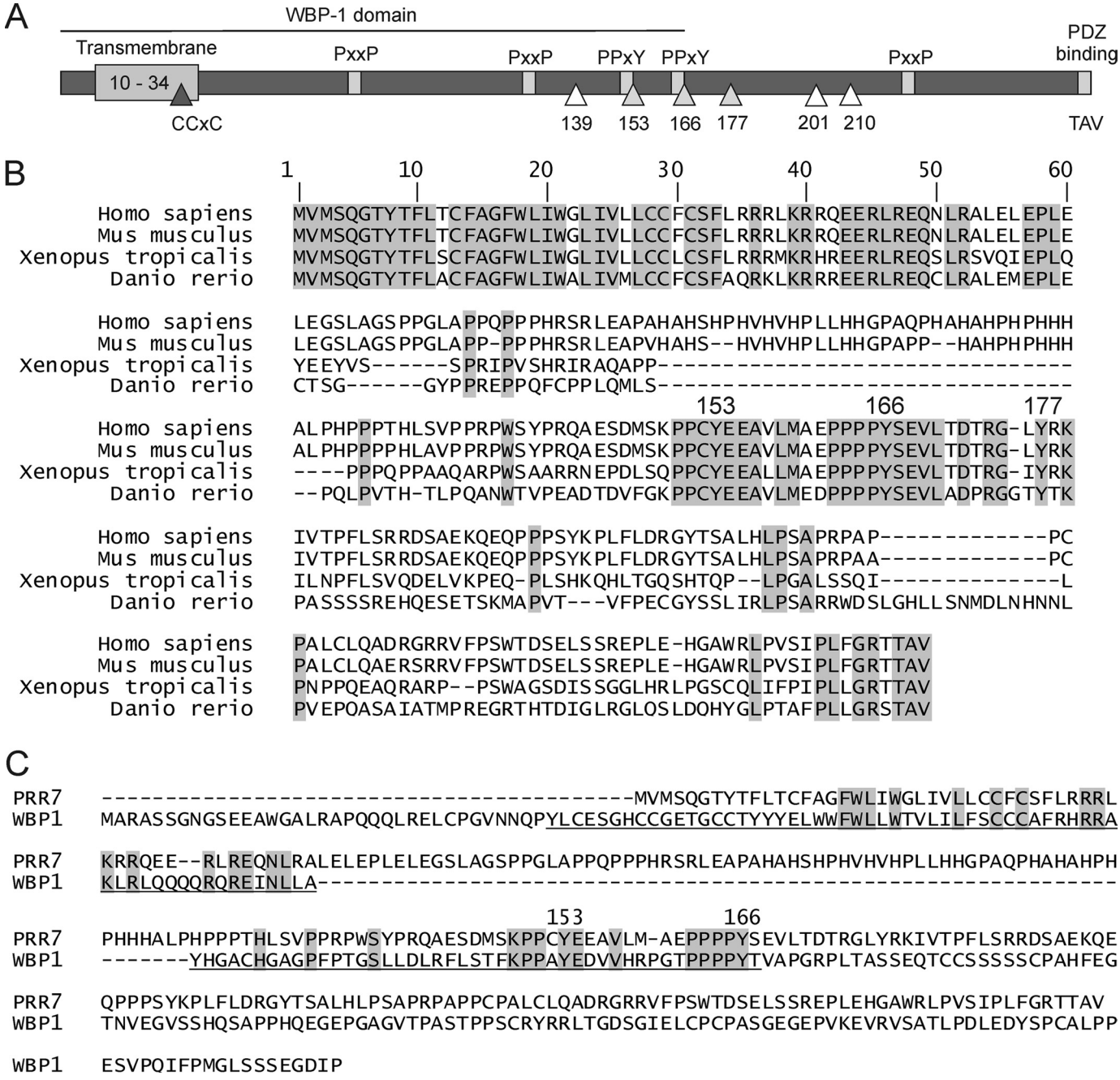

FIGURE 1. **Human PRR7 protein scheme and conservation.** *A*, PRR7 features a short extracellular part (predicted aa 1–9) followed by a single transmembrane segment (predicted aa 10–34), a submembrane palmitoylation motif CC*X*C (aa 28–31), six intracellular tyrosine residues (*gray triangles* for fully conserved residues, *white triangles* for less conserved residues), multiple SH3 domain binding proline-rich motifs (P*XX*P, only conserved motifs are shown, aa 74–77, 123–126, 222–225), group I WW domain binding motifs (PP*XY*, only conserved motifs shown, aa 150–153, 163–166), and a C-terminal PDZ-binding motif (TTAV, aa 271–274). The N-terminal part of PRR7 (aa 1–167) corresponds to the predicted WBP-1 domain as indicated. This scheme is based on GenBank™ protein sequence NP_085044. *B*, shown is alignment of PRR7 protein sequences from four vertebrate species: *Homo sapiens* (human), *Mus musculus* (mouse), *Xenopus tropicalis* (frog), and *Danio rerio* (zebrafish). The sequences were aligned using ClustalW program from the EMBL-EBI website. Absolutely conserved residues are shaded in *gray*. Tyrosine residues conserved in all vertebrates (Tyr-153, Tyr-166, Tyr-177 in humans) are numbered *above the alignment*. *C*, a comparison of human PRR7 and WBP-1 protein sequences is shown. The sequence corresponding to the predicted WBP-1 domain is *underlined*. Identical residues are *shaded in gray*. Two conserved tyrosine residues (Tyr-153 and Tyr-166 in human PRR7) in the predicted WW domain binding motifs are indicated *above the sequences*.

To examine the expression of PRR7 at the protein level, we generated anti-human PRR7 monoclonal antibodies. Unfortunately, none of the generated antibodies could clearly detect PRR7 after immunoblotting of whole primary cell lysates (except for mouse or rat brain tissues; not shown). Moreover, native PRR7 could not be quantitatively immunoprecipitated from cell lysates using these antibodies, suggesting partial blocking of the epitope (not shown). Nevertheless, it was still possible to use immunoprecipitation to concentrate PRR7 protein to the degree sufficient for detection by immunoblotting also in leukocytes. We then used this approach to verify our results from previous experiments. As shown in Fig. 2*D*, PRR7 protein was detected in PBL activated by various stimuli, including activation with anti-CD3 and anti-CD28 antibodies,

TABLE 1

Conservation of PRR7 protein in vertebrates

Orthologous protein sequences were aligned and compared to human PRR7 using ClustalW program. Species in this table are sorted according to the calculated protein identity with human PRR7.

Species	Length	Identity
	aa	*%*
Pongo pygmaeus (*orangutan*)	273	99
Pan troglodytes (*chimpanzee*)	259	98
Macaca mulatta (*macaque*)	276	98
Rattus norvegicus (*rat*)	269	98
M. musculus (*mouse*)	269	97
Spermophilus tridecemlineatus (*squirrel*)	269	97
Canis familiaris (*dog*)	272	97
Bos taurus (*cattle*)	269	97
Echinops telfairi (*tenrec*)	270	95
Sus scrofa (*pig*)	269	94
Monodelphis domestica (*opossum*)	280	81
X. tropicalis (*frog*)	227	56
D. rerio (*fish*)	246	48
Gasterosteus aculeatus (*fish*)	279	44

PHA, or PMA and ionomycin. We could also detect PRR7 protein in several lymphoid cell lines, including Jurkat, Ramos, and MOLT-4 (Fig. 2*E*). The highest protein levels were observed in MOLT-4, which correlated well with the higher PRR7 mRNA level in this cell line (Fig. 2, *B* and *E*).

Overexpression of PRR7 Results in Apoptosis in the Jurkat T Cell Line—Because the level of PRR7 expression in leukocytes (cell lines and primary PBL) was low and its direct immunoprecipitation was inefficient, we generated multiple Jurkat cell lines transfected with PRR7 constructs containing a C-terminal GFP tag. Surprisingly, we were not able to establish a Jurkat cell line with a sufficiently high expression of PRR7. Direct observation of the PRR7-GFP-transfected Jurkat cells excluded a rapid necrotic cell death of the transfectants. Instead, we consistently observed a gradual loss of the PRR7 transfectants from the culture within a few days (not shown). PRR7^{high} cells were stained with the DNA dye, propidium iodide, and analysis of the staining suggested that overexpression of PRR7 protein caused apoptosis (not shown). To exclude the possibility that the apoptosis induction is at least in part the result of the stress caused by the transfection procedure (electroporation), we generated a stable Jurkat clone (J-iPRR7) inducibly expressing full-length HA-tagged PRR7. In this case a modified RheoSwitch Mammalian Inducible Expression System (21) was utilized. It allowed us to tightly regulate the expression of PRR7 using the synthetic compound RSL1. Without RSL1, PRR7 expression was not detectable; maximal expression was achieved in the presence of RSL1 12 h after induction (Fig. 3*A*). Strikingly, we observed that in J-iPRR7 cells, apoptosis could be clearly detected within 24 h of induction by RSL1 and gradually increased with time (Fig. 3, *B* and *C*), suggesting that apoptosis induction was a direct consequence of PRR7 expression. This process could be to a substantial degree inhibited by caspase inhibitor Z-VAD, demonstrating the involvement of caspase-dependent apoptotic pathways (Fig. 3*D*).

Region Surrounding Tyr-166 Is Critical for Apoptosis Induction—To identify the regions of the PRR7 molecule involved in the apoptosis induction, we generated a set of Jurkat cell lines transiently expressing either full-length PRR7-GFP or its mutants gradually truncated from the C terminus (Fig. 3*E*). We also generated a mutant where all the tyrosines in the PRR7 sequence were mutated to phenylalanines (all Y to F) and a mutant lacking the N terminus, including extracellular peptide, transmembrane segment, and the palmitoylation motif (Δ2–39-PRR7-GFP). As expected, expression of the full-length PRR7 resulted in a high degree of apoptosis in Jurkat cells (Fig. 3*F*). Similar results were obtained when aa downstream of Thr-171 were removed, suggesting that the C-terminal region, including the highly conserved Tyr-177 and the PDZ binding motif, are dispensable for apoptosis induction. In contrast, when 12 more aa were removed (Δ159–274-PRR7-GFP), a significant drop in the percentage of apoptotic cells was observed, and only a very mild additional reduction was noticed after further shortening of PRR7 protein by 8 or more aa (Δ151–274-PRR7-GFP) (Fig. 3*F* and not shown). These data suggested that the region critical for the apoptosis induction is located between aa 159 and 171 of PRR7. Importantly, the tyrosine mutant of PRR7 (all Y to F) also induced only a mild level of apoptosis under the same conditions, indicating that one or more tyrosine residues are involved. The only tyrosine in the critical region identified by the deletion mutants is the highly conserved Tyr-166. Thus, our observations suggest that a tyrosine-based motif surrounding this Tyr-166 is essential for the induction of apoptosis by PRR7, although the involvement of other tyrosine residues cannot be completely excluded by this type of analysis.

Finally, the mutant lacking extracellular and transmembrane parts induced the highest level of apoptosis in Jurkat transfectants (Fig. 3*F*). This finding was surprising as we rather expected a loss of function when removing the membrane localization sequences.

Intracellular Localization of PRR7 Mutants Partially Correlates with Apoptosis Induction—Strong pro-apoptotic effects of the construct lacking putative membrane anchoring sequences prompted us to analyze subcellular localization of PRR7 and its mutants. Full-length PRR7 was localized at the plasma membrane and to large vesicular perinuclear structures, which did not co-localize with an early endosomal marker transferrin (not shown) nor with lysosomal marker LAMP-1 (CD107a, Fig. 4, *A* and *B*). The C-terminal tag modifications had no effect on this localization pattern as tagged versions of PRR7 (PRR7-GFP, PRR7-HA) were indistinguishable from non-tagged PRR7 (Fig. 4*A*), suggesting that the C-terminal PDZ binding motif requiring a free carboxyl group at the C terminus for binding (28) is not involved in this process.

Time course analysis of PRR7 in the inducible system revealed that shortly after expression induction by RSL1, PRR7 was found mainly at the plasma membrane and later gradually accumulated in the perinuclear compartment. After RSL1 withdrawal, the plasma membrane staining was lost, and PRR7 could be detected only in the perinuclear cytoplasmic vesicles (Fig. 4*C*). These data suggest a continuous active process of PRR7 removal from the plasma membrane by endocytosis.

We next analyzed PRR7 deletion mutants. C-terminal deletions up to aa 171 (Δ207–274, Δ171–274-PRR7-GFP) did not have any effect on PRR7 localization. However, further shortening of the cytoplasmic part of PRR7 up to aa 159 and 151 (Δ159–274, Δ151–274-PRR7-GFP) resulted in gradual loss of vesicular accumulation and a shift to an almost exclusive sur-

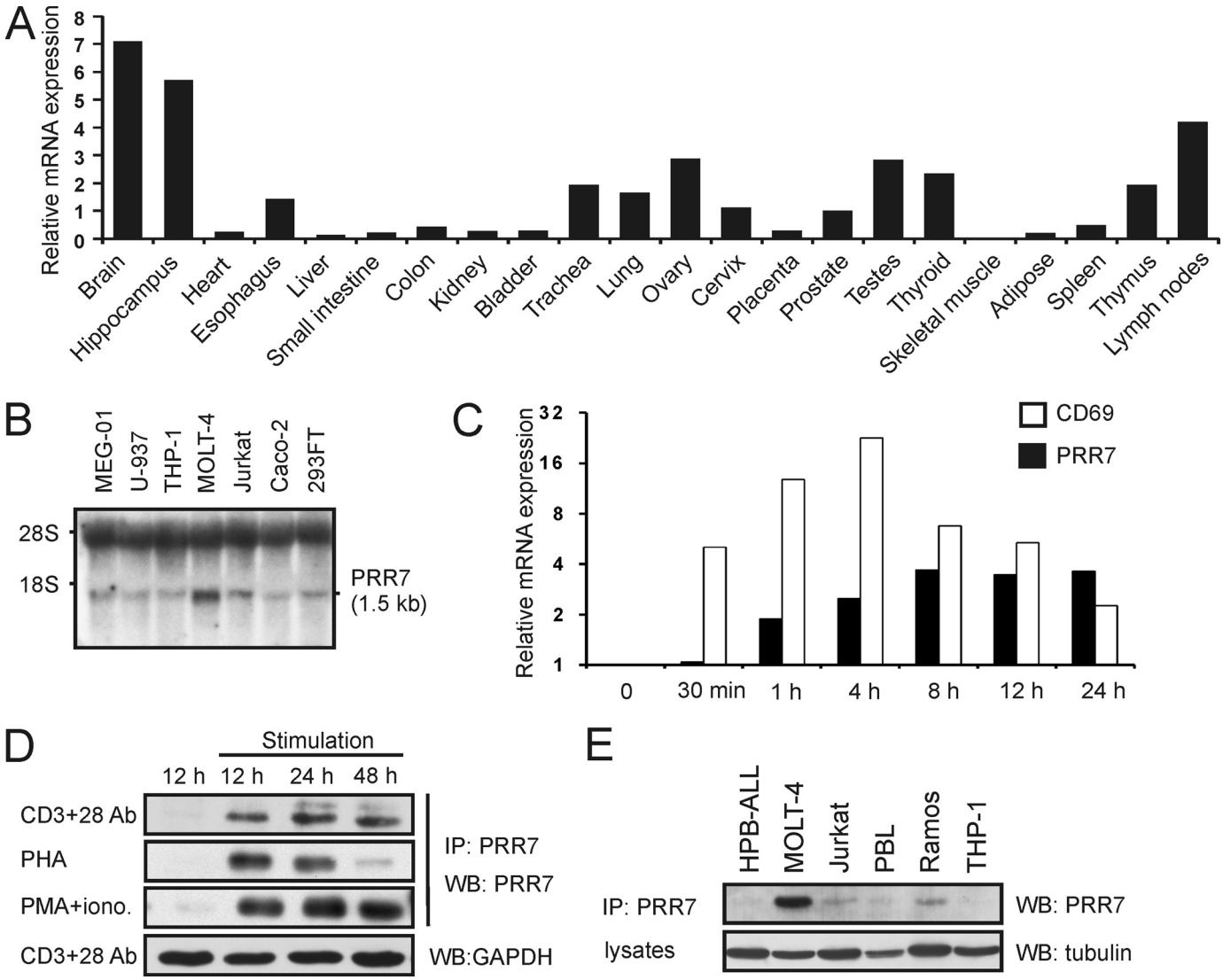

FIGURE 2. **Expression of PRR7 in primary human cells and tissues.** *A*, shown is RT-qPCR analysis of PRR7 mRNA expression in normal human tissues. PCR reactions were done in triplicate, and mean Ct values were used for further data processing in GenEx software. First, data were normalized to GAPDH mRNA expression, and then relative expression values were calculated. An average expression in all tissues corresponds to value 1 on the vertical axis. *B*, Northern blot analysis of PRR7 mRNA in human cell lines is shown. Total RNA (15 μg) was resolved on 1% agarose gel and, after transfer to nylon membrane, probed for PRR7 mRNA. The positions of ribosomal RNA bands 18 S and 28 S are indicated. *C*, shown is an RT-qPCR analysis of kinetics of PRR7 mRNA up-regulation in human PBL after PHA treatment. PCR reactions were done in triplicate, and mean Ct values were used for further data processing in GenEx software. Data were normalized to the optimal reference gene, β2-microglobulin, and relative expression values were calculated. Value 1 on the *vertical axis* corresponds to basal PRR7 mRNA expression in unstimulated PBL. Expression of the activation marker CD69 was used as a positive control. *D*, human PBL were stimulated with plate-bound anti-CD3 IgG and soluble anti-CD28 IgM, PHA, or PMA and ionomycin. Cell lysates were concentrated by immunoprecipitation (*IP*) with the anti-PRR7 mAb (TRAP3-03). Expression of PRR7 was analyzed by immunoblotting (*WB*) using the anti-PRR7 mAb (TRAP3-10). In addition, equivalence of sample sizes was verified via staining of lysates for GAPDH. A representative result for each type of stimulation is provided. *E*, PRR7 was immunoprecipitated from lysates of human cell lines with the anti-PRR7-Sepharose. Expression of PRR7 was analyzed by immunoblotting using the anti-PRR7 mAb. The equivalence of sample sizes was verified via staining of lysates with the anti-tubulin mAb.

face localization (Fig. 4*B*). Additional shortening of PRR7 sequence did not have any further effect on the subcellular localization of this protein (not shown). These results suggest that the region critical for internalization of PRR7 is positioned between aa 151 and 171. Strikingly, this region partially overlaps with the sequence responsible for the apoptosis induction (159–171), suggesting a link between PRR7 internalization and apoptosis. In agreement with this, the PRR7 N-terminal deletion mutant, which caused the highest level of apoptosis (Δ2–39-PRR7-GFP), was localized exclusively in the intracellular vesicular compartment (Fig. 4*B*). The region found to be critical for PRR7 internalization contains two highly conserved tyrosine motifs, suggesting that they may serve as tyrosine-based internalization motifs. However, the all Y to F mutant of PRR7 showed only a mild reduction in the size of intracellular PRR7 compartment (not shown), displaying at the same time strong defects in the apoptosis induction. These results indicated that tyrosines within the critical conserved region are not a part of the tyrosine-based internalization sequences, but rather, they are involved in pro-apoptotic signaling mediated by PRR7. Importantly, these tyrosines form the putative WW domain binding motif of the PRR7 WBP-1 domain, suggesting possible involvement of a WW-containing protein in this process.

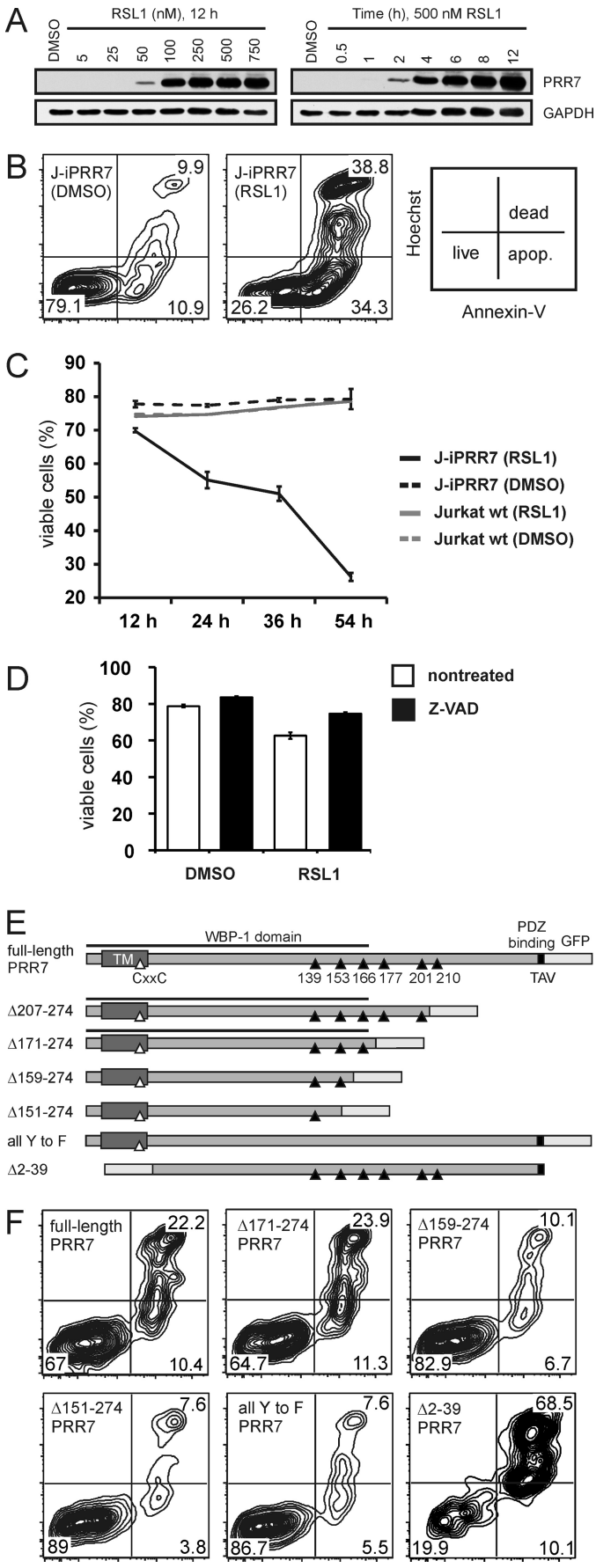

PRR7 Partitions to Large Detergent-resistant Complexes—Similarity to palmitoylated lipid raft-associated TRAPs suggested that PRR7 may employ lipid rafts as signaling platforms. Indeed, we found PRR7 to be palmitoylated in the J-iPRR7 cells (Fig. 5*A*). However, in contrast to these adaptors, PRR7 was found in a different type of detergent (Brij-98)-resistant complexes. These were large (as determined by gel filtration on Sepharose 4B) but almost non-buoyant (as determined by density gradient ultracentrifugation) and resistant to lipid raft-disrupting detergent laurylmaltoside (Fig. 5, *B* and *C*).

Variable Effects of PRR7 on the Activity of Signaling Pathways in J-iPRR7—To elucidate how PRR7 affects T cell signaling pathways, we compared the phenotype of induced *versus* non-induced J-iPRR7 cells. Induction of PRR7 expression led to a mild spontaneous up-regulation of the activation marker CD69 in quiescent cells (Fig. 6*A*). Moreover, treatment of induced J-iPRR7 with PMA and ionomycin resulted in a substantial increase in IL-2 production (Fig. 6*B*), suggesting that these cells are in a partially activated state. In contrast, at the same time, the induced J-iPRR7 cells exhibited an attenuated calcium response (Fig. 6*C*) and reduced global tyrosine phosphorylation (Fig. 6*D*) after TCR stimulation.

Interestingly, we detected strong constitutive tyrosine phosphorylation of PRR7, which was not altered by TCR cross-linking (Fig. 6, *D* and *E*). This observation raised questions about the mechanisms mediating PRR7 phosphorylation and the role of tyrosine phosphorylation in the diverse effects of PRR7 on T cell signaling pathways.

To elucidate the mechanisms of PRR7 phosphorylation, we analyzed lysates of J-iPRR7 cells treated with a specific inhibitor of Src-family kinases (SFK) PP2 by phosphotyrosine immunoblotting. As shown in Fig. 7*A*, PRR7 phosphorylation was almost completely inhibited in the presence of PP2, suggesting that PRR7 is constitutively phosphorylated by SFKs. To identify potential SFKs capable of PRR7 phosphorylation, constructs encoding PRR7 and various tyrosine kinases were co-transfected into COS-7 cells. The results revealed that several SFKs (most strongly Src) are able to phosphorylate PRR7 (Fig. 7*B*). The multiple predicted SH3 domain binding motifs in the intracellular part of PRR7 using iSPOT (29) indicated a possible

FIGURE 3. **PRR7-inducible system and induction of apoptosis by overexpression of PRR7 in Jurkat cells.** *A*, to determine the optimal concentration of RSL1 for PRR7 induction, J-iPRR7 cells were treated with an increasing amount of RSL1 for 12 h (*left panel*). J-iPRR7 cells were treated with 500 nM RSL1, and expression of PRR7 in several time intervals was analyzed by immunoblotting with the anti-PRR7 mAb (TRAP3-10, *right panel*). Staining for GAPDH was used as a sample loading control. *B*, J-iPRR7 cells were induced to express PRR7 or left uninduced (DMSO control). After 54 h, apoptosis in both cultures was determined by annexin V and Hoechst 33258 staining. *C*, J-iPRR7 and Jurkat wt cells were treated with 500 nM RSL1 to induce PRR7 expression or left untreated (DMSO control). Cell viability was determined by flow cytometry after 12, 24, 36, and 54 h. Data are presented as the mean of three experiments (±S.D.). *D*, J-iPRR7 cells were induced to express PRR7 or left uninduced (DMSO control) for 24 h in the presence of the pan-caspase inhibitor, Z-VAD-FMK (10 μM). The percentage of viable cells was determined by propidium iodide (*PI*) staining and flow cytometry. The experiment was done in triplicate cultures, and data are represented as the mean values ± S.D. *E*, shown is a scheme of PRR7-GFP mutants used in this study. Tyrosine residues are represented by *black triangles*. *F*, Jurkat cells were transfected with corresponding plasmid DNA coding for wt or mutated PRR7 fused to GFP. After 48 h, cells were stained with annexin V/Dy647 and Hoechst 33258 to analyze apoptosis in the GFP-positive cells.

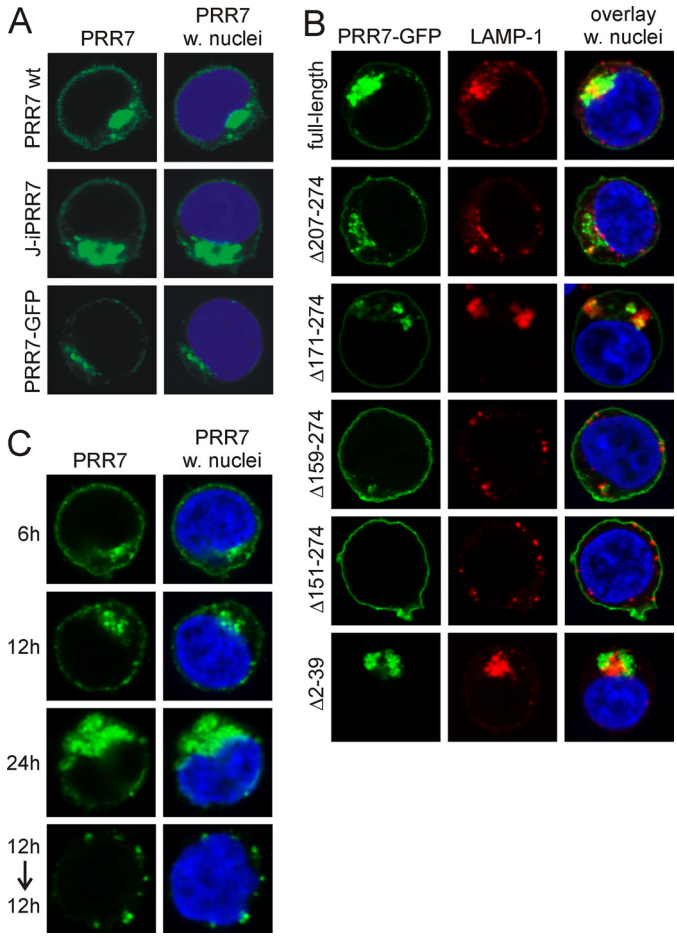

FIGURE 4. **Subcellular localization of full-length PRR7 and deletion mutants in Jurkat cells.** *A*, shown is a comparison of subcellular localization of PRR7 protein with (*w.*) and without tags. Jurkat cells expressing the PRR7 wt protein (without a tag) were fixed 18 h post-transfection and stained with PRR7 antibody. J-iPRR7 (PRR7 with HA-tag) cells were induced for 18 h to express PRR7 with 500 nM RSL1, fixed, and stained with the anti-HA-tag mAb. Jurkat PRR7-GFP transfectants were fixed 18 h post-transfection. Samples were analyzed by confocal microscopy. *B*, cells were transfected with corresponding plasmid DNA, and after 18 h cells were allowed to adhere to poly-lysine-coated coverslips, fixed, stained for lysosomal marker LAMP-1 (CD107a) and DNA dye Hoechst 33258, and analyzed by confocal microscopy. *C*, J-iPRR7 cells were induced to express PRR7 with 500 nM RSL1. Cells were fixed 6, 12, and 24 h afterward or induced for 12 h, washed, and incubated an additional 12 h in fresh medium without RSL1 before fixation. All samples were stained with the anti-HA-tag mAb and DNA dye Hoechst 33258 and analyzed by confocal microscopy.

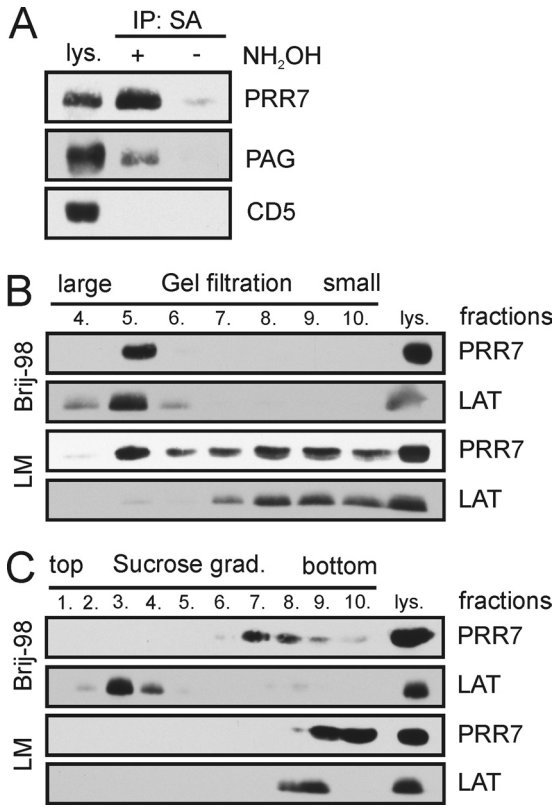

FIGURE 5. **Biochemical characterization of the PRR7 protein.** J-iPRR7 cells were induced to express PRR7 (16 h) and subjected to several biochemical assays. *A*, palmitoylation of PRR7 was examined using the acyl-biotinyl exchange chemistry-based method as described under "Experimental Procedures." A palmitoylated transmembrane adaptor protein, PAG, was used as a positive control; a non-palmitoylated transmembrane protein, CD5, and lysate that was not treated with NH_2OH (hydroxylamine) were used as negative controls. IP, immunoprecipitate. *SA*, streptavidin beads. *B*, Brij-98 or LM lysates of J-iPRR7 cells were subjected to gel filtration on Sepharose 4B, and the separated fractions were analyzed by immunoblotting. A raft-associated transmembrane adaptor protein, LAT, was used as a control. *C*, Brij-98 or LM lysates of J-iPRR7 cells were subjected to density gradient ultracentrifugation, and the separated fractions were analyzed by immunoblotting. The fractions are numbered from the *top*. *10* represents the sediment. The lipid raft protein, LAT, was used as control.

association of PRR7 with SFKs (via their SH3 domains). Thus we immunoprecipitated PRR7 from the induced J-iPRR7 cells and tested the immunoprecipitates for the presence of associated SFKs by immunoblotting. Among the tested SFKs (Src, Lck, Fyn), the only identified binding partner was Src (Fig. 7*C* and not shown).

Mechanisms of PRR7-dependent Regulation of J-iPRR7 Signaling—So far, our observations suggested that PRR7 expression had a dual activating/inhibitory effect. It resulted in selective up-regulation of c-Jun and CD69, whereas at the same time it led to the inhibition of proximal TCR signaling. Among the hypothetical explanations for the inhibitory effects of PRR7 on TCR-mediated signaling was the possibility that the cells are already in the process of apoptosis advanced enough to have negative effects on TCR signal transduction. To test this, we treated J-iPRR7 cells with caspase inhibitor Z-VAD during RSL1-mediated PRR7 induction and then followed a calcium response downstream of TCR. Z-VAD treatment had a negligible effect on calcium response in PRR7-expressing J-iPRR7 cells, suggesting an apoptosis-independent mechanism of PRR7-mediated inhibition of T cell signaling (Fig. 8*A*).

To identify the point where PRR7 interferes with TCR signaling pathways, we treated J-iPRR7 cells with RSL1 to induce PRR7 expression, stimulated the cells by TCR cross-linking, and followed the phosphorylation of individual proteins in the cell lysates. We observed reduced phosphorylation of a number of important signaling molecules, including ZAP-70, LAT, PLCγ1, ERK1/2, and JNK (Fig. 8*B*) after TCR stimulation. The only remarkable exception was the up-regulation of c-Jun protein level, which was also reflected in the increased amount of the phosphorylated form of this transcription factor (Fig. 8*B*).

The reduction in tyrosine phosphorylation of proteins in proximal TCR signaling pathways, including ZAP-70, LAT, and PLCγ1, suggested the effects of PRR7 at the level of TCR itself. To analyze this, we followed the phosphorylation of TCRζ

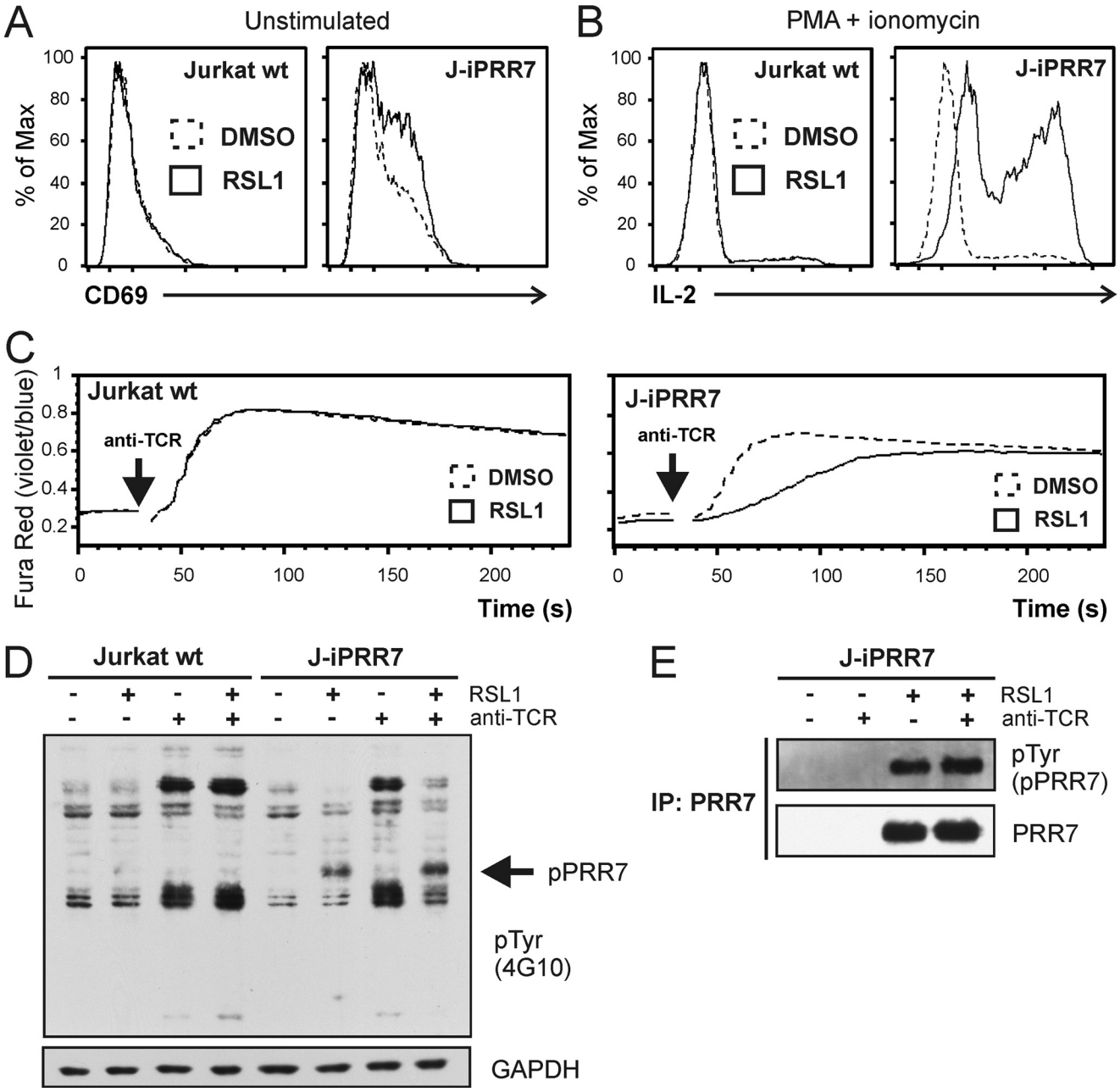

FIGURE 6. **Activated phenotype and impaired TCR signaling in J-iPRR7 cells.** *A*, J-iPRR7 cells were induced for 12 h to express PRR7, stained for the surface lymphocyte activation marker, CD69, and analyzed by flow cytometry. *B*, J-iPRR7 cells were induced to express PRR7. After 12 h, the cells were stimulated for additional 6 h with PMA and ionomycin in the presence of brefeldin A (5 μg/ml), fixed, stained for cytokine IL-2, and analyzed by flow cytometry. *C*, J-iPRR7 cells were induced for 16 h to express PRR7 and then loaded with a calcium indicator dye Fura Red. Calcium response after the anti-TCR IgM (C305, 10 μg/ml) stimulation was measured by flow cytometry. Collected data were analyzed in FlowJo software and plotted as mean fluorescence values. *D*, J-iPRR7 cells were induced to express PRR7 (16 h). Cells were stimulated with the anti-TCR IgM (C305, 10 μg/ml, 2 min) or left unstimulated. Whole cell lysates were analyzed by immunoblotting with the anti-phospho-Tyr mAb (4G10). Membrane was reprobed with GAPDH antibody as a loading control. *E*, J-iPRR7 cells were treated as in *panel D*, and lysate was subjected to immunoprecipitation (*IP*) with the anti-PRR7 mAb. Immunoprecipitated material was analyzed by immunoblotting with the anti-phospho-Tyr mAb (4G10) and the anti-PRR7 mAb.

chain after TCR cross-linking. We observed a substantial reduction in TCRζ phosphorylation both in a basal state and after stimulation in PRR7-expressing cells (Fig. 8*C*). As TCRζ is a substrate SFKs, we next analyzed the activation status of these kinases by immunoblotting with antibodies specific to their activating and inhibitory tyrosines with a focus on Lck, the major Src-family member in T cells. Surprisingly, we observed reduction in the phosphorylation of both regulatory tyrosines (SFK activation loop tyrosine and Lck inhibitory tyrosine) in PRR7-expressing cells. However, we also detected a highly reproducible reduction in total Lck staining (Fig. 8*D*). These data showed that the decreased Lck level is probably the major consequence of PRR7 expression, which is then reflected in the reduced content of both regulatory phosphotyrosines in the samples and reduced activity of downstream signaling pathways.

Finally, to assess the role of SFK activity and tyrosine phosphorylation of PRR7 in the opposing functions of PRR7, we

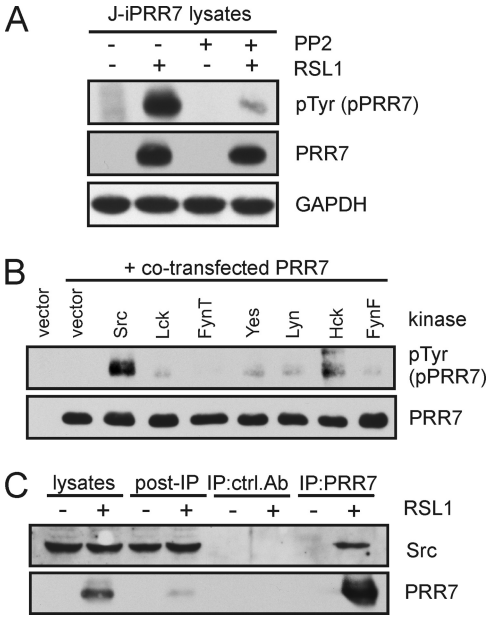

FIGURE 7. **Tyrosine phosphorylation of PRR7 and association of PRR7 with Src.** *A*, J-iPRR7 cells were induced to express PRR7 and simultaneously treated with the SFK inhibitor, PP2 (10 μM), for 18 h or left untreated. Tyrosine phosphorylation status of PRR7 was analyzed by immunoblotting with the anti-phospho-Tyr mAb (4G10). GAPDH staining served as a sample loading control. *B*, PRR7 was co-transfected with Src kinases into COS-7 cells. After 24 h, cells were lysed, and tyrosine phosphorylation of PRR7 was detected by immunoblotting with the anti-phospho-Tyr (4G10) mAb. *C*, J-iPRR7 cells were induced to express PRR7 or left uninduced for 18 h and lysed in LM buffer, and PRR7 was immunoprecipitated (*IP*) using the anti-PRR7-Sepharose or an isotype control mAb. Eluted proteins were analyzed by immunoblotting.

treated J-iPRR7 cells with SFK inhibitor PP2 during the PRR7 induction. Surprisingly, PP2 treatment had only a minor effect on c-Jun up-regulation as well as apoptosis induction (not shown), indicating that the effect of PRR7 on these pathways is independent of SFK signaling. In contrast, PP2 treatment inhibited the up-regulation of CD69 (Fig. 8*E*).

DISCUSSION

Thus far, PRR7 has been described in a single paper (18) as a component of the postsynaptic density (PSD) fraction of the rat forebrain, suggesting that it may play a role in modulating neural activities via interactions with the PSD-95/*N*-methyl-D-aspartate receptor complex or in PSD core formation. Here, we report that PRR7 is expressed in many tissues, including leukocytes, and is significantly up-regulated during T cell activation (Fig. 2, *C* and *D*). Nevertheless, even in activated T cells we had difficulties detecting PRR7 using our monoclonal antibodies on the immunoblot of whole cell lysates, which was most likely the result of both low expression level of PRR7 and suboptimal antibody reactivity. Therefore, we have used mainly Jurkat transfectants transiently or inducibly expressing recombinant PRR7. In these cells, our monoclonal antibodies could readily detect PRR7 in cell lysates and could be used in biochemical studies.

PRR7 is highly evolutionarily conserved (Table 1), suggesting that its function might be preserved across all vertebrates. The intracellular part of this protein (Fig. 1*A*) contains several motifs (proline-rich WW binding motif, tyrosine-based SH2 domain binding and/or internalization motifs, proline-based SH3 binding motifs, and a C-terminal PDZ-binding motif) indicating potential for interactions with other proteins.

The PDZ binding motif is responsible for the reported association with the MAGUK family scaffold protein PSD-95 in neurons (18). We assumed that in leukocytes it could be associated with the leukocyte counterpart of PSD-95, DLG1 (30). However, in our co-transfection experiments, we were not able to confirm such an association, whereas the association with PSD-95 was readily demonstrable under the same conditions (not shown). Src is another binding partner of PRR7, as identified in this work. PRR7 is most likely a substrate of Src, as we observed strong tyrosine phosphorylation of PRR7 in Jurkat cells, which was inhibited by the SFK inhibitor, PP2.

The most striking consequence of PRR7 overexpression in Jurkat T cell line was increased apoptosis. We used multiple deletion mutants to identify the region critical for apoptosis induction. Our analysis limited this region to the sequence between aa 159–171 in the WBP-1 domain of PRR7. Importantly, this region contains only a single tyrosine residue, Tyr-166, suggesting that phosphorylation of this site may be involved. However, our experiments with PP2 treatment of J-iPRR7 cells did not provide sufficient evidence for the role of SFK-mediated PRR7 tyrosine phosphorylation in apoptosis induction (not shown). We could also rule out the activation-induced cell death, as we did not observe any up-regulation of FasL in J-iPRR7 cells nor were we able to block PRR7-induced apoptosis by blocking antibodies to FasL (not shown). Thus, the mechanism of how the region around Tyr-166 mediates pro-apoptotic signaling remains unknown. One of the remaining hypotheses is phosphorylation-independent binding of a WW domain-containing protein to the tyrosine motif in the critical region. However, the identity of such a putative protein remains to be determined.

PRR7 inducibly expressed in the Jurkat cells was initially present at the plasma membrane, and later it was mainly detected in reversible, perinuclear, vesicular structures (Fig. 4, *B* and *C*). Time course analysis of PRR7 localization in the inducible system after RSL1 withdrawal suggests that the perinuclear accumulation is a continuous, active process involving removal from the plasma membrane by endocytosis (Fig. 4*C*).

Interestingly, the region involved in PRR7-mediated internalization partially overlaps with the section critical for PRR7-mediated apoptosis, suggesting the link between PRR7 internalization and induction of apoptosis. However, the region required for PRR7 internalization also includes the sequences outside the area critical for apoptosis. Moreover, the mutation of all PRR7 tyrosine residues that had strong inhibitory effects on apoptosis induction resulted only in a mild reduction in PRR7 internalization (not shown), suggesting that this region mediates apoptosis via other mechanisms then solely by triggering PRR7 endocytosis. On the other hand, the mutant lacking the membrane-anchoring sequences, which localized exclusively in the intracellular compartment, induced the highest degree of apoptosis. Taken together these data suggest that internalization and tyrosine phosphorylation are two independent mechanisms, which may cooperate to efficiently trigger apoptosis in J-iPRR7. An important question remains of how the region between aa 151 and 171 mediates PRR7 inter-

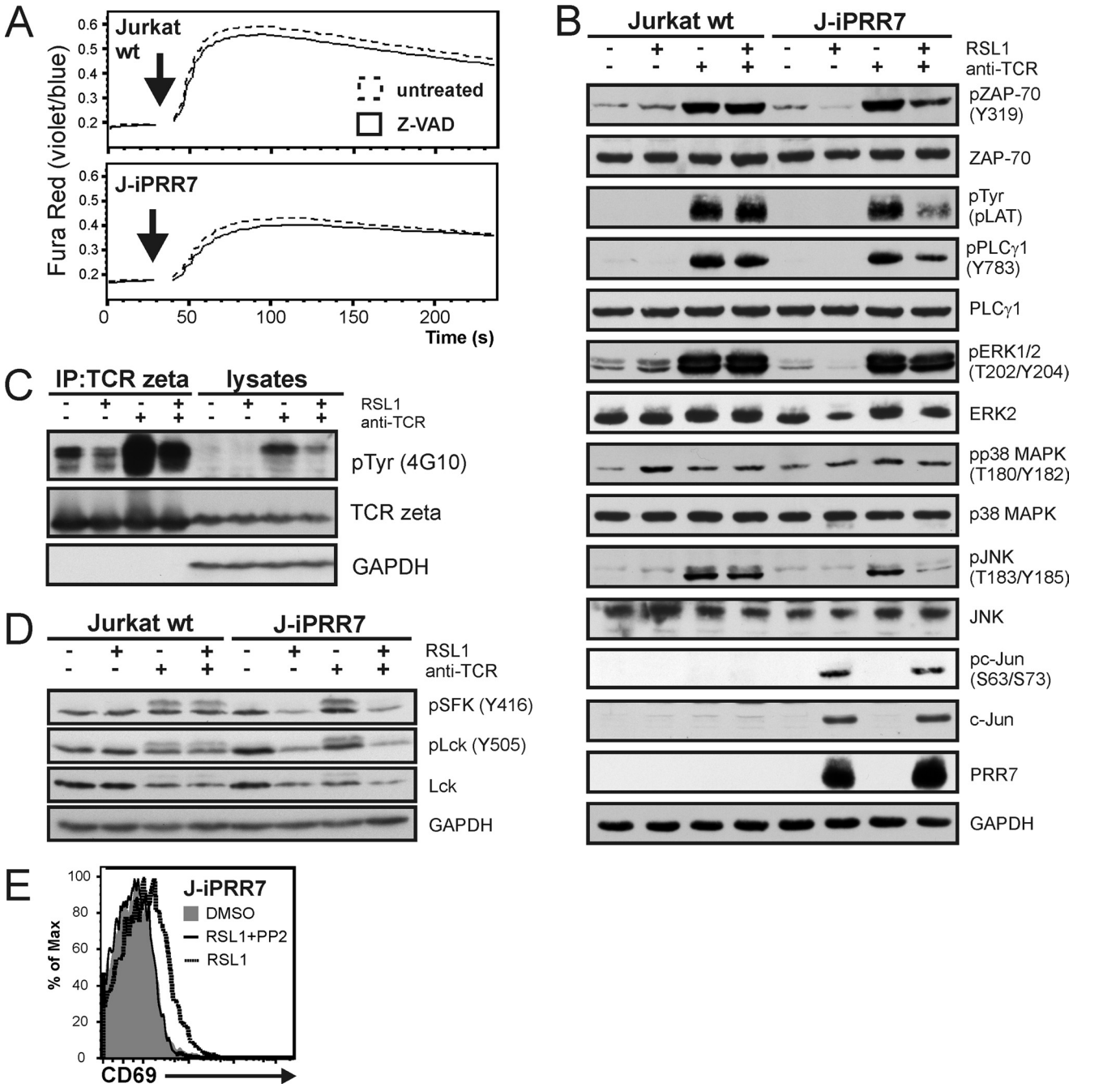

FIGURE 8. **Mechanisms of PRR7 dependent regulation of J-iPRR7 signaling.** *A*, J-iPRR7 cells were induced to express PRR7 in the presence of the pan-caspase inhibitor Z-VAD-FMK (10 μM, 16 h) and then loaded with a calcium indicator dye Fura Red. Calcium response after the anti-TCR IgM (C305, 10 μg/ml, *black arrows*) stimulation was measured by flow cytometry. Collected data were analyzed in FlowJo software and plotted as mean fluorescence values. *B*, J-iPRR7 cells induced to express PRR7 (16 h) were stimulated with the anti-TCR IgM (C305, 10 μg/ml, 2 min) or left unstimulated. Whole cell lysates were analyzed by immunoblotting with antibodies specific for proteins involved in TCR signaling. Phosphorylation status of LAT was detected using anti-Tyr(P) antibody (clone P-TYR-02) developed in our laboratory. Staining of GAPDH was used as a sample loading control. *C*, J-iPRR7 cells were treated as stated above (*panel B*), and lysates were subjected to immunoprecipitation (*IC*) with the anti-TCRζ mAb. Immunoprecipitates and whole cell lysates were immunoblotted with the anti-phospho-Tyr mAb (4G10) and Abs specific for TCRζ and GAPDH (sample loading control). *D*, J-iPRR7 cells were treated as stated above (*panel B*). Whole cell lysates were analyzed by immunoblotting with antibodies specific for phosphorylated forms of Lck, total Lck, and GAPDH (sample loading control). *E*, J-iPRR7 cells were induced to express PRR7 in the presence or absence of PP2 (10 μM, 18 h), stained for CD69, and analyzed by flow cytometry. In all the above assays, Jurkat wt cells and DMSO treatment were used as controls (not shown in *panels C* and *E*).

nalization. Tyrosines 153 and 166 within this critical region are part of potential tyrosine-based internalization sequences fitting the consensus Y*XX*Φ (31). Tyrosine to phenylalanine mutations within similar motifs can substantially reduce the rate of endocytosis (32). Mutations of PRR7 tyrosines had only a mild effect on PRR7 internalization, suggesting that these motifs are not genuine internalization sequences.

Other phenotypic features of the induced J-iPRR7 cells were also quite striking. They exhibited some traits of partially activated or "primed" T cells, including a spontaneous increase in

the expression of the surface activation marker, CD69, and strongly enhanced IL-2 production after PMA and ionomycin stimulation (Fig. 6, *A* and *B*). On the other hand, proximal elements of immunoreceptor signaling cascades (tyrosine phosphorylation of cytoplasmic substrates and cytoplasmic calcium elevation upon TCR cross-linking) were clearly diminished or down-regulated (Fig. 6, *C* and *D*, and 8, *B–D*). A likely explanation is that PRR7 by a so-far unknown mechanism down-regulates protein levels of a critical SFK Lck, which in turn results in the reduction of the activity of all the downstream pathways. On the other hand, a concomitant positive regulatory function of PRR7 was evidenced by a strong up-regulation of AP-1 transcription factor component c-Jun accompanied by a mild induction of the activation marker CD69 in the cells where PRR7 expression was induced (Figs. 6*A* and 8*B*). Intriguingly, c-Jun up-regulation was not affected by PP2 treatment (not shown), suggesting that this phenomenon is independent of Src or other SFKs. Moreover, we did not see any up-regulation of upstream pathways such as JNK or Erk that could lead to c-Jun up-regulation. c-Jun turnover is regulated via ubiquitin-dependent degradation, and thus a plausible hypothesis is that PRR7 somehow interferes with this process. This could lead to up-regulation of c-Jun protein levels independently of the activity of upstream MAP kinase pathways. Interestingly, one of the proteins involved in the regulation of c-Jun turnover is Itch, an E3 ubiquitin ligase of NEDD4 family (33) that also possesses multiple WW domains and could potentially interact with PRR7. However, we could not detect any Itch protein in PRR7 immunoprecipitates (not shown), although it remains possible that the interaction is labile or that some other member of the NEDD4 family is involved in such an interaction.

It can be speculated that increased c-Jun/AP-1 activity is responsible for the primed state of PRR7 expressing Jurkat, resulting in a high level of IL-2 production after stimulation. Although AP-1 sites are important components of the IL-2 promoter (34, 35), additional factors such as NF-AT and NF-κB are required for the full activity. If these are provided, *e.g.* after stimulation with PMA and ionomycin, a strong response can result. Regulation of CD69 expression also involves AP-1, but in contrast to c-Jun, CD69 up-regulation could be inhibited by PP2. A somewhat speculative explanation can be that tonic signaling by TCR (which is dependent on SFK) is required for CD69 expression in addition to c-Jun activity. In Jurkat cells, basal TCR signaling results in low level of CD69 expression (36). It is likely that it can be further potentiated by c-Jun overexpression while still being dependent on SFK-driven basal signaling. In line with this explanation is the observation that PRR7-mediated CD69 up-regulation could be partially blocked by inhibitors of several pathways (NF-AT, NF-κB, and p38 MAPK, SAPK/JNK) known to be initiated by TCR/SFK mediated signaling (not shown).

Although our present results show that PRR7 is able to influence T cell physiology rather dramatically, it remains to be determined whether it plays a regulatory role under more physiological conditions, *e.g.* in the natural process of T cell activation (37). Such roles may be indicated by the evidently tightly controlled expression of PRR7 in resting T cells and its marked up-regulation upon activation (Fig. 2). In contrast, cell types other than T lymphocytes, *e.g.* fibroblasts, may be much less sensitive to increased levels of PRR7 expression; in this context it should be noted that overexpression of full-length PRR7 was well tolerated by COS-7 or HEK293FT cells. Clearly, preparation of conditional *Prr7* gene knock-out mice may provide more definitive answers concerning the roles of PRR7 in various types of cells and tissues.

Acknowledgments—We thank all colleagues who provided the cells, vectors, and antibodies as indicated under "Experimental Procedures."

REFERENCES

1. Simeoni, L., Kliche, S., Lindquist, J., and Schraven, B. (2004) *Curr. Opin. Immunol.* **16,** 304–313
2. Zhang, W., Trible, R. P., and Samelson, L. E. (1998) *Immunity* **9,** 239–246
3. Brdička, T., Cerný, J., and Horejší, V. (1998) *Biochem. Biophys. Res. Commun.* **248,** 356–360
4. Brdicka, T., Pavlistová, D., Leo, A., Bruyns, E., Korínek, V., Angelisová, P., Scherer, J., Shevchenko, A., Hilgert, I., Cerný, J., Drbal, K., Kuramitsu, Y., Kornacker, B., Horejsí, V., and Schraven, B. (2000) *J. Exp. Med.* **191,** 1591–1604
5. Kawabuchi, M., Satomi, Y., Takao, T., Shimonishi, Y., Nada, S., Nagai, K., Tarakhovsky, A., and Okada, M. (2000) *Nature* **404,** 999–1003
6. Brdicka, T., Imrich, M., Angelisová, P., Brdicková, N., Horváth, O., Spicka, J., Hilgert, I., Lusková, P., Dráber, P., Novák, P., Engels, N., Wienands, J., Simeoni, L., Osterreicher, J., Aguado, E., Malissen, M., Schraven, B., and Horejsí, V. (2002) *J. Exp. Med.* **196,** 1617–1626
7. Janssen, E., Zhu, M., Zhang, W., Koonpaew, S., and Zhang, W. (2003) *Nat. Immunol.* **4,** 117–123
8. Brdicková, N., Brdicka, T., Angelisová, P., Horváth, O., Spicka, J., Hilgert, I., Paces, J., Simeoni, L., Kliche, S., Merten, C., Schraven, B., and Horejsí, V. (2003) *J. Exp. Med.* **198,** 1453–1462
9. Hur, E. M., Son, M., Lee, O. H., Choi, Y. B., Park, C., Lee, H., and Yun, Y. (2003) *J. Exp. Med.* **198,** 1463–1473
10. Zhu, M., Janssen, E., Leung, K., and Zhang, W. (2002) *J. Biol. Chem.* **277,** 46151–46158
11. Marie-Cardine, A., Kirchgessner, H., Bruyns, E., Shevchenko, A., Mann, M., Autschbach, F., Ratnofsky, S., Meuer, S., and Schraven, B. (1999) *J. Exp. Med.* **189,** 1181–1194
12. Bruyns, E., Marie-Cardine, A., Kirchgessner, H., Sagolla, K., Shevchenko, A., Mann, M., Autschbach, F., Bensussan, A., Meuer, S., and Schraven, B. (1998) *J. Exp. Med.* **188,** 561–575
13. Liu, Y., and Zhang, W. (2008) *J. Leukoc. Biol.* **84,** 842–851
14. Horejsí, V. (2004) *Immunol. Lett.* **92,** 43–49
15. Horejsí, V., Otáhal, P., and Brdicka, T. (2010) *FEBS J.* **277,** 4383–4397
16. Fuller, D. M., and Zhang, W. (2009) *Immunol. Rev.* **232,** 72–83
17. Koelsch, U., Schraven, B., and Simeoni, L. (2008) *J. Immunol.* **181,** 5930–5939
18. Murata, Y., Doi, T., Taniguchi, H., and Fujiyoshi, Y. (2005) *Biochem. Biophys. Res. Commun.* **327,** 183–191
19. Krogh, A., Larsson, B., von Heijne, G., and Sonnhammer, E. L. (2001) *J. Mol. Biol.* **305,** 567–580
20. Hobbs, S., Jitrapakdee, S., and Wallace, J. C. (1998) *Biochem. Biophys. Res. Commun.* **252,** 368–372
21. Lessard, J., Aicha, S. B., Fournier, A., Calvo, E., Lavergne, E., Pelletier, M., and Labrie, C. (2007) *Prostate* **67,** 808–819
22. Qiao, L., Schürmann, G., Betzler, M., and Meuer, S. C. (1991) *Gastroenterology* **101,** 1529–1536
23. Fraser, J. D., Goldsmith, M. A., and Weiss, A. (1989) *Proc. Natl. Acad. Sci. U.S.A.* **86,** 7133–7137
24. Otáhal, P., Angelisová, P., Hrdinka, M., Brdicka, T., Novák, P., Drbal, K., and Horejsí, V. (2010) *J. Immunol.* **184,** 3689–3696
25. Wan, J., Roth, A. F., Bailey, A. O., and Davis, N. G. (2007) *Nat. Protoc.* **2,** 1573–1584

26. Finn, R. D., Mistry, J., Tate, J., Coggill, P., Heger, A., Pollington, J. E., Gavin, O. L., Gunasekaran, P., Ceric, G., Forslund, K., Holm, L., Sonnhammer, E. L., Eddy, S. R., and Bateman, A. (2010) *Nucleic Acids Res.* **38,** D211–D222
27. Chen, H. I., and Sudol, M. (1995) *Proc. Natl. Acad. Sci. U.S.A.* **92,** 7819–7823
28. Saras, J., and Heldin, C. H. (1996) *Trends Biochem. Sci.* **21,** 455–458
29. Brannetti, B., and Helmer-Citterich, M. (2003) *Nucleic Acids Res.* **31,** 3709–3711
30. Round, J. L., Tomassian, T., Zhang, M., Patel, V., Schoenberger, S. P., and Miceli, M. C. (2005) *J. Exp. Med.* **201,** 419–430
31. Bonifacino, J. S., and Traub, L. M. (2003) *Annu. Rev. Biochem.* **72,** 395–447
32. Jadot, M., Canfield, W. M., Gregory, W., and Kornfeld, S. (1992) *J. Biol. Chem.* **267,** 11069–11077
33. Gao, M., Labuda, T., Xia, Y., Gallagher, E., Fang, D., Liu, Y. C., and Karin, M. (2004) *Science* **306,** 271–275
34. Jain, J., Valge-Archer, V. E., and Rao, A. (1992) *J. Immunol.* **148,** 1240–1250
35. Castellanos, M. C., Muñoz, C., Montoya, M. C., Lara-Pezzi, E., López-Cabrera, M., and de Landázuri, M. O. (1997) *J. Immunol.* **159,** 5463–5473
36. Roose, J. P., Mollenauer, M., Ho, M., Kurosaki, T., and Weiss, A. (2007) *Mol. Cell. Biol.* **27,** 2732–2745
37. Krammer, P. H., Arnold, R., and Lavrik, I. N. (2007) *Nat. Rev. Immunol.* **7,** 532–542

Btk is a positive regulator in the TREM-1/DAP12 signaling pathway

Tereza Ormsby[1,2], Eva Schlecker[1], Janina Ferdin[1], Anja Sibylle Tessarz[1], Pavla Angelisová[2], Afitap Derya Köprülü[3], Michael Borte[4], Klaus Warnatz[5], Ilka Schulze[6], Wilfried Ellmeier[3], Václav Hořejší[2] and Adelheid Cerwenka[1]

[1]German Cancer Research Center (DKFZ), Innate Immunity, Heidelberg, Germany; [2]Institute of Molecular Genetics, Academy of Sciences of the Czech Republic, Division of Molecular Immunology, Prague, Czech Republic; [3]Division of Immunobiology, Institute of Immunology, Center for Pathophysiology, Infectiology and Immunology, Medical University of Vienna, Vienna; [4]Diagnostic and Research Center for Primary Immunodeficiency, Leipzig, Germany; [5]Center of Chronic Immunodeficiency, Research group Clinical Immunology, Freiburg, Germany; [6]Center for Chronic Immunodeficiency, Research group Pediatric Immunology, Freiburg, Germany

Correspondence to Adelheid Cerwenka, German Cancer Research Center (DKFZ/D080), Im Neuenheimer Feld 280, D-69120, Heidelberg, Germany; e-mail: a.cerwenka@dkfz-heidelberg.de; phone: +49-6221-424480; fax: +49-6221-423755

Short title: Btk in TREM-1/DAP12 signaling

Scientific section designation: Immunobiology

Abstract

The triggering receptor expressed on myeloid cells 1 (TREM-1) has been implicated in the production of pro-inflammatory cytokines and chemokines during bacterial infection and sepsis. For downstream signal transduction, TREM-1 is coupled to the ITAM-containing adaptor DAP12. Here, we demonstrate that Bruton`s tyrosine kinase (Btk), a member of the Tec kinases, becomes phosphorylated upon TREM-1 triggering. In U937-derived cell lines, in which expression of Btk was diminished by shRNA-mediated knock-down, phosphorylation of Erk1/2 and PLCγ1 and Ca^{2+} mobilization were reduced after TREM-1 stimulation. Importantly, TREM-1-induced production of the pro-inflammatory cytokines, TNF-α and IL-8, and up-regulation of activation/differentiation cell surface markers were impaired in Btk knock-down cells. Similar results were obtained upon TREM-1 stimulation of BMDCs of *Btk*$^{-/-}$ mice. The analysis of cells containing Btk mutants revealed that intact membrane localization and a functional kinase domain were required for TREM-1-mediated signaling. Finally, after TREM-1 engagement, TNF-α production by PBMCs was reduced in the majority of patients suffering from X-linked agammaglobulinemia (XLA), a rare hereditary disease caused by mutations in the *Btk* gene. In conclusion, our data identify Btk as a positive regulator in the ITAM-mediated TREM-1/DAP12 pathway and suggest its implication in inflammatory processes.

Introduction

TREM-1 belongs to the immunoglobulin (Ig)-like superfamily of receptors. In humans, TREM-1 is expressed on neutrophils and $CD14^{high}$ monocytes.[1] TREM-1 expression is further up-regulated by TLR ligands. Binding of TREM-1 to endogenous ligand(s) expressed on granulocytes and platelets and present in sera of septic patients,[2-4] as well as to exogenous ligands on Marburg and Ebola viruses,[5] has been described. The exact nature of TREM-1 ligand(s), however, remains elusive. Engagement of TREM-1 by agonistic monoclonal antibodies (mAbs) results in respiratory burst, degranulation, phagocytosis, secretion of pro-inflammatory cytokines such as tumor necrosis factor-α (TNF-α), of the chemokines, interleukin-8 (IL-8) and monocyte chemotactic protein-1 (MCP-1), and in the up-regulation of cell surface expressed differentiation/activation markers.[1] In animal models of lipopolysacharide (LPS)-induced septic shock and microbial sepsis caused by live *Escherichia coli*, application of a soluble TREM-1-Ig fusion protein greatly increased survival of experimental animals indicating the importance of TREM-1 in the amplification of inflammation.[6]

TREM-1 possesses a short intracellular part that lacks intrinsic signaling motifs. Instead, it is coupled to the immunoreceptor tyrosine-based activation motif (ITAM)-containing adaptor protein, DAP12.[1] TREM-1 engagement leads to Ca^{2+} mobilization and phosphorylation of several proteins including DAP12, extracellular-signal regulated kinase (Erk1/2), phospholipase Cγ (PLCγ)[1] and the adaptor protein NTAL that further interacts with Grb2.[7] Recently, it was reported that the adaptor protein CARD9 is essential for TREM-1-induced secretion of TNF-α, IL-2 and IL-12p40 by mouse bone marrow-derived dendritic cells (BMDCs).[8]

Btk, a member of the Tec family of protein tyrosine kinases (PTKs), is involved in signaling via a variety of receptors including the B cell receptor (BCR), cytokine receptors and integrins.[9, 10] Loss of Btk function causes X-linked agammaglobulinemia (XLA), a rare primary immunodeficiency disease.[11, 12] Mutations causing XLA have been described in all Btk domains as well as in non-coding sequences of the gene.[13] XLA is manifested by severe defects in early B cell development, resulting in an almost complete absence of peripheral B cells and Igs of all classes. Affected individuals suffer from recurrent bacterial and enteroviral infections.[9] In mice, the R28C point mutation in the pleckstrin homology (PH) domain of Btk leads to X-linked immunodeficiency (*Xid*).[14]

In innate immune cells, the role of Btk is less clear. Btk has been implicated in several pathways in myeloid cells.[10] Btk associates with certain TLRs and their downstream signaling molecules.[15] Contradictory results were obtained from studies of TLR stimulation of monocytes of XLA

patients. In one report, relative to healthy controls, monocytes of XLA patients secreted reduced amounts of TNF-α upon LPS stimulation.[16] On the other hand, Perez *et al*.[17] described that monocytes of XLA patients showed similar TNF-α expression upon TLR4 triggering, compared to healthy individuals. In mouse osteoclasts, Btk mediates signaling in response to RANKL stimulation, and *Tec*$^{-/-}$*Btk*$^{-/-}$ mice show an osteopetrotic phenotype.[18] Osteoclasts from XLA patients showed defective resorption activity *in vitro* but bone density and bone turnover markers were not altered in XLA patients. In serum of XLA patients, increased levels of inflammatory cytokines were detected. Addition of this serum restored the activity of XLA osteoclasts and led to the normalization of bone density *in vitro*.[19] Moreover, Btk is involved in Fcγ receptor-mediated phagocytosis in mouse peritoneal macrophages.[20] The role of Btk in DAP12-mediated signaling in monocytes/macrophages is currently unknown.

Here, we demonstrate an important role of Btk in ITAM-mediated TREM-1/DAP12 signaling in myeloid cells. Btk was required for secretion of pro-inflammatory cytokines, Erk1/2 phosphorylation and Ca^{2+} flux. These data identify Btk as a promising target for the treatment of inflammatory diseases.

Material and Methods

Mice

Tec-deficient mice[21] and Btk-deficient mice[22] (purchased from Jackson Laboratory) were intercrossed and maintained in the animal facility of the Medical University of Vienna in concordance with all standards of animal care. Mice were backcrossed onto a C57BL/6 background for at least eight generations. All animal experiments were approved by the appropriate governmental authorities.

Patients

Eight unrelated male patients diagnosed with XLA, as defined by the World Health Organization (WHO) classification, and twelve healthy individuals were analyzed in this study after informed consent was obtained. This study was approved by the Research Ethics Committee, Medical University of Heidelberg, Germany. All patients received regular Igs substitution therapy and were free of serious infection at the time of blood sampling. All blood samples from XLA patients were taken before Ig treatment. Detailed clinical and molecular information about the XLA patients is depicted in Table S1.

Cell culture and plasmids

All cell lines derived from the human myelomonocytic cell line U937 were cultured in RPMI 1640 supplemented with 10% FCS, 2 mM glutamine, 100 U/ml penicillin and 100 µg/ml streptomycin (Invitrogen Life Technologies). Human PBMCs were obtained from peripheral blood by gradient centrifugation using Ficoll-Paque Plus (GE Healthcare) (Figure 6) or using Polymorphprep (Axis-Shield) (Figure 1D), according to the manufacturer´s instructions, and cultured in X-vivo 20 (Lonza). For a detailed description of BMDCs generation, see Supplemental methods.

Vectors, shRNA and cDNA constructs used in this study and methods for the generation of stable cell lines are also described in the Supplemental methods.

Stimulation of cells for signal transduction

For cross-linking experiments, cells were incubated with primary mAb (10 µg/ml) for 20 minutes at 4°C, washed twice with warm RPMI 1640 medium and incubated with secondary mAb (10 µg/ml) for 5 minutes at 37°C. For experiments with inhibitors, cells were incubated with PP2, Syk inhibitor IV BAY 61-3606 (both 16 µM, Calbiochem) or DMSO for 20 minutes at

37°C. Primary human PBMCs were incubated for 30 min on ice with 2% Venimmun N before stimulation.

Cells (5×10^7/ml) were stimulated with the indicated mAb (10 µg/ml) for 5 minutes at 37°C. Subsequently, cells were washed twice with cold PBS and lysed in 1 ml (per 5×10^7 cells) of LM lysis buffer (1% lauryl-β-D-maltoside (Calbiochem), 20 mM Tris (pH 7.5) 100 mM NaCl, 10% glycerol, 10 mM EDTA (pH 8.0), 50 mM NaF, 1/100 v/v of freshly prepared pervanadate, Complete Protease Inhibitor Cocktail (Roche Diagnostics)) for 30 minutes at 4°C. Subsequently, postnuclear supernatants were subjected to immunoprecipitation (IP).

Erk phosphorylation and Ca^{2+} assay are described in Supplemental methods.

Immunoprecipitation and whole cell lysates

For IP with covalently coupled mAb, postnuclear supernatants were pre-cleared with IgG2b-CNBr-Sepharose 4B beads to eliminate nonspecifically binding proteins. The flow through was enriched for tyrosine-phosphorylated (pY) proteins using anti-pY (clone 4G10)-CNBr-Sepharose 4B beads for 2–3 hours at 4°C. For IP with uncoupled mAb, postnuclear supernatants were pre-cleared with Protein A Ultralink Resin (Thermo Fisher Scientific). The flow through was incubated with the anti-Myc-tag or the anti-Btk Ab for 30 minutes at 4°C, added to 25-40 µl of Protein A Ultralink Resin and samples were incubated for additional 2-3 hours at 4°C. Bound proteins were eluted with 2×concentrated Laemmli buffer, resolved by SDS-PAGE followed by immunoblotting.

For analysis of whole cell lysates, 5×10^6 cells were lysed for 30 minutes at 4°C in 100 µl of LM lysis buffer. Postnuclear supernatants were mixed at a 1:1 ratio with 2×concentrated non-reduced Laemmli buffer, heated for 5 minutes at 95°C and reduced with 1% DTT. Proteins were resolved by SDS-PAGE followed by immunoblotting.

Stimulation of cells with immobilized Abs

For cytokine production, human PBMCs from healthy donors or XLA patients, mouse BMDCs and U937-TD-derived cells (5×10^5/ml) were stimulated with the mAb, anti-TREM-1, anti-FLAG or the respective isotype control mAb as indicated in the text, immobilized to tissue culture plastic (20 µg/ml). In addition, U937-TD-derevied cells were treated with Phorbol 12-Myristate 13-Actetate (PMA) (1 ng/ml, Sigma-Aldrich) and mouse BMDCs were stimulated with PMA (20 ng/ml) and ionomycin (100 ng/ml, Sigma-Aldrich). Supernatants were collected at the indicated time points and the amounts of secreted TNF-α, IL-8 or MIP-2 were analyzed by ELISA (R&D Systems) according to the manufacturer´s instructions.

For the analysis of up-regulation of differentiation/activation markers, cells were harvested, stained with the indicated mAbs and analyzed by flow cytometry using FACSCalibur (BD Biosciences). Subsequent data analyses were performed using the FlowJo software (Tree Stars). Abs used in this study are described in the Supplemental methods.

Results

The protein tyrosine kinase Btk is phosphorylated upon TREM-1 triggering

To gain insight into signaling events downstream of TREM-1, the U937-TD cell line that ectopically expresses the FLAG-tagged TREM-1 (FLAG-TREM-1) and DAP12 was used.[7] The parental myelomonocytic cell line U937 does not express endogenous TREM-1 and has very low levels of endogenous DAP12 (data not shown). U937-TD cells express high levels of FLAG-TREM-1 and human leukocyte antigen class I (HLA-I) (Figure 1A). We have shown previously that stimulation of U937-TD cells with anti-TREM-1 or anti-FLAG mAbs led to phosphorylation of several proteins including Erk1/2 kinase and the adaptor protein NTAL, to increased cytokine and chemokine production as well as enhanced Ca^{2+} flux. Incubation with an isotype-matched anti-HLA-I mAb did not induce these events and was used as a negative control.[7]

To identify novel regulators in the TREM-1/DAP12 pathway, we focused on proteins known to be involved in Ca^{2+} mobilization in ITAM-based signaling pathways, such as BCR-mediated signaling in B cells. Accordingly, we selected Btk, a member of the Tec family of PTKs, as a candidate. Indeed, immunoblotting using an anti-Btk pY551 mAb followed by an anti-Btk Ab revealed highly increased levels of Btk pY551 after TREM-1 triggering, compared to incubation with the isotype-matched anti-HLA-I mAb (Figure 1B). In addition, phosphorylation of Btk on Y223 upon TREM-1 triggering was observed (data not shown).

To address the possibility that Btk phosphorylation resulted from signaling of Fc receptors, U937-TD cells were stimulated using $F(ab`)_2$ fragments of the anti-FLAG mAb, alone or cross-linked with $F(ab`)_2$-specific goat anti-mouse $F(ab`)_2$ fragments (Figure 1B). $F(ab`)_2$ fragments of the anti-FLAG mAb or the goat anti-mouse $F(ab`)_2$ alone did not induce Btk phosphorylation. However, their cross-linking led to Btk phosphorylation similar to the levels observed during stimulation with anti-TREM-1 or anti-FLAG mAbs (Figure 1B). In the same experiment, we did not observe phosphorylation of the related kinase, Tec, which is also expressed in U937-TD cells (data not shown). Moreover, Btk phosphorylation was observed after TREM-1 stimulation in primary human PBMCs that contained 14% TREM-1^+ monocytes (Figure 1C). In PBMCs, only $CD14^+$ monocytes express TREM-1 and thus respond to TREM-1 stimulation (data not shown).[1]

To determine which kinases are required for Btk phosphorylation upon TREM-1 stimulation, U937-TD cells stably expressing Myc-tagged Btk (Myc-Btk) were stimulated via TREM-1 in the

presence or absence of the Src kinase inhibitor, PP2, the Syk kinase inhibitor, Syk IV, or the solvent control, DMSO (Figure 1D). Triggering with the anti-FLAG mAb in the presence of DMSO led to pronounced Btk phosphorylation. In contrast, the presence of Src or Syk kinase inhibitors during the stimulation greatly reduced Btk tyrosine phosphorylation.

Our data indicate that Btk becomes phosphorylated downstream of TREM-1 in a Src and Syk kinase dependent manner, suggesting that Btk might play an important role in the TREM-1/DAP12 signaling pathway.

Btk is a positive regulator of TREM-1 signaling and function

To evaluate the function of Btk in TREM-1 signaling, Btk knock-down cell lines were established. Two different target sequences, one localized in the SH2 domain (B#1 shRNA) of Btk, the other localized in the SH3 domain (B#2 shRNA) of Btk, were selected.[23] U937-TD cells were transduced with constructs containing these oligonucleotides or the vector control (VC) resulting in the U937-TD-B#1, U937-TD-B#2 and U937-TD-VC cell lines, respectively. Figure 2A shows that the B#1 shRNA efficiently reduced Btk expression in U937-TD cells, leading to approximately 96% down-regulation of Btk expression relative to the vector control cells. B#2 shRNA impaired Btk expression less efficiently, resulting in 40% down-regulation. Expression of the related kinase, Tec, was not affected by the shRNAs directed against Btk, which indicates the specificity of the selected oligonucleotides (data not shown). Furthermore, all cell lines expressed similar levels of FLAG-TREM-1 on the cell surface (data not shown). For subsequent experiments, U937-TD cells transduced with a construct containing oligonucleotides delivering shRNA directed against GFP (U937-TD-GFP), were used as an additional control.[7]

The stimulation of TREM-1 in U937-TD cells leads to TNF-α and IL-8 production and to up-regulation of the differentiation/activation markers, CD11c and CD86.[1, 7] To investigate whether Btk affects these processes, U937-TD-VC, U937-TD-B#1, U937-TD-B#2 and U937-TD-GFP were incubated with plate-bound isotype-matched control or anti-FLAG mAbs or with PMA and the production of TNF-α and IL-8 was analyzed. Triggering of TREM-1 for 8, 16, 24 and 48 hours in U937-TD-B#1 led to greatly decreased levels of TNF-α and IL-8 relative to U937-TD-VC (Figure 2B and data not shown). Moreover, lower percentages of $CD11c^{+}CD86^{+}$ cells were detected after TREM-1 stimulation for 24 and 48 hours of the U937-TD-B#1 cell line (Figure 2C and data not shown). U937-TD-B#2 cells behaved similar to U937-TD-VC cells suggesting that these cells still expressed sufficient levels of Btk for it to perform its function. In addition, cytokine secretion and up-regulation of activation markers in U937-TD-GFP cells was

indistinguishable from U937-TD-VC cells. Upon treatment with PMA that bypasses ITAM-based signaling[24] no significant differences in cytokine production and up-regulation of CD11c and CD86 were observed. In our previous study,[7] TREM-1 stimulation of U937-TD cells in the presence of LPS resulted in highly elevated amounts of TNF-α and IL-8. In Btk knock-down cells (U937-TD-B#1), impaired TNF-α and IL-8 production was observed not only upon TREM-1 stimulation alone but also in combination with LPS (Figure S1). Stimulation of U937-TD cells by LPS alone led to undetectable or low[7] levels of TNF-α. It has been described that Erk1/2 becomes phosphorylated after TREM-1 ligation.[1, 7] Indeed, Erk1/2 phosphorylation was induced after TREM-1 engagement by the anti-FLAG mAb and upon anti-FLAG $(Fab')_2$ cross-linking (Figure S2). As depicted in Figure 2D, at 2 minutes post-stimulation, levels of Erk1/2 phosphorylation in U937-TD-B#1 cells were similar to U937-TD-VC cells. However, at later time points, they were greatly reduced, suggesting that Btk controls sustained levels of Erk1/2 phosphorylation after TREM-1 triggering. In addition, triggering of TREM-1 in the presence of the PI3K inhibitor, LY294002, led to decreased levels of Erk1/2 phosphorylation (Figure 2E).

Members of the Tec kinase family were shown to be important for Ca^{2+} mobilization following antigen receptor engagement.[25] Indeed, the Btk knock-down cell line, U937-TD-B#1, exhibited a reduced Ca^{2+} response upon stimulation via TREM-1 as compared to control cells (Figure 2F). PLCγ is an important regulator of the initiation of Ca^{2+} flux.[26] Among two PLCγ isoforms, PLCγ1 is the prominent isoform expressed in U937 cells (data not shown). After TREM-1 triggering, phosphorylation of PLCγ1 was reduced but, similar to Ca^{2+} elevation, was not completely abolished in U937-TD-B#1 cells (Figures 2G).

In summary, our data demonstrate that Btk is a positive regulator of cytokine production, of up-regulation of the differentiation/activation markers CD11c and CD86, of sustained Erk1/2 phosphorylation, of Ca^{2+} mobilization and PLCγ1 phosphorylation in the TREM-1/DAP12 pathway.

Expression of Btk insensitive to the B#1 shRNA restores the defects in Btk knock-down cells

To confirm that the observed functional defects were due to the down-regulation of Btk expression by RNA silencing, a Btk construct insensitive to the B#1 shRNA was designed. Nucleotides in the target sequence of the B#1 shRNA were mutated by site-directed mutagenesis to disable binding of the B#1 shRNA but preserve the amino acid sequence of Btk (Figure 3A).

The U937-TD-B#1 cell line was transduced by either an empty vector or the vector containing Btk insensitive to B#1 shRNA to establish U937-TD-B#1-VC_{ins} and U937-TD-B#1-$Btk_{insB\#1}$WT, respectively. In parallel, U937-TD-VC cells were transduced by an empty vector to produce U937-TD-VC-VC_{ins} with endogenous Btk expression. Figure 3B illustrates that Btk expression in the rescue cell line U937-TD-B#1-$Btk_{insB\#1}$WT was increased to about 50% of the amount in U937-TD-VC-VC_{ins} cells containing endogenous Btk. Expression of FLAG-TREM-1 by these cell lines was similar to the parental cell lines (data not shown).

We first investigated whether TREM-1-induced cytokine secretion and up-regulation of CD11c and CD86 were affected upon TREM-1 triggering in the Btk rescue cell line. Indeed, in U937-TD-B#1-$Btk_{insB\#1}$WT, the levels of TNF-α and IL-8 (Figure 3C) as well as the percentages of $CD11c^{+}CD86^{+}$ cells (Figure 3D) were significantly increased up to 50% of the amounts produced by cells containing endogenous Btk. The extent of functional responses correlated with the level of Btk expression in U937-TD-B#1-$Btk_{insB\#1}$WT cells (Figure 3B). Furthermore, no differences in cytokine production or in up-regulation of CD11c and CD86 were observed upon treatment with PMA, demonstrating a similar intrinsic signaling potential of these cells. Likewise, Erk1/2 phosphorylation was improved in U937-TD-B#1-$Btk_{insB\#1}$WT cells (Figure 3E). After engagement of TREM-1, a modest but consistent increase in Ca^{2+} mobilization was observed in U937-TD-B#1-$Btk_{insB\#1}$WT cells compared to that of Btk knock-down cells (Figure 3F).

In summary, transduction of Btk insensitive to B#1 shRNA in U937-TD-B#1 cells led to the recovery of cytokine secretion, up-regulation of CD11c and CD86, and Erk1/2 phosphorylation reaching around 50% of its original levels. The extent of this rescue of functional responses correlated with the relative amounts of Btk expressed in these cells. Our data confirm that the functional defects observed in Btk knock-down cells were due to their decreased levels of Btk.

Intact membrane localization and a functional kinase domain are required for function of Btk in the TREM-1 signaling pathway

We next investigated whether certain domains of Btk were required for TREM-1 signaling and function. In order to inactivate these domains, point mutations were introduced as illustrated in Figure 4A. The point mutation, E41K, in the PH domain reportedly correlates with increased phosphorylation and translocation to the plasma membrane.[27] The R28C mutation in the PH

domain impairs Btk binding to PIP_3 in the plasma membrane[28] and the K430E mutation targets the kinase domain of Btk, rendering it inactive.[29]

U937-TD-B#1 cells were stably transduced with constructs containing Btk WT, E41K, R28C or K430E insensitive to B#1 shRNA or an empty vector. Figure 4B shows expression of Btk in these cell lines. Expression of FLAG-TREM-1 was comparable in all cell lines except for U937-TD-B#1-$Btk_{insB\#1}$R28C that consistently revealed slightly higher amounts of TREM-1 on the cell surface (data not shown).

First, cytokine production and up-regulation of CD11c and CD86 upon TREM-1 triggering were investigated (Figures 4C, D). Cells expressing Btk E41K displayed significantly higher levels of TNF-α and IL-8 relative to U937-TD-B#1-$Btk_{insB\#1}$WT and U937-TD-B#1-VC_{ins} cells. The up-regulation of CD11c and CD86 was consistently increased in cells expressing Btk E41K. In cells carrying the Btk R28C or K430E mutations, greatly reduced cytokine production and percentages of $CD11c^+CD86^+$ cells upon TREM-1 triggering were observed.

Then, TREM-1-induced Erk1/2 phosphorylation was analyzed in U937-TD-B#1-VC_{ins}, U937-TD-B#1-$Btk_{insB\#1}$WT and U937-TD-B#1-$Btk_{insB\#1}$E41K, R28C and K430E cells (Figure 4E). After TREM-1 triggering, cells expressing Btk E41K displayed slightly increased Erk1/2 phosphorylation compared to WT. In contrast, Erk1/2 phosphorylation was lower in cells carrying Btk R28C or K430E.

Finally, we investigated whether Ca^{2+} flux was affected in the Btk mutant cell lines. Upon TREM-1 engagement, Ca^{2+} mobilization was enhanced in U937-TD-B#1-$Btk_{insB\#1}$E41K (Figure 4F). By contrast, in cells expressing Btk R28C or K430E mutants the Ca^{2+} response was decreased.

Our results indicate that TREM-1-induced cytokine production, up-regulation of activation markers, Erk1/2 phosphorylation and Ca^{2+} mobilization are dependent on intact plasma membrane localization of Btk and its kinase activity.

TREM-1-induced cytokine secretion is reduced in BMDCs generated from *Btk*$^{-/-}$ mice

Our recent study revealed that mouse TREM-1 is expressed by subsets of blood monocytes, blood granulocytes and by BMDCs. Upon TREM-1 stimulation, BMDCs, but not other TREM-1 expressing cell populations, produce pro-inflammatory cytokines.[30]

To investigate whether Btk affects TREM-1 function in mouse primary cells, BMDCs were generated from bone marrow precursors of WT and *Btk*$^{-/-}$ mice by a 3-day culture in GM-CSF-containing medium. Since the related Tec kinase might compensate for Btk function in

Btk$^{-/-}$ mice, we also analyzed BMDCs from *Tec*$^{-/-}$ and *Tec*$^{-/-}$*Btk*$^{-/-}$ mice.[21] On all BMDCs similar expression of TREM-1, CD86, MHC class II or CD40 was observed by flow cytometry (Figure 5A and data not shown).

Upon TREM-1 triggering, production of TNF-α and macrophage inflammatory protein 2 (MIP-2) was significantly reduced by *Btk*$^{-/-}$ BMDCs, but only slightly impaired by *Tec*$^{-/-}$ BMDCs. Moreover, in *Tec*$^{-/-}$*Btk*$^{-/-}$ BMDCs, cytokine secretion was almost completely abolished (Figure 5B). All cells produced comparable amounts of cytokines upon treatment with PMA and ionomycin. Similar results were obtained at 8, 24 and 36 hours time points (data not shown). No up-regulation of CD86, CD80 or CD40, upon TREM-1 triggering was observed regardless whether BMDCs were derived from WT or knock-out mice (data not shown).

PBMCs from the majority of tested XLA patients secrete decreased levels of TNF-α after TREM-1 stimulation

To study the role of Btk in primary human cells, TREM-1-induced TNF-α production in patients with XLA (Table S1), a rare hereditary disease caused by mutations in the *Btk* gene,[11, 12] was examined. Also within PBMCs of XLA patients, only CD14^{+} monocytes expressed TREM-1 (data not shown). Similar TREM-1 expression by healthy donors (average MFI = 153.7 ± 87.3) and XLA patients (average MFI = 134.5 ± 37.8) on CD14^{+} monocytes was observed (Figure 6A). Upon TREM-1 triggering, TNF-α production was greatly impaired in PBMCs of seven out of eight XLA patients (Figure 6B). The median value of TNF-α production normalized to 5×10^{4} of CD14^{+} cells for healthy controls was 275 pg/ml and for XLA patients 99 pg/ml (P = 0.055, determined by Mann Whitney test). PBMCs from one patient produced extremely high amounts of TNF-α (1642.5 ± 153 pg/ml) upon TREM-1 stimulation. The reasons for this hyper-responsiveness upon TREM-1 stimulation are currently unknown and will be addressed in future studies. In summary, our data indicate that Btk is a positive regulator of TNF-α production in TREM-1-mediated signaling in primary human PBMCs.

Discussion

TREM-1 is implicated in the amplification of inflammatory responses and sepsis.[6] A better understanding of the TREM-1/DAP12 signaling pathway could help in designing novel therapies to control inflammatory diseases. Here, we demonstrate that after TREM-1 stimulation, Btk, a member of the Tec family of PTKs, becomes phosphorylated at Y551 in a Src and Syk kinase dependent manner. Y551 is located in the activation loop of Btk that was shown to be required for its intact kinase activity.[31] Phosphorylation at Y223 in the SH3 domain of Btk results from an internal autokinase activity of Btk and serves as an additional indicator of Btk activation.[31] Of note, we observed increased phosphorylation at Y223 of Btk upon TREM-1 triggering as well (data not shown). Thus, upon TREM-1 engagement, Btk becomes phosphorylated and activated.

Using several approaches, such as knocking-down Btk expression by RNA interference, studying BMDCs from *Btk*$^{-/-}$ mice and the analysis of PBMCs from patients suffering from XLA immunodeficiency, we demonstrate that Btk is a positive regulator of TNF-α production upon TREM-1 stimulation. Upon LPS stimulation of human monocytes, Btk is involved in the stabilization of mRNA of TNF-α, which was associated with an increase in the phosphorylation of p38 mitogen-activated protein kinase (MAPK).[16] We did not observe increased phosphorylation of p38 upon TREM-1 triggering in U937-TD cells (data not shown). Instead, we observed increased Erk1/2 phosphorylation after TREM-1 stimulation. In this context, it has been shown that after LPS stimulation, elevated levels of Erk1/2 phosphorylation correlated with higher production of TNF-α.[32] In Btk knock-down cells, Erk1/2 phosphorylation was similar to that of control cells at early time points, but later it was greatly reduced. These data suggest that after TREM-1 engagement, Btk sustains enhanced levels of Erk1/2 phosphorylation. A similar observation was published previously in Btk-deficient DT40 cells after BCR stimulation.[33]

Upon LPS stimulation, Btk was implicated in the phosphorylation of the p65 subunit of NFκB, which was dependent on the intact kinase activity of Btk.[34] Our analysis of cells carrying different mutants of Btk revealed that a functional Btk kinase domain was essential for TREM-1-induced cytokine production. In this context, NFκB was shown to be activated by TREM-1 triggering.[35] In addition, weak phosphorylation of interleukin-1 receptor-associated kinase 1 (IRAK1), a kinase implicated in the activation of NFκB downstream of TLRs, was demonstrated after TREM-1 triggering.[36] It is possible that Btk is involved in the phosphorylation of downstream substrates, such as the p65 subunit of NFκB, after TREM-1 engagement, facilitating TNF-α production. Moreover, NFκB is involved in the regulation of transcription of the *Btk* gene[37] which might further amplify an on-going pro-inflammatory immune response.

Our results obtained with BMDCs from knock-out mice reveal an important role of Btk in the regulation of TREM-1-induced TNF-α production. TNF-α production upon TREM-1 stimulation was only minimally affected by the absence of just Tec kinase. We did not observe Tec phosphorylation after engagement of the TREM-1 pathway in U937-TD cells (data not shown), suggesting a subordinate role of Tec in TREM-1 signaling.

After BCR engagement, Btk mediates an increase in intracellular Ca^{2+} required for the activation of transcription factors such as NFAT.[25, 38] It was shown that Btk phosphorylates PLCγ1 at several tyrosine residues, including Y783, which is necessary for its maximal lipid hydrolase activity.[39] We observed greatly impaired Ca^{2+} flux and PLCγ1 phosphorylation in Btk knock-down cells after TREM-1 triggering which was dependent on intact R28 in the PH of Btk and functional kinase domain of Btk. Neither Ca^{2+} flux nor PLCγ1 phosphorylation were completely abolished in Btk knock-down cells. Accordingly, it was shown that Syk kinase is absolutely essential for Ca^{2+} flux and PLCγ phosphorylation while Btk regulates the magnitude of these processes after stimulation via BCR.[38, 40]

In our study, we used different Btk mutants to dissect the molecular requirements underlying the function of Btk downstream of TREM-1. U937-TD cells carrying the Btk E41K mutation exhibited increased cytokine production, up-regulation of activation markers, Erk1/2 phosphorylation and Ca^{2+} mobilization as compared to control cells. The E41K mutation of Btk was shown to be hyperphosphorylated[27] and to exhibit stronger association with membrane phospholipids,[41] resulting in higher amounts of Btk at the plasma membrane.[27] In concordance with our study, increased Ca^{2+} mobilization was observed after BCR engagement in *Btk*$^{-/-}$ DT40 cells reconstituted with Btk E41K.[42] However, transgenic mice expressing Btk E41K suffer from similar but more severe B cell defect as compared to *Xid* mice.[43]

U937-TD cells carrying Btk R28C displayed greatly impaired responses to TREM-1 stimulation compared to control cells. The R28C mutation disables Btk to bind to PIP_3 in the plasma membrane.[28] Thus, Btk R28C cannot relocalize from the cytosol to the close proximity of the plasma membrane where activation of PLCγ takes place. Modifications at position 28 are common alterations occurring in XLA patients[44] and the reason for the B cell phenotype observed in *Xid* mice.[14]

The Btk K430E mutation targets the kinase domain of Btk, rendering it inactive. We observed that in U937-TD cells expressing Btk K430E cytokine production, up-regulation of activation markers, Erk1/2 phosphorylation and Ca^{2+} mobilization were impaired as compared to U937-TD cells carrying Btk WT. In contrast, in *Btk*$^{-/-}$ DT40 cells reconstituted with Btk K430E, Ca^{2+} mobilization is fully restored.[45] In this study, it was proposed that besides its kinase activity, Btk

might also function as an adaptor protein that facilitates Ca^{2+} flux. Similarly, Btk`s tumor suppressor activity is fully restored by the kinase inactive form of Btk.[46] Of note, Btk R525Q, another kinase inactive mutant, did not reconstitute BCR-induced Ca^{2+} flux.[38] We conclude that the function of Btk might depend on the cellular context and pathways studied.

Thus, intact localization in the plasma membrane and intact kinase activity of Btk are essential for its function in the TREM-1/DAP12 signaling pathway. Apart from known targets such as PLCγ, Btk might phosphorylate other yet unidentified molecules downstream of TREM-1. Although the comparison of overall tyrosine phosphorylation patterns of Btk knock-down cells did not reveal any apparent differences (data not shown), our future studies will seek to identify the unknown targets of Btk in the TREM-1 pathway. Together with Btk these molecules might represent suitable targets for chemical intervention in patients with inflammatory diseases.

Our experiments revealed greatly reduced TNF-α production by PBMCs from seven out of eight tested XLA patients as compared to healthy controls upon TREM-1 stimulation. XLA patients carry mutations in the *Btk* gene leading to the complete loss or dysfunction of Btk.[11, 12] Since the exact nature of the TREM-1 ligand(s) is currently unknown, the implications of our findings regarding the clinical manifestation of XLA patients, such as their high susceptibility to infection, remain unclear. Elevated levels of inflammatory cytokines including TNF-α were detected in the serum of XLA patients.[19] Our data suggest that these high levels of TNF-α arise from TREM-1-unrelated pathways. The stimulation of monocytes of XLA patients with LPS resulted in controversial findings. One study reported defects in TNF-α production by monocytes of XLA patients upon LPS stimulation[16] whereas another study observed similar levels of TNF-α expression.[17] Thus, the contribution of TLR4 signaling to the high TNF-α serum levels in XLA patients requires further investigation. In one patient, extremely high amounts of TNF-α production (1642.5 ± 153 pg/ml) were detected upon TREM-1 stimulation of PBMCs. The reasons for this increased TNF-α production are currently not known and are under investigation in our laboratory.

In conclusion, Btk is a positive regulator of the TREM-1 signaling pathway that leads to TNF-α production. It is well established that TNF-α is a key mediator of inflammatory responses and sepsis. Therefore, it is tempting to speculate that inhibition of Btk with specific small molecular compounds might be a promising strategy in the treatment of inflammation and sepsis.

Acknowledgements

This work was supported by a Marie Curie Excellence Grant (to A.C.). P.A. and V.H. are supported by project of 1M0506 (MSMT, Czech Republic). T.O. is partially supported by the Faculty of Sciences, Charles University in Prague (Czech Republic).

The authors thank G. Superti-Furga (Center for Molecular Medicine, Austrian Academy of Sciences, Vienna, Austria) for providing constructs containing human Btk, O. Witt (Clinical Cooperation Unit Pediatric Oncology, DKFZ, Heidelberg, Germany) for initiating the contacts for the XLA study, S. Ehl (Center for Chronic Immunodeficiency, Research group Pediatric Immunology, Freiburg, Germany), A. Rölle, M. Kegel, J. Ormsby and P. Willis for critically reading the manuscript.

Authorship

T.O. designed and performed the experiments, analyzed the data and wrote the manuscript; E.S. performed experiments with XLA patients; J.F., A.S.T. and P.A. helped with experiments; A.D.K. and W. E. provided knock-out mice; K.W., M.B. and I.S. helped with the recruitment of XLA patients; V.H. and A.C. oversaw the project, designed experiments and co-wrote the manuscript.

Conflict of interest disclosure

The authors declare no competing financial interests.

References

1. Bouchon A, Dietrich J, Colonna M. Cutting edge: inflammatory responses can be triggered by TREM-1, a novel receptor expressed on neutrophils and monocytes. *J Immunol.* May 15 2000;164(10):4991-4995.

2. Gibot S, Buonsanti C, Massin F, et al. Modulation of the triggering receptor expressed on the myeloid cell type 1 pathway in murine septic shock. *Infect Immun.* May 2006;74(5):2823-2830.

3. Haselmayer P, Grosse-Hovest L, von Landenberg P, Schild H, Radsak MP. TREM-1 ligand expression on platelets enhances neutrophil activation. *Blood.* Aug 1 2007;110(3):1029-1035.

4. El Mezayen R, El Gazzar M, Seeds MC, McCall CE, Dreskin SC, Nicolls MR. Endogenous signals released from necrotic cells augment inflammatory responses to bacterial endotoxin. *Immunol Lett.* Jul 31 2007;111(1):36-44.

5. Mohamadzadeh M, Coberley SS, Olinger GG, et al. Activation of triggering receptor expressed on myeloid cells-1 on human neutrophils by marburg and ebola viruses. *J Virol.* Jul 2006;80(14):7235-7244.

6. Bouchon A, Facchetti F, Weigand MA, Colonna M. TREM-1 amplifies inflammation and is a crucial mediator of septic shock. *Nature.* Apr 26 2001;410(6832):1103-1107.

7. Tessarz AS, Weiler S, Zanzinger K, Angelisova P, Horejsi V, Cerwenka A. Non-T cell activation linker (NTAL) negatively regulates TREM-1/DAP12-induced inflammatory cytokine production in myeloid cells. *J Immunol.* Feb 15 2007;178(4):1991-1999.

8. Hara H, Ishihara C, Takeuchi A, et al. The adaptor protein CARD9 is essential for the activation of myeloid cells through ITAM-associated and Toll-like receptors. *Nat Immunol.* Jun 2007;8(6):619-629.

9. Lindvall JM, Blomberg KE, Valiaho J, et al. Bruton's tyrosine kinase: cell biology, sequence conservation, mutation spectrum, siRNA modifications, and expression profiling. *Immunol Rev.* Feb 2005;203:200-215.

10. Koprulu AD, Ellmeier W. The role of Tec family kinases in mononuclear phagocytes. *Crit Rev Immunol.* 2009;29(4):317-333.

11. Tsukada S, Saffran DC, Rawlings DJ, et al. Deficient expression of a B cell cytoplasmic tyrosine kinase in human X-linked agammaglobulinemia. *Cell.* Jan 29 1993;72(2):279-290.

12. Vetrie D, Vorechovsky I, Sideras P, et al. The gene involved in X-linked agammaglobulinaemia is a member of the src family of protein-tyrosine kinases. *Nature.* Jan 21 1993;361(6409):226-233.

13. Valiaho J, Smith CI, Vihinen M. BTKbase: the mutation database for X-linked agammaglobulinemia. *Hum Mutat.* Dec 2006;27(12):1209-1217.

14. Rawlings DJ, Saffran DC, Tsukada S, et al. Mutation of unique region of Bruton's tyrosine kinase in immunodeficient XID mice. *Science.* Jul 16 1993;261(5119):358-361.

15. Jefferies CA, Doyle S, Brunner C, et al. Bruton's tyrosine kinase is a Toll/interleukin-1 receptor domain-binding protein that participates in nuclear factor kappaB activation by Toll-like receptor 4. *J Biol Chem.* Jul 11 2003;278(28):26258-26264.

16. Horwood NJ, Mahon T, McDaid JP, et al. Bruton's tyrosine kinase is required for lipopolysaccharide-induced tumor necrosis factor alpha production. *J Exp Med.* Jun 16 2003;197(12):1603-1611.

17. Perez de Diego R, Lopez-Granados E, Pozo M, et al. Bruton's tyrosine kinase is not essential for LPS-induced activation of human monocytes. *J Allergy Clin Immunol.* Jun 2006;117(6):1462-1469.

18. Shinohara M, Koga T, Okamoto K, et al. Tyrosine kinases Btk and Tec regulate osteoclast differentiation by linking RANK and ITAM signals. *Cell.* Mar 7 2008;132(5):794-806.

19. Danks L, Workman S, Webster D, Horwood NJ. Elevated cytokine production restores bone resorption by human Btk-deficient osteoclasts. *J Bone Miner Res.* Jan;26(1):182-192.

20. Jongstra-Bilen J, Puig Cano A, Hasija M, Xiao H, Smith CI, Cybulsky MI. Dual functions of Bruton's tyrosine kinase and Tec kinase during Fcgamma receptor-induced signaling and phagocytosis. *J Immunol.* Jul 1 2008;181(1):288-298.

21. Ellmeier W, Jung S, Sunshine MJ, et al. Severe B cell deficiency in mice lacking the tec kinase family members Tec and Btk. *J Exp Med.* Dec 4 2000;192(11):1611-1624.

22. Khan WN, Alt FW, Gerstein RM, et al. Defective B cell development and function in Btk-deficient mice. *Immunity.* Sep 1995;3(3):283-299.

23. Heinonen JE, Smith CI, Nore BF. Silencing of Bruton's tyrosine kinase (Btk) using short interfering RNA duplexes (siRNA). *FEBS Lett.* Sep 11 2002;527(1-3):274-278.

24. Nel AE, Navailles M, Rosberger DF, et al. Phorbol ester induces tyrosine phosphorylation in normal and abnormal human B lymphocytes. *J Immunol.* Nov 1985;135(5):3448-3453.

25. Fluckiger AC, Li Z, Kato RM, et al. Btk/Tec kinases regulate sustained increases in intracellular Ca2+ following B-cell receptor activation. *EMBO J.* Apr 1 1998;17(7):1973-1985.

26. Wilde JI, Watson SP. Regulation of phospholipase C gamma isoforms in haematopoietic cells: why one, not the other? *Cell Signal.* Oct 2001;13(10):691-701.

27. Li T, Rawlings DJ, Park H, Kato RM, Witte ON, Satterthwaite AB. Constitutive membrane association potentiates activation of Bruton tyrosine kinase. *Oncogene.* Sep 18 1997;15(12):1375-1383.

28. Salim K, Bottomley MJ, Querfurth E, et al. Distinct specificity in the recognition of phosphoinositides by the pleckstrin homology domains of dynamin and Bruton's tyrosine kinase. *EMBO J.* Nov 15 1996;15(22):6241-6250.

29. Li T, Tsukada S, Satterthwaite A, et al. Activation of Bruton's tyrosine kinase (BTK) by a point mutation in its pleckstrin homology (PH) domain. *Immunity.* May 1995;2(5):451-460.

30. Zanzinger K, Schellack C, Nausch N, Cerwenka A. Regulation of triggering receptor expressed on myeloid cells 1 expression on mouse inflammatory monocytes. *Immunology.* Oct 2009;128(2):185-195.

31. Rawlings DJ, Scharenberg AM, Park H, et al. Activation of BTK by a phosphorylation mechanism initiated by SRC family kinases. *Science.* Feb 9 1996;271(5250):822-825.

32. Shinohara H, Inoue A, Toyama-Sorimachi N, et al. Dok-1 and Dok-2 are negative regulators of lipopolysaccharide-induced signaling. *J Exp Med.* Feb 7 2005;201(3):333-339.

33. Jiang A, Craxton A, Kurosaki T, Clark EA. Different protein tyrosine kinases are required for B cell antigen receptor-mediated activation of extracellular signal-regulated kinase, c-Jun NH2-terminal kinase 1, and p38 mitogen-activated protein kinase. *J Exp Med.* Oct 5 1998;188(7):1297-1306.

34. Doyle SL, Jefferies CA, O'Neill LA. Bruton's tyrosine kinase is involved in p65-mediated transactivation and phosphorylation of p65 on serine 536 during NFkappaB activation by lipopolysaccharide. *J Biol Chem.* Jun 24 2005;280(25):23496-23501.

35. Gibot S, Kolopp-Sarda MN, Bene MC, et al. A soluble form of the triggering receptor expressed on myeloid cells-1 modulates the inflammatory response in murine sepsis. *J Exp Med.* Dec 6 2004;200(11):1419-1426.

36. Fortin CF, Lesur O, Fulop T, Jr. Effects of TREM-1 activation in human neutrophils: activation of signaling pathways, recruitment into lipid rafts and association with TLR4. *Int Immunol.* Jan 2007;19(1):41-50.

37. Yu L, Mohamed AJ, Simonson OE, et al. Proteasome-dependent autoregulation of Bruton tyrosine kinase (Btk) promoter via NF-kappaB. *Blood.* May 1 2008;111(9):4617-4626.

38. Takata M, Kurosaki T. A role for Bruton's tyrosine kinase in B cell antigen receptor-mediated activation of phospholipase C-gamma 2. *J Exp Med.* Jul 1 1996;184(1):31-40.

39. Humphries LA, Dangelmaier C, Sommer K, et al. Tec kinases mediate sustained calcium influx via site-specific tyrosine phosphorylation of the phospholipase Cgamma Src homology 2-Src homology 3 linker. *J Biol Chem.* Sep 3 2004;279(36):37651-37661.

40. Takata M, Sabe H, Hata A, et al. Tyrosine kinases Lyn and Syk regulate B cell receptor-coupled Ca2+ mobilization through distinct pathways. *EMBO J.* Mar 15 1994;13(6):1341-1349.

41. Fukuda M, Kojima T, Kabayama H, Mikoshiba K. Mutation of the pleckstrin homology domain of Bruton's tyrosine kinase in immunodeficiency impaired inositol 1,3,4,5-tetrakisphosphate binding capacity. *J Biol Chem.* Nov 29 1996;271(48):30303-30306.

42. Kang SW, Wahl MI, Chu J, et al. PKCbeta modulates antigen receptor signaling via regulation of Btk membrane localization. *EMBO J.* Oct 15 2001;20(20):5692-5702.

43. Dingjan GM, Maas A, Nawijn MC, et al. Severe B cell deficiency and disrupted splenic architecture in transgenic mice expressing the E41K mutated form of Bruton's tyrosine kinase. *EMBO J.* Sep 15 1998;17(18):5309-5320.

44. Vihinen M, Kwan SP, Lester T, et al. Mutations of the human BTK gene coding for bruton tyrosine kinase in X-linked agammaglobulinemia. *Hum Mutat.* 1999;13(4):280-285.

45. Tomlinson MG, Woods DB, McMahon M, et al. A conditional form of Bruton's tyrosine kinase is sufficient to activate multiple downstream signaling pathways via PLC Gamma 2 in B cells. *BMC Immunol.* 2001;2:4.

46. Middendorp S, Zijlstra AJ, Kersseboom R, Dingjan GM, Jumaa H, Hendriks RW. Tumor suppressor function of Bruton tyrosine kinase is independent of its catalytic activity. *Blood.* Jan 1 2005;105(1):259-265.

Figure legends

Figure 1: Btk becomes phosphorylated after TREM-1/DAP12 triggering. (A) U937-TD cells were stained with anti-TREM-1, anti-FLAG or anti-HLA-I (open histograms) or isotype-matched control mAbs (filled histograms) followed by staining with goat anti-mouse-PE Abs and analyzed by flow cytometry. (B) U937-TD cells were incubated with the indicated stimuli for 5 min at 37°C. pY proteins were immunoprecipitated from postnuclear supernatants using covalently coupled IgG2b-Sepharose followed by anti-pY-Sepharose. Phosphorylation was detected by immunoblotting with anti-Btk pY551 and anti-Btk Abs. (C) Human PBMCs containing 14% TREM-1^+ monocytes were incubated with the indicated stimuli for 2 min. Btk was immunoprecipitated from postnuclear supernatants using the anti-Btk Ab and Protein A Ultralink Resin. Immunoblotting was performed with anti-Btk pY551 and anti-Btk Abs. (D) U937-TD cells transduced with Myc-tagged Btk were placed in medium alone or in the presence of DMSO or the Src kinase inhibitor, PP2, or the Syk inhibitor IV for 20 min at 37°C. Subsequently, cells were incubated with the indicated stimuli for 5 min at 37°C. Btk was immunoprecipitated from postnuclear supernatants using the anti-Myc-tag mAb and Protein A Ultralink Resin. Immunoblotting was performed with anti-Btk pY551 and anti-Btk Abs. IP: immunoprecipitation; pY: phosphotyrosine.

Figure 2: TREM-1 signaling is impaired in Btk knock-down cells. (A) Whole cell lysates of U937-TD-derived cells were analyzed by immunoblotting with anti-Btk and anti-β-actin mAbs. LumiImager signals of Btk and β-actin were quantified and the ratio between Btk and β-actin was calculated. (B, C) U937-TD-derived cells were incubated for 16 (B) or 48 (C) hours with either plate-bound anti-FLAG or isotype-matched control mAbs or PMA. (B) Supernatants were analyzed by ELISA for TNF-α and IL-8. Data are displayed as mean ± SD of at least duplicates of ELISA. (C) Cells were analyzed for expression of the differentiation/activation markers, CD11c and CD86, by flow cytometry. (D) U937-TD-derived cells were incubated with medium alone or with isotype-matched anti-HLA-I or with anti-FLAG mAbs for the indicated time periods. Postnuclear supernatants were analyzed by immunoblotting with anti-pErk1/2 and anti-Erk1 Abs. LumiImager signals were quantified, and the ratio between pErk1/2 and Erk1 was calculated. (E) U937-TD cells were incubated with medium, isotype-matched anti-HLA-I or with anti-FLAG mAbs in the presence or absence (w/o) of LY294002 or DMSO for 5 min. Postnuclear supernatants were analyzed by immunoblotting with anti-pErk1/2 and anti-β-actin Abs. Signals were quantified, and the ratio between pErk1/2 and β-actin was calculated.

(F) Ca^{2+} mobilization of the Indo-1 AM-labeled U937-TD-derived cells was analyzed by flow cytometry. Cells were stimulated with mAb at the time point indicated by the arrow. (G) U937-TD-derived cells were stimulated with isotype-matched anti-HLA-I or anti-FLAG mAbs for the indicated time periods. Postnuclear supernatants were analyzed by immunoblotting with anti-PLCγ1 pY783 and anti-PLCγ1 Abs. One representative experiment of two (G), of three (A and F), of seven (B), of five (C) and of four (D) independent experiments is shown. n.d: not detectable.

Figure 3: Expression of Btk insensitive to the B#1 shRNA restores the defects of the Btk knock-down cell line. (A) A schematic picture of the construct used to prepare the Btk rescue cell line, U937-TD-B#1-$Btk_{insB\#1}$WT, is depicted. (B) Whole cell lysates of U937-TD-derived cells were analyzed by immunoblotting with anti-Btk and anti-β-actin mAbs. LumiImager signals of the ratio between Btk and β-actin are displayed as mean ± SD from seven independent experiments. (C, D) U937-TD-derived cells were incubated with either plate-bound anti-FLAG or isotype-matched control mAbs or PMA. (C) ELISA analysis of supernatants collected after 8 (TNF-α) or 16 (IL-8) hours. Data are displayed as mean ± SD from ELISA performed at least in duplicates of duplicate cultures. (D) Expression analysis of CD11c and CD86 after 48 hours by flow cytometry is shown. Data are displayed as mean ± SD from duplicate cultures. (E) U937-TD-derived cells were stimulated with the anti-FLAG mAb for 5 minutes. Postnuclear supernatants were analyzed by immunoblotting with anti-pErk1/2 and anti-Erk1 Abs. LumiImager signals were quantified, and the ratio between pErk1/2 and Erk1 was calculated. (F) Ca^{2+} mobilization of Indo-1 AM-labeled U937-TD-derived cells was analyzed by flow cytometry. Cells were stimulated with the anti-FLAG mAb at the time point indicated by the arrow. One representative experiment of seven (B), of five (C, F), of four (D) and of three (E) independent experiments is shown. * $P < 0.05$ and ** $P < 0.005$ (Student`s t-test). ins: insensitive; WT: wild-type.

Figure 4: Intact plasma membrane localization and a functional kinase domain of Btk are essential for Btk function after TREM-1 triggering. (A) Schematic illustration of $Btk_{insB\#1}$ mutants introduced into U937-TD-B#1 cells. (B) Whole cell lysates of U937-TD-derived cells were analyzed by immunoblotting with anti-Btk and anti-β-actin or anti-α-tubulin mAbs. LumiImager signals of the ratio between Btk and the indicated housekeeping protein are displayed as mean ± SD from seven independent experiments. (C, D) U937-TD-derived cells were incubated with either plate-bound anti-FLAG or isotype-matched control mAbs or PMA.

(C) Supernatants were collected after 8 (TNF-α) or 16 (IL-8) hours and cytokine production was analyzed by ELISA. Data are displayed as mean ± SD of at least duplicates of ELISA from duplicate cultures. (D) Expression analysis of CD11c and CD86 after 48 hours by flow cytometry is depicted. Data are displayed as mean ± SD from duplicate cultures. (E) U937-TD derived cells were stimulated with the anti-FLAG mAb for 5 minutes. Postnuclear supernatants were analyzed by immunoblotting with anti-pErk1/2 and anti-Erk1 mAbs. LumiImager signals were quantified, and the ratio between pErk1/2 and Erk1 was calculated. (F) Ca^{2+} mobilization of Indo-1 AM-labeled U937-TD-derived cells was analyzed by flow cytometry. Cells were stimulated with the anti-FLAG mAb at the time point indicated by the arrow. One representative experiment of seven (B), of four (C, D), of three (E) and of five (F) independent experiments is shown. * $P < 0.05$ and ** $P < 0.003$ (Student`s t-test).

Figure 5: Btk is required for TREM-1-induced cytokine production in mouse BMDCs. BMDCs were generated from bone marrow cells of WT, *Btk*$^{-/-}$, *Tec*$^{-/-}$ and *Tec*$^{-/-}$*Btk*$^{-/-}$ mice in GM-CSF-containing medium. (A) On day 3, BMDC from WT and *Tec*$^{-/-}$*Btk*$^{-/-}$ mice were stained with isotype-matched (dashed line) or anti-TREM-1 (full line) mAbs and analyzed by flow cytometry. (B) On day 4, cells were incubated for 8 hours with either plate-bound isotype-matched control or plate-bound anti-TREM-1 mAbs or with PMA and ionomycin. Supernatants were analyzed by ELISA for TNF-α and MIP-2. Data are displayed as mean ± SD of at least duplicates of ELISA from duplicate cultures. Figure shows one representative result out of three independent experiments. * $P < 0.01$, ** $P < 0.006$ and *** $P < 0.0001$ (Student`s t-test). iono: ionomycin.

Figure 6: Cytokine production in PBMCs from XLA patients after TREM-1 triggering. (A) Expression of TREM-1 on PBMCs of healthy controls and of XLA patients was analyzed by flow cytometry. Representative histograms show overlays of staining with isotype-matched (dashed line) or anti-TREM-1 (full line) mAbs gated on $CD14^+$ cells. (B) PBMCs were prepared from peripheral blood of XLA patients and healthy individuals by Ficoll-Paque gradient centrifugation. Cells were incubated with plate-bound isotype control or anti-TREM-1 mAbs for 24 hours and TNF-α production was analyzed by ELISA. Due to the lack of B cells in XLA patients, slightly increased frequency of TREM-1^+ cells was observed (healthy controls: 21.4 ± 5.4%; XLA: 30.3 ± 8.0%). Thus, levels of TNF-α production were normalized to 5×10^4 of $CD14^+$ cells. Median value of group is depicted in the graph as a line.

Figure 1

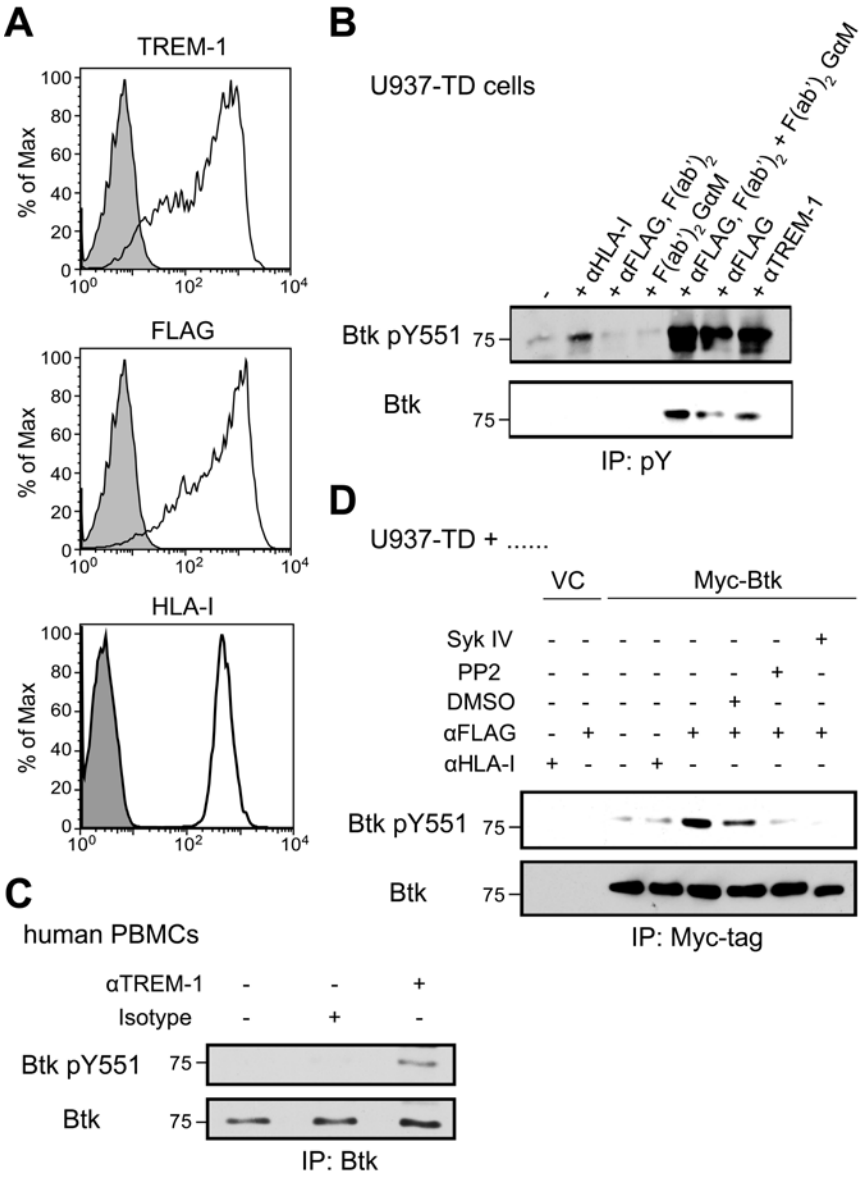
A
TREM-1
FLAG
HLA-I
% of Max
B
U937-TD cells
- + αHLA-I + αFLAG, F(ab')2 + F(ab')2 GαM + αFLAG, F(ab')2 + F(ab')2 GαM + αFLAG + αTREM-1
Btk pY551
Btk
IP: pY
C
human PBMCs
αTREM-1
Isotype
Btk pY551
Btk
IP: Btk
D
U937-TD + ...
VC
Myc-Btk
Syk IV
PP2
DMSO
αFLAG
αHLA-I
Btk pY551
Btk
IP: Myc-tag

Figure 2

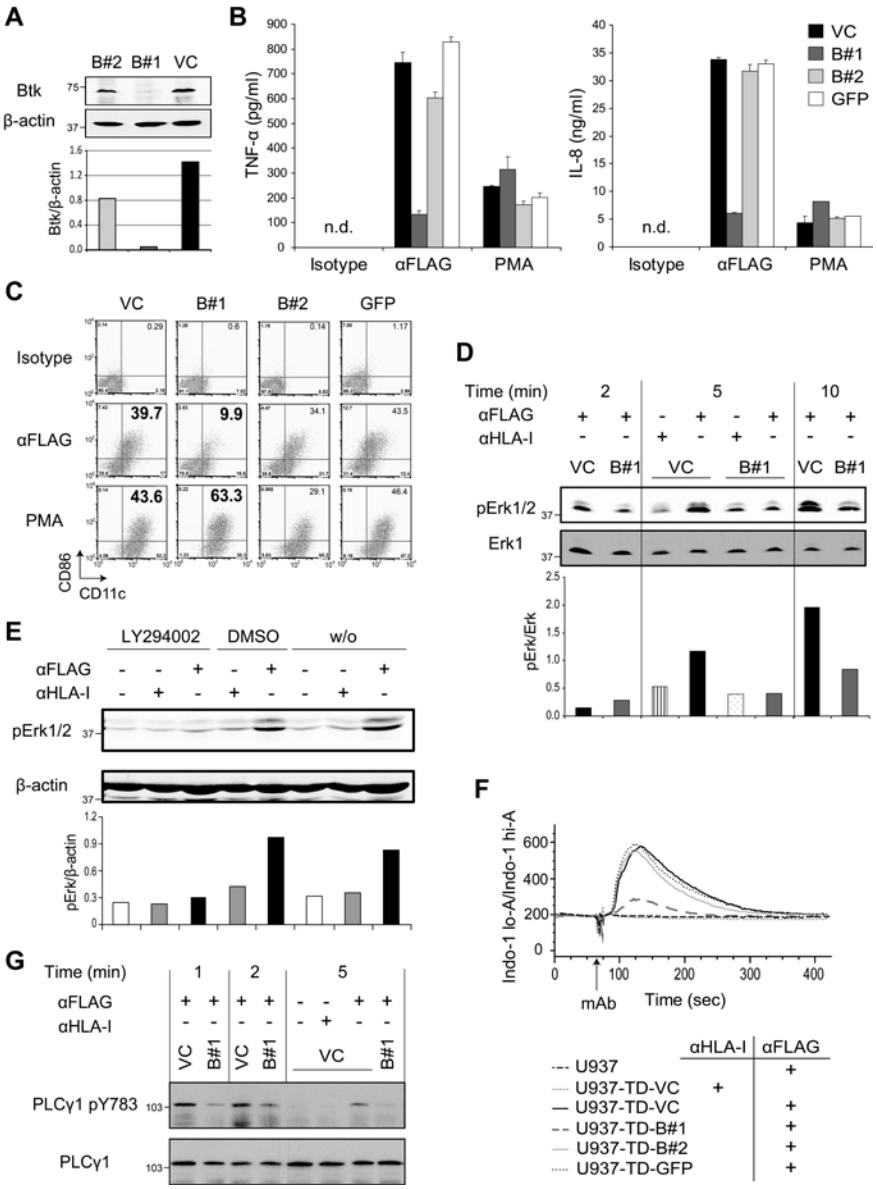
A
B#2 B#1 VC
Btk
β-actin
Btk/β-actin
B
TNF-α (pg/ml)
n.d.
Isotype
αFLAG
PMA
IL-8 (ng/ml)
VC
B#1
B#2
GFP
C
VC B#1 B#2 GFP
Isotype
αFLAG
PMA
39.7
9.9
43.6
63.3
CD86
CD11c
D
Time (min) 2 5 10
αFLAG
αHLA-I
VC B#1 VC B#1 VC B#1
pErk1/2
Erk1
pErk/Erk
E
LY294002 DMSO w/o
αFLAG
αHLA-I
pErk1/2
β-actin
pErk/β-actin
F
Indo-1 lo-A/Indo-1 hi-A
mAb
Time (sec)
αHLA-I αFLAG
U937 +
U937-TD-VC +
U937-TD-VC +
U937-TD-B#1 +
U937-TD-B#2 +
U937-TD-GFP +
G
Time (min) 1 2 5
αFLAG
αHLA-I
VC B#1 VC B#1 VC B#1
PLCγ1 pY783
PLCγ1

Figure 3

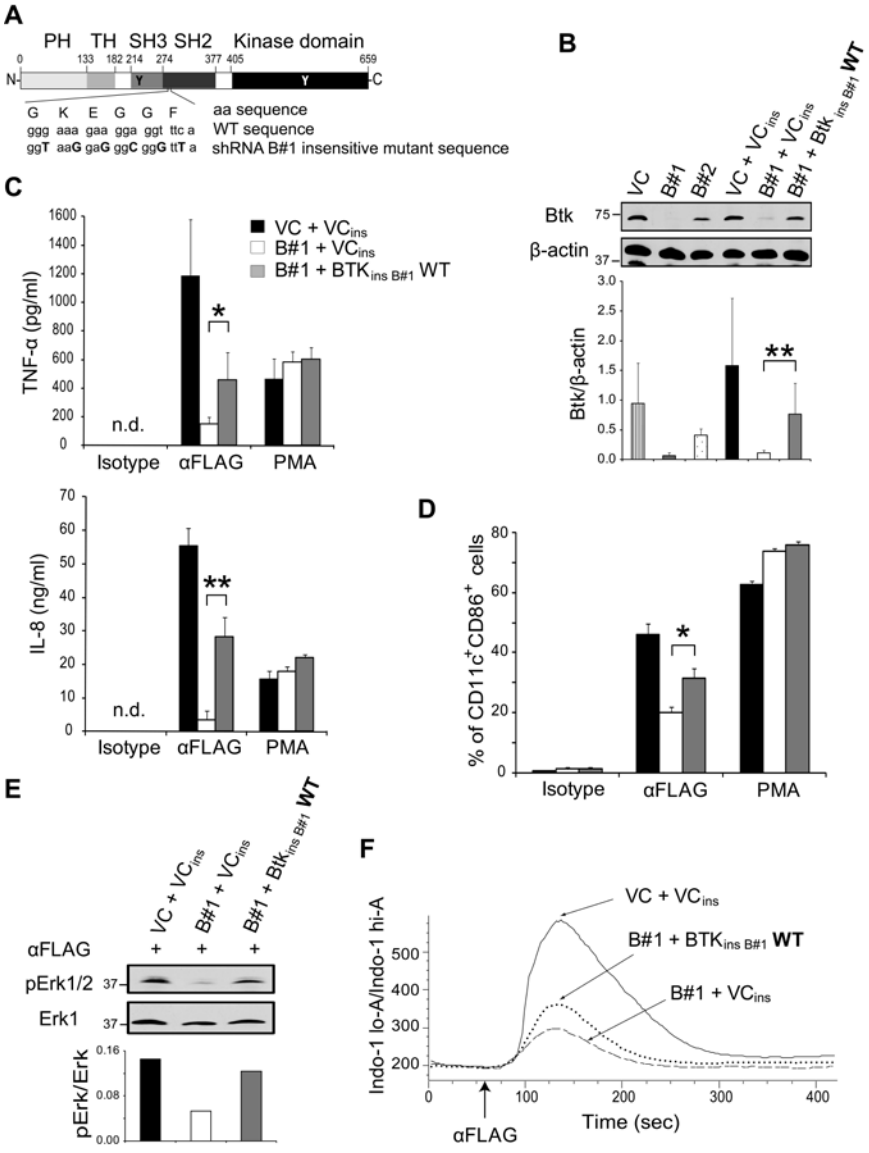
A
PH TH SH3 SH2 Kinase domain
0 133 182 214 274 377 405 659
N C
G K E G G F aa sequence
ggg aaa gaa gga ggt ttc a WT sequence
ggT aaG gaG ggC ggG ttT a shRNA B#1 insensitive mutant sequence
B
VC B#1 B#2 VC + VCins B#1 + VCins B#1 + Btkins B#1 WT
Btk
β-actin
Btk/β-actin
C
VC + VCins
B#1 + VCins
B#1 + BTKins B#1 WT
TNF-α (pg/ml)
IL-8 (ng/ml)
n.d.
Isotype αFLAG PMA
D
% of CD11c+CD86+ cells
E
αFLAG
pErk1/2
Erk1
pErk/Erk
F
Indo-1 lo-A/Indo-1 hi-A
Time (sec)
αFLAG

Figure 4

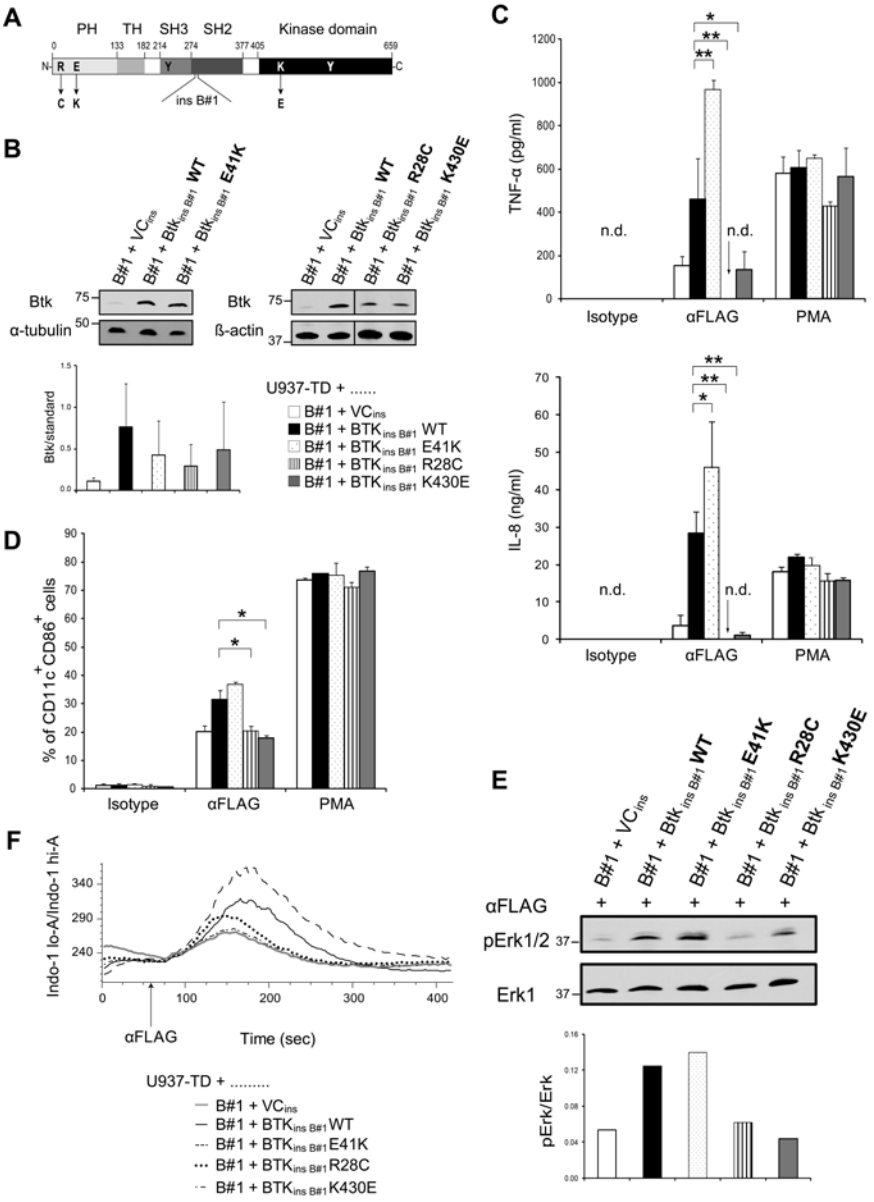
A
PH
TH
SH3
SH2
Kinase domain
ins B#1
B
Btk
α-tubulin
ß-actin
Btk/standard
U937-TD + ...
B#1 + VCins
B#1 + BTKins B#1 WT
B#1 + BTKins B#1 E41K
B#1 + BTKins B#1 R28C
B#1 + BTKins B#1 K430E
C
TNF-α (pg/ml)
IL-8 (ng/ml)
n.d.
Isotype
αFLAG
PMA
D
% of CD11c+CD86+ cells
E
αFLAG
pErk1/2
Erk1
pErk/Erk
F
Indo-1 Io-A/Indo-1 hi-A
Time (sec)

Figure 5

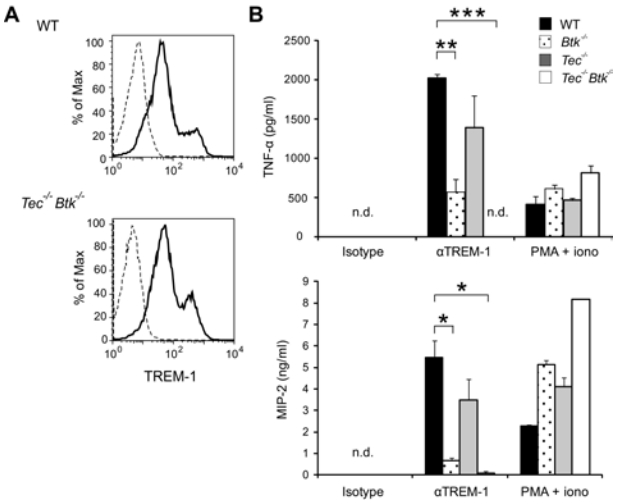
A
WT
% of Max
Tec-/- Btk-/-
TREM-1
B
WT
Btk-/-
Tec-/-
Tec-/- Btk-/-
TNF-α (pg/ml)
n.d.
Isotype
αTREM-1
PMA + iono
MIP-2 (ng/ml)

Figure 6

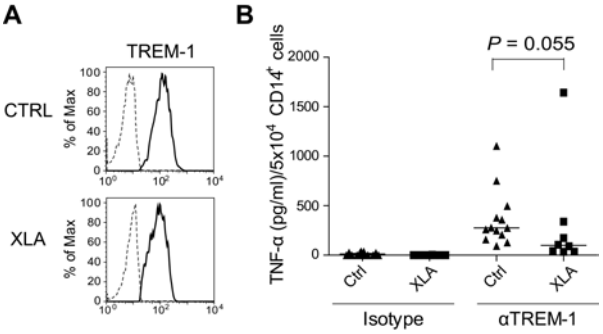
A
TREM-1
CTRL
XLA
% of Max
B
P = 0.055
TNF-α (pg/ml)/5x10^4 CD14+ cells
Ctrl
XLA
Ctrl
XLA
Isotype
αTREM-1

Supplemental methods

Generation of mouse BMDCs

Mouse BMDCs were differentiated from BM cells isolated from femur and tibiae of the hind legs. Cell suspensions were filtered through a 40 µM cell strainer and incubated for 2–3 minutes in 0.5 ml ACK buffer per leg for erythrocytes lysis. After washing, cells were cultured overnight in DMEM supplemented with 10% FCS, 2 mM glutamine, 100 U/ml penicillin, 100 µg/ml streptomycin, 1/100 v/v non-essential amino acids, 1 mM sodium pyruvate, 50 µM β-mercaptoethanol (Invitrogen Life Technologies) and 10% GM-CSF containing supernatant from the cell line X6310-GM-CSF, provided by Prof. T. Decker (University of Vienna, Vienna, Austria). Non-adherent cells were harvested and cultured for additional four days.

Vectors

The pMXs-IN vector was described previously[7] and used for expression of Myc-tagged Btk in U937-TD cells. The pMXs-ILyt2 vector was generated by exchanging LNGFR in pMXs-IN for Lyt2 (truncated mouse CD8) and used for expression of Btk constructs insensitive to B#1 shRNA. The RVH1_LNGFR vector (kindly provided by Prof. R. Medzhitov, Yale University, New Haven, CT) was described previously[7] and used for expression of shRNA oligonucleotides.

Short hairpin RNA constructs

The following oligonucleotides encoding shRNAs that targets Btk were used: B#1 (5′-GATCCCCGGGAAAGAAGGAGGTTTCATTCAAGAGATGAAACCTCCTTCTTTCCCTTTTTGGAAC-3′); and B#2 (5′-GATCCCCGAAGCTTAAAACCTGGGAGTTCAAGAGACTCCCAGGTTTTAAGCTTCTTTTTGGAAC-3′).[23] These oligonucleotides were annealed and ligated into the RVH1_LNGFR vector. The construct bearing shRNA directed against GFP was described previously.[7]

cDNA constructs and generation of stable cell lines

cDNA of human Btk WT and E41K were amplified from pRVC-TAP-hBtk and pSGT-hBtk* E41K, respectively, provided by Prof. G. Superti-Furga (Center for Molecular Medicine, Austrian Academy of Sciences, Vienna, Austria). N-terminally Myc-tagged Btk was amplified from pRVC-TAP-hBtk. The forward primer contained the sequence of Myc-tag: 5′-CGCGGATCCATGGAACAAAAACTTATTTCTGAAGAAGATCTGGCCGCAGTGATTCTGG-3′. Amplified cDNAs were inserted into the pMXs-IN vector.[7] Btk constructs insensitive

to the B#1 shRNA were generated by site-directed mutagenesis using the primer 5′-GCAACTGCTAAAGCAAGAGGGTAAGGAGGGCGGGTTTATTGTCAGAGACTCCAG CAAAG-3′ following standard protocols and ligated into the pMXs-ILyt2 vector. Point mutations, Btk R28C and K430E, were generated by site-directed mutagenesis of construct $Btk_{insB\#1}$WT following standard protocols and ligated into the pMXs-ILyt2 vector.

To prepare stable transfectants of the U937-TD cell line, which ectopically expresses FLAG-TREM-1 and DAP12, the protocol described before by Tessarz *et al*[7] was used. To enrich transduced cells, cells were pre-sorted using anti-LNGFR or anti-mouse CD8 mAbs coupled magnetic beads (MACS, Miltenyi Biotec) followed by flow cytometric sorting by FACSVantage SE (BD Biosciences).

Antibodies

The following antibodies were used: anti-FLAG (clone M2) and anti-human β-actin from Sigma-Aldrich; anti-α-tubulin from Oncogene; anti-Myc tag, anti-human Btk, anti-human phospho-PLCγ1 Tyr783, anti-human PLCγ1 and anti-phospho Erk1/2 (Thr202/Tyr204) from Cell Signaling Technology; anti-human HLA-I (clone MEM-147) from Exbio; anti-phosphotyrosine (clone 4G10) from Upstate Biotechnology; purified or PE-conjugated anti-human TREM-1 and purified or PE-conjugated anti-mouse TREM-1 from R&D Systems; anti-human Btk, anti-human Btk pY551/Itk pY551, anti-human Erk1, FITC-conjugated anti-mouse CD11c, APC-conjugated anti-human CD11c, PE-conjugated anti-human CD86, PE-conjugated anti-human NGFR and purified NA/LE Rat IgG2aκ Isotype control from BD Biosciences; APC-conjugated anti-mouse CD11b, APC-conjugated anti-mouse CD8, PE-conjugated rat IgG2aκ from BioLegend; purified or PE-conjugated mouse IgG1κ (clone MOPC-21C) from BD Biosciences (Figure 2) or BioLegend (Figure 3 and 4); anti-human Btk (M-138) from Santa Cruz Biotechnology: PE-conjugated goat $F(ab')_2$ anti-mouse IgGs from Biosource; $F(ab')_2$ goat anti-mouse IgG+IgM from Jackson ImmunoResearch; goat anti-mouse IgG horseradish peroxidase conjugate and goat anti-rabbit IgG horseradish peroxidase conjugate from Biorad.

$F(ab')_2$ fragments of the anti-FLAG M2 mAb were prepared essentially following standard protocols using incubation of the mAb with immobilized pepsin (Thermo Fisher Scientific) in acetate buffer pH 5 for 6 hours.

Erk phosphorylation

Cells (5×10^6) were stimulated in RPMI 1640 without FCS with the mAbs (10 µg/ml) for the indicated time period at 37°C. After washing, cells were resuspended in 100 µl of LM lysis

buffer (additionally containing crystal of DNase). Lysates were subjected to three freeze-thaw cycles followed by incubation at 4°C for 30 minutes. Postnuclear supernatants mixed with reducing Laemmli buffer were resolved by SDS-PAGE followed by immunoblotting using anti-pErk1/2 and anti-Erk or β-actin Abs. The ratio between pErk1/2 and Erk1 or β-actin resp. was determined by a LumiImager (Roche Diagnostics). Quantification of the protein signals was performed using the LumiAnalyst software (Roche Diagnostics).

Ca^{2+} flux

Cells (3×10^6/ml) were washed with RPMI 1640 without FCS and loaded with 1 µM Indo-1 AM (Molecular Probes) at 37°C for 30 minutes. Cells were washed twice with RPMI 1640 without FCS and kept at 37°C till measurement. Ca^{2+} flux was induced with the indicated mAb (10 µg/ml) and measured for additional 360 seconds using FACSVantage SE (BD Biosciences).

Supplemental table

Table S1: Clinical and molecular information about the XLA patients

Patient	Age	Mutation	IgG trough levels [g/l]	Treatment (Ig) [mg/kg]	PBMCs [counts x10^6/ml]	B cells [%]
1	8	R562W	8.4	125/week sc	1.21	0
2	2	c.776+5delG	7.9	500/3 weeks iv	1.75	0
3	20	Intron 7: 721+1 G ->C	6.8	100/week sc	0.59	0
4	16	H519N	10.9	150/week sc	1.29	0
5	31	R28C	8.1	75/week sc	0.96	0.2
6	12	V626G	11	174/week sc	1.35	0
7	11	H519R	9.4	700/month iv	1.10	0
8	38	W421X	7.7	93/week sc	0.76	0.1

sc indicates subcutaneous; iv, intravenous.

Supplemental data

Figure legends

Figure S1: Cytokine production upon TREM-1 and TLR4 engagement is impaired in Btk knock-down cells. U937-TD-derived cells were incubated with plate-bound anti-FLAG with or without LPS (1 µg/ml) or isotype-matched anti-HLA class I mAbs, LPS (1 µg/ml) or PMA (5 ng/ml) for 16 hours. Production of TNF-α (upper panel) and IL-8 (lower panel) was measured by ELISA. Data are displayed as mean ± SD of at least duplicates of ELISA from duplicate cultures. n.d: not detectable.

Figure S2: Similar Erk phosphorylation is induced after TREM-1 engagement by anti-FLAG and anti-FLAG (Fab')$_2$ cross-linking. U937-TD-VC cells were incubated with the indicated stimuli for 5 min. Postnuclear supernatants were analyzed by immunoblotting with anti-pErk1/2 and anti-Erk1 Abs.

Figure S1

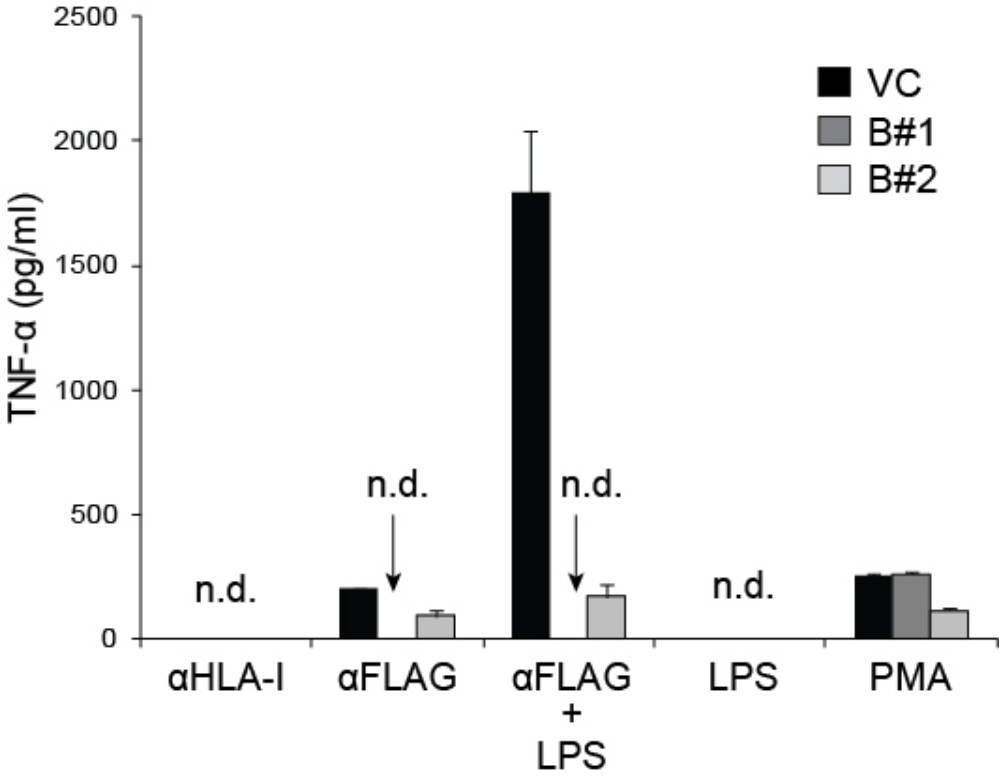
2500
2000
1500
1000
500
0
TNF-α (pg/ml)
VC
B#1
B#2
n.d.
n.d.
n.d.
n.d.
αHLA-I
αFLAG
αFLAG + LPS
LPS
PMA

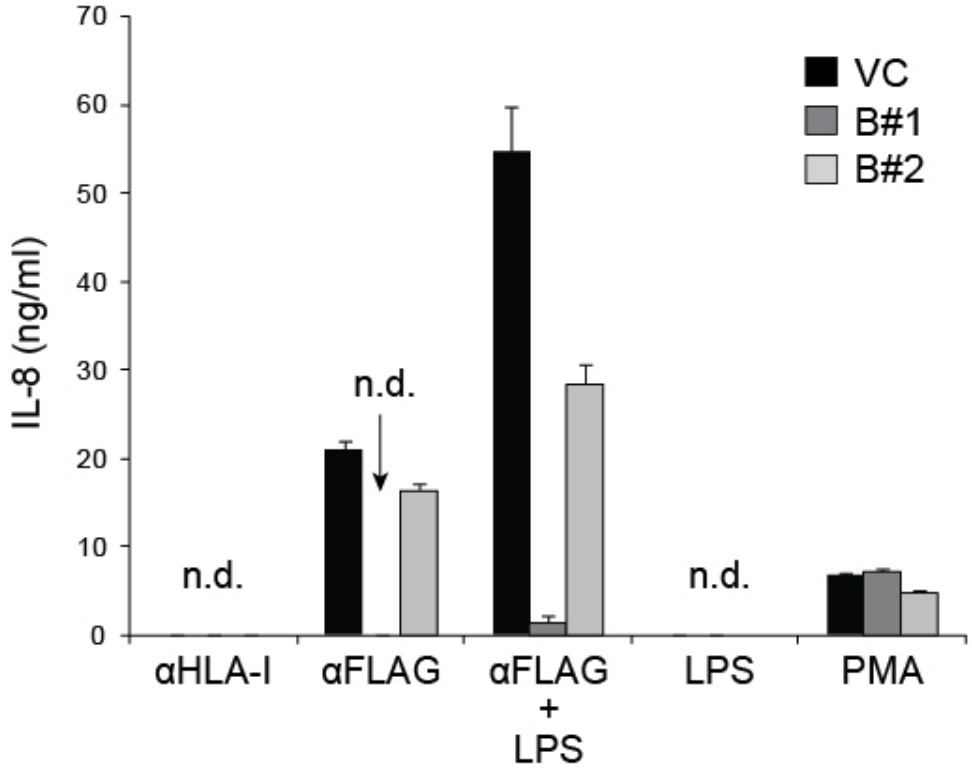
70
60
50
40
30
20
10
0
IL-8 (ng/ml)
VC
B#1
B#2
n.d.
n.d.
n.d.
n.d.
αHLA-I
αFLAG
αFLAG + LPS
LPS
PMA

Figure S2

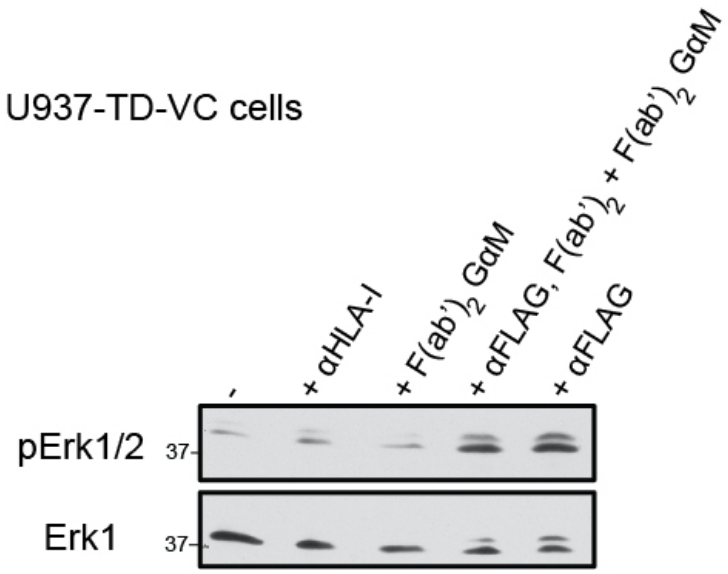
U937-TD-VC cells
-
+ αHLA-I
+ F(ab')2 GαM
+ αFLAG, F(ab')2 + F(ab')2 GαM
+ αFLAG
pErk1/2
37
Erk1
37